Anticorrosion Potentials of Derived Chitosan and Polyaspartic Acid Modified with Organic Compounds on Steel in Acidizing Environment.

BY

OBASI, ANNUNCIETA CHUKWUDUMEBI (B.Eng.)

(20194197838)

A THESIS SUBMITTED TO THE POSTGRADUATE SCHOOL, FEDERAL UNIVERSITY OF TECHNOLOGY, OWERRI

IN PARTIAL FULFILLMENT OF THE REQUIREMENTS FOR THE AWARD OF MASTERS IN ENGINEERING (M.ENG) IN POLYMER SCIENCE AND ENGINEERING

SEPTEMBER2023.

CERTIFICATION

We certify that this work: **"Anticorrosion Potentials of Derived Chitosan and Polyaspartic Acid Modified with Organic Compounds on Steel in Acidizing Environment."** was carried out by **Obasi Annuncieta Chukwudumebi** (**20194197838**) in partial fulfillment for the award of the degree of Masters in Engineering (**M.ENG**) in Polymer Science and Engineering, in the Department of Polymer and Textile Engineering of the Federal University of Technology, Owerri.

.....
Engr Dr. P.I. Anyanwu
Principal Supervisor

13/11/2023
Date

.....
Engr. Dr. S.C. Nwanonenyi

13/11/2023
Date

.....
Engr. Dr. M.N. Akanbi

13/11/2023
Date

.....
Engr. Dr. I.O. Eze
Head of Department
Polymer and Textile Engineering

13/11/2023
Date

.....
Engr .Prof. Remy Uche.
Dean, School of Engineering
Engineering Technology

24/01/24
Date

.....
Prof. B.O. Esonu
Dean of Postgraduate School

.....
Date

.....
Engr. Prof. M.C. Menkiti
External Supervisor

.....
Date

DEDICATION

This work is dedicated to God Almighty for His unending love towards me and my family members.

I also dedicate this work to my wonderful husband and children whose support contributed immersively to the progress of this work.

This work is also dedicated to those who believed that “whatever is worth doing is worth doing well”.

ACKNOWLEDGEMENTS

To say that this work is all my idea, I will be lying. It is on this note that I want to acknowledge with sincere gratitude my Principal Supervisor, and Co Supervisor Engr. Dr. P.I. Anyanwu and Engr. Dr. S.C. Nwanonenyi whose act of fatherly love and understanding guided me in producing this overwhelming work in the academic field.

To my Head of Department, Department of Polymer and Textile Engineering, Engr. Dr. I.O. Eze, for his contribution towards making this work a success.

My appreciation also extends to all the board members of the Department of Polymer and Textile, especially all the Professors and Senior colleagues whose contribution comes in kind words and advice.

I also acknowledge the Department of Chemistry and Pharmacy of Madonna University for providing the equipment and access to laboratory units for the synthesis.

I in a special way acknowledge Dr. D.I. Njoku and Dr. B.I. Onyeachu who contributed greatly to the success of this work.

I can’t forget in a hurry to sincerely acknowledge the City University HK and HKMU HK, SAR, China, for assisting with the electrochemical, surface analysis, and imaging techniques.

I won’t forget to acknowledge my Dad, Mr. Godwin C. Obasi, my Mum, Mrs. Esther A. Obasi, and my Uncle Prof. P.C. Obasi whose own contribution brought me where I am today.

This work is supported by FUTO granting me a study fellowship for my Master's Degree.

Obasi, Annuncieta Chukwudumebi

Table of Content

List of Tables

List of Figures

List of Abbreviations

Abbreviations	Meaning
CTS	Chitosan
NAHD	Nicotinic acid hydriazide
PAA	Polyaspartic acid
EIS	Electrochemical impedance spectroscopy
PDP	Potentiodynamic polarization
FTIR	Fourier transformed infrared spectroscopy
XPS	X-ray photoelectron spectroscopy
CTS-PAA	Chitosan-modified polyaspartic acid
CTS-NAHD	Chitosan modified nicotinic acid hydriazide
SEM	Scanning electron microscopy
Uv-vis	Ultraviolet visible
E_a	Activation energy
B.E	Binding energy
R_{ct}	Charge transfer resistance
r^2	Goodness of fitting parameter

ABSTRACT

The anticorrosion potentials of derived chitosan and polyaspartic acid modified with organic compounds on steel in an acidizing environment were investigated using gravimetric and electrochemical methods. Chitosan (CTS) and polyaspartic acid (PAA) were synthesized from oyster shells and L-aspartic acid respectively. The oyster shell synthesized chitosan was modified using polyaspartic acid and nicotinic acid hydrazide (NAHD) respectively. The modified polymers (CTS-PAA) and (CTS-NAHD) obtained were used to investigate corrosion inhibition of mild steel in 1.0 M HCl solution.The synthesized chitosan, polyaspartic acid, and modified polymers were characterized using FT-IR and UV-vis respectively. Corrosion studies were performed using gravimetric (weight loss), electrochemical (electrochemical impedance spectroscope, EIS, and potentiodynamic polarization, PDP), and computational techniques respectively. Gravimetric results obtained revealed that inhibitor efficiency of the modified polymers increased with the rise in inhibitor concentration at room temperature (CTS-PAA and CTS-NAHD had an efficiency of 96.5% and 86.6% at a concentration of 200mg/L) at room whereas their response with time (24hrs, 72hrs, 120hrs & 168hrs) and temperature (40-60^{o}C) variations respectively showed reversed cases. The electrochemical test, EIS, and PDP showed that CTS-PAA gave the highest inhibition efficiency than CTS-NAHD at 86.3% and 89% respectively. The adsorption isotherms results confirmed that adsorption of CTS-PAA and CTS-NAHD on the mild steel surface followed Langmuir adsorption isotherm. Surface analysis carried out on the mild steel using X-ray photoelectron spectroscopy, XPS, and scanning electron microscope, SEM respectively probed the evidence of corrosion protection. The computational results obtained revealed that there existsa correlation between the electron molecular structures of modified inhibitors and their inhibition efficiency, and the theoretical results obtained are in agreement with experimental data.
Therefore, the modification of chitosan has aided in solving the global problem of corrosion in Engineering.

Keywords: Chitosan, Polyaspartic acid, nicotinic acid anhydride, steel, corrosion, inhibition.

CHAPTER ONE
INTRODUCTION

1.1 Background of Study

Corrosion is a natural process whereby a material usually metals deteriorates in the presence of oxygen and water as they interact with their environments. Corrosion is a high-cost problem that causes the collapse and failure of oil pipelines, bridges, and buildings and the leakage of chemical plants. Corroded electrical contacts because fire outbreaks and other problems, corroded medical implants lead to blood poisoning, and air pollution has caused corrosion damage to works of art around the world. Corrosion intimidates the safe disposal of radioactive waste that must be stored in containers for tens of thousands of years (239 ECS Meeting, 2019).In 2020 and 2021, Nigeria national oil spill detection and response agency (NOSDRA) recorded 822 combined oil spill summing to 28,003 barrels of oil spewed in the environment creating direct impact on the farmers and residents of those areascaused by corrosion (Adeyanju&Oyekunle 2019).

Corrosion occur when the atoms on the metal surfacee.g.oxygen, hydrogen; electrical current or even dirt and bacteria attack the entire surfaces of the metal. Most metals are easily oxidized and they tend to lose electrons to oxygen (and other substances) in the air or water. As oxygen is reduced (gains electrons), it forms an oxide with the metal. Corrosion can also happen when metals like steel are placed under too much stress causing the material to crack.

The deterioration of metals as a result of corrosion is a global challenge. According to NACE, “unmitigated corrosion costs of the U.S. economy is over $500 billion each year, or roughly 3.1 percent of our GDP” (NACE, 2016). The cost of corrosion worldwide is estimated to be US$2.5 trillion, which is equivalent to 3.4% of the global GDP (Koch, 2017). In Nigeria, about $18.5 million is used annually to solve the problem of corrosion in industries and more than 65% of this cost is taken by the

oil and gas industries due to the kind ofequipmentthey use and their operation conditions.(Adeyanju&Oyekunle 2019) These costs do not include individual safety or environmental consequences. Through near misses, incidents, forced shutdowns (outages), accidents, etc., several industries have come to understand that lack of management towards corrosion can be very costly and lead to material wastage but proper corrosion management leads to significant cost savings over the lifetime of an asset (NACE, 2016).

Mild steel is a type of carbon steel that contains a low level of carbon. Mild steel otherwise known as low carbon steel contains roughly between 0.05 % and 0.25 % of carbon by weight. This is contrary to high-carbon steel, which is composed of up to 2.5 % carbon by weight. Carbon steels are used for automobile body parts, plates, and wire products. However, it is highly susceptible to corrosion in an acid medium, and hydrochloric (HCl) acid is the solvent most often employed for chemical cleaning. HCl is commonly used for the neutralization of alkaline agents, and as a bleaching agent, in the food, textile, metal, and rubber industries.(Fekry & Mohamed, 2010)To arrest the corrosion of steel in acidic environemnts such as the aggressive environemnts created by oil well acidizing, contnued effors is reqauired to provide low-cost and ecofriedly methods of controling corrosion in Nigeria oil and gas sectors and in other industries.

1.1.1 Polymeric inhibitors for controlling metal corrosion in acidic media:

Polymers are gigantic molecules that are formed by the combination of small molecules known as monomers. Polymers can be obtained from either inorganic or organic sources and inhibitors from polymeric compounds have the potential to reduce effectively the corrosion rate of metal surfaces in mildly aggressive mediums or environments when added in small concentrations (Tiu & Advincula, 2015). Polymers can be modified with organic or inorganic additives to improve their inhibitive properties (Milewska et al., 2013). The use of polymers as corrosion

inhibitors has attracted significant attention recently. Polymers are used as corrosion inhibitors because, through their functional groups they form complexes with metal ions and on the metal surface these complexes cover a large surface area, thereby isolating the surface of the metal and protecting it against the access of corrosive agents present in the solution or electrolyte (Liu et al., 2021).

1.1.2 Modification of natural polymers for corrosion inhibition:

Natural polymers are modified due to the limited presence of adsorption sites /functional groups necessary to improve corrosion protection in acidic environments. Thus, the grafting of functional compounds aided by several coupling and catalysts has been explored for polymer modification and different degrees of anticorrosion improvement have been achieved. Several reactions including catalyzed dehydration, amidation, esterification, aminolysis, etc., have been employed to modify natural polymers to achieve species with improved solubility, thermal stability, and effective inhibition performance (El et al., 2020).

1.2 Problem Statement

The impact of corrosion is felt in three areas of concern; economics, safety (including health), and environmental damage (Umoren et al., 2020). Some of the consequences of corrosion include mechanical damage to pumps and other infrastructural facilities, reduction in the value of metal components due to deterioration of appearance, contamination of fluids in pipes and vessels, perforation of vessels and pipes allowing escape of their contents, and possible harm to the surroundings, hazards or injuries to people arising from structural failure or breakdown (examples, bridges, cars, etc) and reductions of metal thickness leading to loss of mechanism strength and structural failure (Bradford, 2001). Annual loss due to corrosion is estimated to be 3 to 5% of GNP.

Therefore, it is very important to study the investigation of metal corrosion and inhibition in aggressive systems to; explore the basic nature of corrosion and its many processes, review some basic environmental and material selection considerations, and describe the discoveries that can help prevent and control corrosion damage of mild steel.

1.3 Objective of study

The objective of this research is to study the anticorrosion potentials of derived chitosan modified with poly-aspartic acid modified and nicotinic acid hydriazideon mild steel in an acidizing environment.

Other specific objectives include the following;

(i) To derive chitosan from Oyster shells, polyaspartic acid from aspartic acid monomers, and to modify the derived chitosan with both polyaspartic acid and the nicotinic acid hydrazide, distinctively.

(ii) To characterize the modified polymers using spectroscopic techniques (FTIR and UV-vis) for successful synthesis and inhibition performance via interaction with metal substrate (SEM, XPS).

(iii) To evaluate the inhibition efficiency of the modified chitosan using the gravimetric testing technique, EIS, PDP, SEM,XPSand theoretical (DFT, Monte Carlo) approaches.

1.4 Scope of Study

The study will be limited to:

- Mild steel as the adsorbent and 1 M HCl as the corrosive medium
- Temperature effects to provide the associated thermodynamic properties **(ΔG, ΔH, Ea, ΔS).**
- Characterization of the polymers to confirm successful preparation **using**

FTIR

- Corrosion tests **(gravimetric and electrochemical techniques)**
- Theoretically evaluation (**DFT –density functional theory and MDS – molecular dynamics)**

1.5 Justification of Study

Mild steel is often deployed in service in different aqueous aggressive environments, with consequent corrosion damage. Corrosion-inhibiting additives are one of the major ways to control corrosion in aggressive media. But, due to the toxicity and lack of eco-friendliness of synthetic and chromate-based inorganic corrosion inhibitors the use of non-toxic additives is encouraged. In this regard, the use of natural polymers is gaining popularity due to their cost-effectiveness, biodegradability, and multiple attachment sites. Interestingly, they are cheap and renewable.

CHAPTER TWO

LITERATURE REVIEW

2.1 Metal Corrosion and Natural Polymeric Inhibitors:

One of the practical ways to alleviate the corrosion of metals in acid media is the use of corrosion-inhibiting additives. Due to the campaign by several environmental agencies, researchers got attracted to the use of biodegradable and eco-friendly additives as corrosion inhibitors. Polymers are employed as corrosion inhibitors because of their ability to form complexes with the metal ions on the surfaces of the metal with a large surface area (Umoren & Solomon, 2020). The complex ions formed prevent the corrosive agents present in the solution from penetrating the metal surface. Polymeric inhibitors from both synthetic and naturally derived are among the effective organic inhibitors that have been proposed/reported for acid corrosion because of biodegradability, cheapness, and effectiveness. However, biopolymers or naturally derived polymeric compounds are biodegradable, eco-friendly, and cheap compared to the synthetic and inorganic polymeric compounds counterparts. In this regard, polymeric inhibitors from natural sources have been reported as a potential alternative for acid corrosion due to their biodegradability, low cost, and effectiveness. For instance, natural polymers (carbohydrates and biopolymers) such as chitosan, sodium alginate, glucose, gellan gum, hydroxypropyl cellulose, aspartic acid, hyaluronic acid, carboxymethyl cellulose, etc., have been studied and used to inhibit corrosion in acidic media. (Solomon et al., 2010) reported on the inhibitive and adsorption behavior of carboxymethyl cellulose on mild steel corrosion in sulphuric acid solution. They used chemical methods to assess the inhibitive and adsorption behavior of carboxymethyl cellulose (CMC) for mild steel in H_2SO_4 solution at 30 - 60^{o}C. From their results, CMC acted as a good corrosion inhibitor to mild steel, and the inhibiting effect increased as the concentration of

CMC increased and reduced as the temperature increased. The adsorption of CMC on the surface of mild steel was found to follow Langmuir and Dubinin–Radushkevich adsorption isotherm models. The inhibition mechanism was further corroborated by the values of activation parameters obtained from the experimental data.

Nwanonenyi et al., 2017 investigated the use of millet starch to control the corrosion of mild steel in 0.5M HCl. The investigation was carried out using gravimetric corrosion testing technique, potentiodynamic polarization technique, thermometric and mathematical computational technique and it was observed that the inhibition efficiency of millet starch increased with an increase in concentration.

Cui et al., 2011also reported on polyaspartic acid as a green corrosion inhibitor for carbon steel. The inhibiting effect of the biodegradable and eco-friendly corrosion inhibitor polyaspartic acid (PAA) on the deterioration of carbon steel in 0.5 M H_2SO_4 was studied using weight loss, potentiodynamic polarization, electrochemical impedance spectroscopy (EIS), and scanning electron microscopy (SEM) techniques. The results obtained from the polarization curve clearly stated that PAA is a good inhibitor. The result from EIS reveals that the corrosion inhibition ability of PAA increased with increasing concentration, and a maximum inhibition efficiency of 80.33 % was recorded. SEM also showed that PAA formed a film layer on the inhibited sample. The adsorption of this inhibitor followed the Freundlich adsorption isotherm.

Jmiai et al., 2017 investigated the behavior of sodium alginate on copper in a 1M hydrochloric acid medium using combined gravimetric and electrochemical techniques. The inhibition efficiency against acid corrosion of 83% at a sodium alginate (SA) concentration of 0.1mg/L was obtained. The Langmuir adsorption isotherm revealed that SA can be adsorbed on the surface of copper. The interaction between the surface of SA and Cu was confirmed by X-ray spectrometry while the

protective effect at the micro level was confirmed by Atomic force spectrometry (AFS) (Jmiai et al., 2017).

Obot et al., 2017studied sodium alginate (SA) as an effective inhibitor against the corrosion of API X60 steel in neutral 3.5% NaCl using gravimetric and electrochemical techniques (OCP, EIS, and EFM). The results show that the inhibition efficiency of the SA increased with the increase in SA concentration but was lowered at a higher temperature (70 °C). The electrochemical measurements show that the SA increases the steel corrosion-resisting ability and also decreases the corrosion kinetics through the formation of an adsorbed layer which reduces the wettability of the steel surface based on contact angle measurement. SEM-EDAX was used to confirm the inhibition of SA on API X60 steel surfaces. The sodium alginate adsorbs on the steel surface through a physisorption mechanism. The adsorption phenomena result in decreased localized pitting corrosion of the API X60 steel in 3.5% NaCl solution. Theoretical results using quantum chemical calculations and Monte Carlo simulations provide further atomic-level insights into the interaction of SA with a steel surface.

Dang et al., 2015investigated the inhibition effect of the environmentally friendly inhibitor sodium alginate on AZ31 magnesium alloy in 3.5 wt% sodium chloride solution**.** The results show that sodium alginate can successfully reduce the corrosive nature of AZ31 magnesium alloy. As the concentration of SA increases, the inhibition efficiency increases up to 90 % at an SA concentration of 500 ppm. The inhibition efficiency increased due to the increase in the adsorption of sodium alginate on the bare surface of magnesium alloy, where it complexes with magnesium hydroxide to form a continuous compact film, which slows down the corrosion of the alloy (Dang et al., 2015).

Mobin et al., 2017 reported polysaccharide from Plantago as a green corrosion inhibitor for carbon steel in 1 M HCl solution. The mucilage of Plantagoiscomprised of highly branched polysaccharide, arabinosyl (galacturonic acid) rhamnosylxylan

(AX), which is responsible for the corrosion inhibition of the carbon steel. The gravimetric method, potentiodynamic polarization, electrochemical impedance spectroscopy (EIS), scanning electron microscopy (SEM), atomic force microscopy (AFM), UV–vis spectroscopy, and FTIR were used to check the inhibition efficiency and the adsorption properties of AX on carbon steel. Thermodynamic and activation parameters also showed that the adsorption of AX on carbon steel was predominantly chemical. Quantum chemical analysis supports the proposed mechanism of inhibition.

Fares et al., 2012 reported on Pectin as a promising green corrosion inhibitor of aluminum in hydrochloric acid solution. At 8.0g/L 10 ^{o}C, an inhibition efficiency of 91% was obtained which reduced with increasing temperature (i.e., 40 ^{o}C =31%). However, with increased pectin concentration, the activation energy, the enthalpy of activation, and the entropy of activation increased. The adsorption process was more favored at lower temperatures with larger negative standard free energy. Adsorption of pectin macromolecules on the aluminum surface followed by Langmuir adsorption isotherm.

Mobin et al., 2017 investigated a biopolymer fromtragacanth gum, (Arabinogalactan) AG, for its adsorption and corrosion inhibition abilities on carbon steel corrosion in 1 M HCl. They used potentiodynamic polarization measurements, gravimetric method, atomic force microscopy, UV−visible spectroscopy, scanning electron microscopy, and electrochemical impedance spectroscopy to determine the adsorptive nature of AG in the acidic medium. The results showed that the inhibition efficiency of AG increased up to 96.3 % as the temperature and AG concentration increased. The thermodynamics and activation parameters were calculated and the AG adsorption followed Langmuir adsorption isotherm.

Umoren et al., 2019 explored the use of natural polymers as green corrosion inhibitors for AZ31 magnesium alloy in a saline environment. Seven natural polymers such as dextran (Dex), chitosan (CHI), carboxymethyl cellulose (CMC),

hydroxyl ethyl cellulose (HEC), sodium alginate (ALG), pectin (PEC), and gum Arabic (GA) were used for anti-corrosion properties on AZ31 Mg alloy in 3.5 wt % NaCl solution. It was observed that GA, CHI, PEC, CMC, and Dex increased the corrosion inhibition of the magnesium alloy, compared with ALG and. Surface imaging studies were carried out using SECM, SEM, EDX, and AFM techniques, and the results concur with the other experimental results and showed effective corrosion inhibition. FTIR, X-ray photoelectron spectroscopy, and UV-vis results disclose that $Mg(OH)_2$ co-existed with adsorbed inhibitor complexes.

2.2 Metal corrosion and modified natural polymeric inhibitors:

Due to the inherent thermal instability, insolubility, limited heteroatoms, and conjugated double bonds in the many bio-polymer chains, the structural modification of these polymers with a variety of compounds to improve their overall anti-corrosion performance is a priority area. As such, several natural polymers have been modified with different organic molecules or compounds. For instance,(El et al., 2020) reported on the modification of chitosan using Cinnamaldehyde as a bio-derived corrosion inhibitor for copper in an acid environment. In a single-step procedure, they cross-linked chitosan using cinnamaldehyde following microwave irradiation to produce cinnamaldehyde-modified chitosan (Cinn-CS) for copper in 1M hydrochloric acid. The electrochemical investigation was carried out using the impedance measurements, and potentiodynamic polarization, supported with surface analysis and computational studies.

Srivastava et al., 2018 reported as the first to investigate the functionalization of Chitosan using polyethylene glycol as a novel biological macromolecule corrosion Inhibitor in 1M HCl. Weight loss method, surface morphology (AFM), electrochemical measurements, and quantum chemical investigation were used to study the inhibition efficiency, and a maximum corrosion inhibition efficiency of 93.9 % was recorded at a concentration of 200 mg/L. The adsorption of the inhibitor

film obeyed Langmuir adsorption isotherm and exhibited both physical and chemical adsorptive interactions. The electrochemical technique also indicated that there was an increase in the polarization resistance which supported the adsorption and inhibition behavior. The experimental findings were supported by the data of quantum chemical calculations.

Zhang et al., 2015 investigated polyamine-grafted chitosan copolymer and evaluated the corrosion inhibition performance of carbon steel in an acidic environment. They synthesized two chitosan derivatives. Methyl acrylate was first grafted to chitosan by reacting the chitosan with methyl acrylate through Micheal addition reaction. Afterward, the resultant was reacted with ethylenediamine and triethylenetetramine respectively to give ethylene diamine grafted chitosan (CS MAA EN) and triethylenetetramine grafted chitosan copolymers (CS MAA TN). The copolymers were characterized using FT-IR. The inhibition abilities were investigated using potentiodynamic polarization, gravimetric measurements, electrochemical impedance spectroscopy, and metallographic microscopy. The copolymers showed good inhibition efficiency on carbon steel in 5% HCl at 25^0C. The results showed that (CS MAA EN) had a higher inhibition efficiency of 90% than (CS MAA TN) which had an 85% inhibition efficiency.

Gao et al., 2020 synthesized eco-friendly corrosion inhibitor lignin derivatives with excellent corrosion resistance behavior in HCl solution. Lignin was grafted to (2,3-epoxypropyl) trimethyl ammonium chloride EPTAC. The inhibition efficiency was investigated using adsorption thermodynamic analysis, electrochemical methods, and molecular dynamic simulation. The results showed that a protective film layer was formed on the iron surface by the lignin- EPTAC giving rise to an excellent 97.80 % inhibition efficiency at the concentration of 100 mg/L. The surface of the steel was smoothened to 26.6 nm from its initial 99.3 nm and the lignin molecule adsorption follows the Langmuir adsorption isotherm.

Sharma et al., 2019 synthesized 8-hydroxyquinoline grafted-alginate as a biobased corrosion inhibitor on mild steel in 1M HCl solution. The modified alginate was characterized by F-TIR and NMR spectral data. The inhibition efficiency of the modified alginate was investigated using surface morphology, electrochemical measurement, density functional theory, and molecular dynamics simulation method and in comparison, the results of the modified alginate were seen to be more advantageous than the unmodified alginate.

Xing et al., 2017 investigated calcium alginate gel beads loaded with benzotriazole. This process was achieved by a piercing solidifying method. Cu-benzotriazole complexes were introduced first on the surface of the gel bead via the interaction of benzotriazole and Cu^{2+} to extend the release time of benzotriazole. The amount of benzotriazole present in Cu-benzotriazole was determined by thermogravimetric analysis and the process of releasing benzotriazole was determined by UV-vis spectrometer. Polarization and electrochemical impedance spectrum techniques were used to determine the inhibition efficiency of the Cu-benzotriazole calcium alginate gel bead on steel in a 3.5% NaCl solution. The result shows that the inhibition efficiency of 5.0g/L Cu-benzotriazole calcium alginate gel bead on steel in 3.5% NaCl solution was higher up to 87.06% at 24 hours with low corrosion current density than steel in 3.5% NaClsolution(Xing et al., 2017).

Chai et al., 2020 reported on the modification of polyaspartic acid using dopamine as a green corrosion inhibitor for mild steel in an acid medium. He studied the inhibition ability of dopamine-modified polyaspartic acid (PASP Dop) at different concentrations and temperatures using weight loss and electrochemical measurements. The results reveal that PASP Dop has a high adsorption rate in 0.5M H_2SO_4 and it obeys Langmuir adsorption isotherm. Potentiodynamic polarization was used to determine the inhibition efficiency of PASP Dop on mild steel in 0.5 M H_2SO_4 solution at 100 ppm as 90.9 % at a temperature of 298 K while weight loss measurement reveals that PASP Dop has good temperature adaptability.

Sangeetha et al., 2015 reported on corrosion mitigation of N-2-hydroxy-3-trimethyl ammonium propyl-chitosan chloride as an inhibitor on mild steel (HTACC).

He used gravimetric measurement and electrochemical experiments to determine the effect of HTACC on mild steel in 1 M HCl. They recorded 98.9% inhibition efficiency at 500ppm. The inhibition efficiency of HTACC increases with an increase in its concentration and decreases with an increase in temperature. The modified chitosan was characterized by FTIR and NMR. Polarization studies show that HTACC acts as both anodic and cathodic curves, and electrochemical impedance spectroscopy reveals that inhibition occurred through inhibitor metal surface adsorption. A scanning electron microscope shows that a protective film was formed on the surface of the metal by the inhibitor.

Solomon et al., 2017 reported on the modification of chitosan using silver nanoparticles (AgNPs-Chi) and its corrosion inhibitor effect on St37 steel in 15% H_2SO_4 solution. The inhibition effect was studied using weight loss and electrochemical techniques in addition to surface morphological examination. They recorded an inhibition efficiency of 94% unlike in the unmodified chitosan which could fairly protect the surface of the steel by 45%. Langmuir adsorption isotherm was used to describe the mode of adsorption of AgNPs-Chi on the surface of the steel. The result of the surface screening shows the adsorption of AgNPs-Chi molecules on steel.

Fekry & Mohamed, 2010 investigated the acetyl thiourea chitosan (ATUCS) as an eco-friendly inhibitor for mild steel in a sulfuric acid environment. Potentiodynamic polarization scanning electron microscopy and electrochemical impedance spectroscopy were used to study the electrochemical behavior of mild steel in 0.5M H_2SO_4 and ATUCS-containing solution. The EIS result indicates that the resistance (Rt) increases slightly as the immersion time increases which means that there is a slight reduction in corrosion rate with time. The polarization technique also reveals that the inhibition efficiency of mild steel increases with an increase in the polymer

concentration and decreases with increasing temperature. ATUSC was confirmed to exhibit good inhibition efficiency of 94.5% at0.76mM concentration. The inhibition efficiency depends on the polymer concentration, temperature, and immersion time.

Li et al., 2014 reported on the modification of chitosan using aminothiourea for corrosion inhibition and heavy metal ion adsorbent. They used formaldehyde as linkages to modify chitosan with thiosemicarbazide (TSFCS) and thiocarbohydrazide (TCFCS) to get two derivatives of chitosan. FTIR, thermal gravity analysis, differential scanning calorimetry, and elemental analysis were used to study and characterize the modified polymer. Scanning electron microscopy was used to determine the surface morphology of the polymer. The behavior of 304 steel in 2 % acetic acid in the presence of different inhibitors at different concentrations was evaluated and found that TCFCS showed the best result of 92 % at 60 mg/L using potentiodynamic polarization.

El-deeb et al., 2018 evaluated modified lignin extracted from wheat straw and used as a corrosion inhibitor for aluminum in alkaline solution. The extracted lignin was modified by hydrolysis to get LG-OH and carboxylation reaction to have LG-COOH. The extracted lignin and modified lignin were characterized by spectroscopic and thermal analysis. The corrosion inhibition of these species was studied in 1.0M NaOH on aluminum using potentiodynamic polarization techniques and morphological characterization. The result shows that the carboxyl modified lignin LG-COOH has a lower corrosion current density I_{corr} than the hydrolyzed lignin and the unmodified lignin. The experimental results show maximum inhibition efficiency with LG-COOH followed by LG-OH, then unmodified lignin (LG). The inhibition efficiency is ascribed to the high adsorption active site on LG-COOH. The adsorption of the inhibitors obeyed Langmuir adsorption isotherm.

Lahrour et al., 2019 reported on glycerin-grafted starch as a corrosion inhibitor of C-Mn steel in 1M HCl solution. They synthesized starch from maize and then grafted it with glycerin to form a bio copolymer which was used as a green corrosion inhibitor

to avoid the toxicological effect of conventional synthetic polymer. FTIR and NMR were used to characterize the bio copolymer while a corrosion inhibition test such as a weight loss test was carried out to ascertain an inhibition efficiency of 94% at a concentration of 300 mg/L. The inhibition efficiency was found to have increased with an increase in the biopolymer concentration and the corrosion current densities decreased with an increase in inhibition concentration. The potential density and corrosion density obtained correspond to the gravimetric test.

Farhadian et al., 2021 chemically modified hydroxyethyl cellulose (CHEC) and used it as an efficient eco-friendly inhibitor for the corrosion of mild steel in a 15% HCl environment at elevated temperature. NMR and ATR-FTIR were used to determine the molecular weight and chemical structure of CHEC. They reported on a facial and practical way by which the inhibition activity of natural polymers can be improved under high temperature, so, hydroxyethyl cellulose was modified with polyurethane and was used as a corrosion inhibitor in suppressing mild steel. Electrochemical impedance spectrometer, weight loss measurement, open circuit potential, potentiodynamic polarization, etc., were used to assess the corrosion inhibition and it was found that 1% of polyurethane prepolymer could increase the inhibition efficiency of CHEC in acid solution at elevated temperature.

XPS result shows that CHEC was adsorbed on the mild steel and caused an inhibition efficiency of 93% at 80^0 C temperatures and the morphology of the mild steel shows the protective roles of the additives.

Liu et al., 2021 reported on the anti-corrosion performance and mechanism of dextrin and its grafted copolymer on steel in an acid solution. They grafted caprolactam and copolymerized it with dextrin through a chemical synthesis method to get dextrin grafted copolymer which was used as a corrosion inhibitor in 1.0 M HCl solution. FTIR was used to characterize the grafted copolymer and also to ensure a successful and proper grafting. Thereafter, the corrosion inhibition performance on steel was investigated with a weight loss test, EIS, SEM,

potentiodynamic polarization curve, scanning electrochemical microscopy, and contact angle experiments. The results show that the modified inhibitor exhibited excellent inhibition performance. It was also observed that the corrosion inhibition efficiency increased with an increase in the inhibitor concentration until it reached a certain concentration, but as the temperature rose, it began to decrease gradually. The grafted dextrin was recorded to have a better corrosion inhibition efficiency of 82.38 % at a concentration of 300 mg/L.

Ochoa et al., 2013 modified cassava starch as a potential corrosion inhibitor for sustainable development. Carboxymethylated cassava starch (CMS) and activated cassava starch (ACS) were studied as corrosion inhibitors for XC35 carbon steel in NaCl solution. FTIR and back titration were used to characterize the modified cassava starch and electrochemical techniques were used to ascertain the inhibitive properties of the modified starch at room temperature. X-ray photoelectron spectroscopy was used to determine the chemical composition of the protective film formed by the starch. The results revealed that the inhibitive film is composed of an iron/hydroxide mixture in which the starch molecules are incorporated. The electrochemical measurement shows that the activated starch AS acts as a mixed-typed inhibitor while carboxymethylated starch inhibits mainly the anodic reaction. Potentiodynamic polarization showed that at a concentration 600 mg/L CMS gave an inhibition efficiency of 84 % while AS showed 98 % inhibition efficiency.

Chugh et al., 2020 investigated the relationship between the degree of substitution and metal protecting ability of cinnamaldehyde-modified chitosan. They synthesized five different chitosan cinnamaldehyde Schiff bases by varying their degree of substitution using chitosan and cinnamaldehyde as the monomeric units. FTIR and NMR were used to characterize the biopolymers. Surface characterization was done using different techniques such as atomic force microscopy (AFM), scanning electrochemical microscopy (SECM), scanning electron microscopy with energy dispersive spectroscopy (SEM-EDS), and X-ray photoelectron spectroscopy (XPS)

to provide important information about the adsorption of the biopolymers at the metal surface leading to the inhibition of the corrosion of the mild steel. Gravimetric tests and electrochemical methods were used to study the anti-corrosion properties of the biopolymer on mild steel in 0.5M H_2SO_4. They also ascertained the inhibition efficiency of the biopolymers using electrochemical impedance spectroscopy, gravimetric test, and potentiodynamic polarization and the result was satisfactory following each other.

2.3 Metal corrosion and synthetic polymeric corrosion inhibitors:

Roy et al., 2014 investigated the corrosion inhibition of mild steel in 1M HCl by polyacrylamide grafted guar gum together with various grafting percentages and the effect of intramolecular synergism. FTIR showed the sites in which the grafted polymers are bonded during metal adsorption. The polymer was seen to have been grafted up to 86% and it behaves as a mixed-type inhibitor. It forms a protective layer on the surface of the mild steel following Langmuir adsorption isotherm. Scanning electron microscopy reveals that the surface of the inhibitor-coated steel was smoother compared with the surface of mild steel without an inhibitor. They conducted a weight loss test and found out that the inhibition efficiency of the guar gum grafted polyacrylamide-coated mild steel increased up to 93% after 5hours of immersion and greater than 90% after 50hours of immersion.

Shukla & Quraishi, 2011 investigated the effect of some substituted aniline-formaldehyde polymers on mild steel corrosion in an HCl medium. Polyaniline formaldehyde, poly(p-chloroaniline) formaldehyde, and poly(o-toluidene) formaldehyde were used as corrosion inhibitors on mild steel in hydrochloricacid medium. Linear polarization, weight loss measurement, Tafel polarization, and electrochemical impedance spectroscopy techniques were employed for the tests. The very high inhibition efficiency was recorded at a very low concentration. The result also confirms that all the inhibitors are mixed-type inhibitors and they all

participated in the reaction in the form of a surface metal inhibitor complex. Atomic force microscopy was studied and it revealed that the metal surface was not affected after the use of an inhibitor in hydrochloric acid medium.

Ansari & Quraishi, 2015 reported on the effect of 3 components (aniline, formaldehyde, and piperazine) on the corrosion of mild steel in an HCl medium. The three polymeric Schiff base was synthesized and studied as corrosion inhibitors in 1M HCl. Electrochemical impedance spectroscopy, weight loss measurement, and potentiodynamic polarization techniques were carried out and the result showed that formaldehyde, aniline, and piperazine (AFPP) polymeric Schiff base exhibited an inhibition efficiency of 98 % on mild steel in 1 M HCl solution. Potentiodynamic polarization techniques also showed that AFPP is a mixed type of inhibitor but predominant at the cathodic site. The inhibitor adsorption followed Langmuir adsorption isotherm.

Kilmartin et al., 2002 reported on the corrosion inhibition of polyaniline and poly(o-methoxyaniline) on stainless steel in HCl and H_2SO_4 solutions. Polyaniline films were deposited on the stainless steel by electrochemical deposition and the corrosion performance was monitored in acidic solution by open circuit potential. Impedance spectroscopy and cyclic voltammetry show that poly(o-methoxyaniline) was polymerized successfully on stainless steel electrode and corrosion inhibition similar to that of polyaniline was recorded. The result showed that both polyaniline and poly(o-methoxyaniline) formed a passive oxide film on the stainless steel which protected the metal from corrosion.

Manickavasagam et al., 2002 studied poly(styrene sulphonic acid)-)-doped polyaniline as a mild steel corrosion inhibitor in hydrochloric acid. Polystyrene sulphonic acid doped polyaniline was synthesized and used as a corrosion inhibitor in 1M HCl on mild steel. Galvanostatic polarization, weight loss measurement, electroporation studies, and a.c impedance measurement were carried out and a.c impedance and hydrogen permeation clearly showed that the compound exhibited an

effective corrosion inhibition on mild steel. The polymer is predominantly an anodic inhibitor and it brought down the extent to which hydrogen enters the metal. The adsorption of the compound on the surface of the metal followed Temkin's adsorption isotherm.

2.4 Metal corrosion and polymer blend as corrosion inhibitors:

The combination of polymers has been shown to improve the overall inhibition performance. Hence, research on blends has been investigated in recent times.

Umoren & Ebenso, 2008 investigated polyvinylpyrrolidone (PVP) and polyacrylamide (PA) blend as corrosion inhibitors for aluminum in an acidic medium. Using thermometric techniques, weight loss measurement, and hydrogen evolution, they studied the behavior of aluminum in HCl in both the presence and absence of PVP, PA and their blend at a temperature range of 30-60^{o}C. The inhibition efficiency increased with an increase in the inhibitor concentration but decreased with an increase in temperature. PVP exhibited higher inhibition efficiency than PA but optimum inhibition efficiency was observed when the two were blended at a ratio of 3:1 (PVP: PA). The inhibitor adsorption obeyed Temkin, Freundlich, and Flory Huggins adsorption isotherms.

Rashid et al., 2014 reported on a polyaniline-palm oil blend for anticorrosion of mild steel in a saline medium. The protective performance of mild steel coated with polyaniline- palm oil blend in 3% NaCl solution was evaluated using open-circuit potentials, electrochemical impedance spectroscopy, potentiodynamic polarization, and electrochemical method. Because of the physical interaction between the coating and mild steel, the surface of the mild steel was covered with a dark green layer and the coating does not involve the use of an organic solvent. The result from EIS and potentiodynamic polarization confirm that the blend has more positive oxidation potentials

Umoren, 2011 worked on the synergistic inhibition effect of polyethylene glycol – polyvinylpyrrolidone blends for corrosion inhibition of mild steel in a sulphuric acid medium. He investigated the individual inhibition efficiency of the compounds and their blend using hydrogen evolution techniques and weight loss measurement at a temperature range of 30-60 ^{o}C. The inhibition efficiency was found to be synergistically at its optimum on the blend ratio of 1:3 (PED: PVP) as the inhibitor concentration increased but decreased at elevated temperatures. The experimental data obtained fits the Temkin adsorption isotherm.

Moraga et al., 2006 reported on the blending of 2,5-dimethoxy aniline (PDMA) and fluoropolymers as a coating for corrosion inhibition of stainless steel. They prepared a heterogeneous blend of the polymers through casting using a ternary system which allows the compatibilization of the polymer mixture and also improves the adhesion of the coating to the stainless steel. Wide scan x-ray photoelectron spectroscopy showed that the surface of the steel was covered totally by the polymer. At zero current, chronopotentiometry was used to determine the open-circuit potentials. Environmental and thermal stability were higher on the blend. An energy dispersive spectrometer was carried out and it showed that the blend exhibited higher resistance to fog than PDMA and both PDMA and the blend behave as both physical and electrochemical barriers, showing superior inhibition resistance when compared to PDMA.

Umoren et al., 2014 reiterated that studies involving the use of polymer blend or mixture in mitigating corrosion in an aggressive environment are scarce. Thus, they investigated the effect of polyethyleneglycol-polyvinyl pyrrolidone blend as corrosion inhibition of aluminum in HCl solution using combined gravimetric and gasometric techniques complemented with surface imagine technique (AFM). The results show that the corrosion rate increases with temperature, time, and surface coverage of the blend on the metal surface decreases with an increase in the different blend ratios. In general, the experimental results reveal that the inhibition efficiency

of the polymer blends was higher than that of the individual polymers which supports that blending influences the performance of the inhibition mixture.

2.5 Research Gap

The effectiveness of naturally derived polymers like chitosan in preventing corrosion can be improved by modifying them with organic molecules containing heteroatoms. However, previous reports on this topic lacked a detailed explanation of the mechanism behind the improved anti-corrosion effects.

To address this knowledge gap, our project focused on describing the process of enhanced anti-corrosion effects of modified naturally derived polymers, specifically chitosan grafted with poly-aspartic acid. We could calculate the electronic and adsorption properties for the first time, which helped us understand the process of enhanced adsorption.

Additionally, we expanded our understanding of modifying naturally derived polymers for anti-corrosion applications by modifying chitosan with nicotinic acid hydrazide and detailing the mechanism behind its anti-corrosion protection. This is new information that has not been reported before.

CHAPTER THREE
MATERIALS AND METHODS

3.1 Materials

The materials used in this work include the following;

(a) Inhibitors

Oyster shells were sourced from Calabar, Cross-rivers State Nigeria,and were used for the synthesis of chitosan. L-Aspartic acid was purchased from Rhawn Reagent China and was polymerized to Polyaspartic acid.

(b) Metals

The metal used was mild steel. A mild steel (MS) specimen was obtained from the FUTO workshop. Each sheet which was 0.1cm in thickness was mechanically pressed-cut into coupons of dimensions 5 cm x 5 cm. Mild steel coupons were first polished with different grades of silicon carbide paper (SiC) ranging from 150 to 1000 to remove the adhered rust and to expose fresh and smoothened surfaces. The polished coupons are degreased in absolute ethanol, washed with distilled water, dried in warm air, and stored in a free moisture environment before immersion for the gravimetric experiment.

The test metal samples for the electrochemical experiment were machined into 1cm by 1cm and fixed in polytetrafluoroethylene (PTFE) rods by epoxy resin in such a way that only one surface of area 1cm was left uncovered. The electrodes (cubic specimen of metal samples) used were polished with emery papers (from 800 to 1200 grits), rinsed with distilled water, degreased by ethanol, and dried in acetone.

(c) Reagents

NaOH pellets and 37 % Hydrochloric acid were purchased from ChemisciencesOwerri Imo State. BDH analytical grade was used as sourced without further purification. HCl was used to prepare the corrodent solution (1.0 M HCl) via

serial dilution while 10 M NaOHsolutionswere used for chitosan preparation. Distilled water was used for all solution preparations. Ethanol (96%, analytical grade) was used to wash the metals after immersion, and also the mussel powder to remove the green pigment. Ammonium hydroxide (NH_4OH), nicotinic acid hydrazide, formaldehyde, glutaraldehyde, acetone, etc., were used as sourced without further purification.

(d) Laboratory materials and glass wares

Other materials used in this research were bristle brushes, beakers, conical flasks, volumetric flask glass rod, hooks, plastic thread, thermometer, Memmert-WTB thermostatic water bath, electric stove, T-l series WANT digital weighing machine of 0.001digits, filtrationfunnel, silicon carbide paper, filter paper, stopwatch, Babyliss electric hair drying machine and a Hotpoint class 3 SA3 electric oven, magnetic stirrer machine with temperature control.

3.2 Method: The following methods were adopted in this research work.

3.2.1 Polymer synthesis

(a) Chitosan Synthesis:

Oyster shells were collected from the local market at Calabar, South-South of Nigeria. They were washed with distilled water to remove leaves, sand, and other impurities and desiccated at room temperature. Then, the oyster shell was air dried for 2 days, oven dried at 50 ◦C for 6 h, and ground to reduce its particle sizes; this was made to pass through analytical 250μm mesh sizes. The ground shells were kept away from dust before processing. The waste was kept at room temperature before use.

Steps involved in deriving chitosan: The following steps are involved in the derivation of chitosan from oyster shells.

i) Washing and rinsing of the oyster shell

ii) Grinding of the shell into fine powder

iii) Demineralization

This was carried out by adding 12.5 M HCl solution to the Oyster shells. Carefully pour the HClinto the oyster shell to avoid bubbling away the shell. The reaction proceeded at room temperature under agitation at 250 rpm for predetermined times (0.5, 2, or 6 h). Afterward, the demineralized shells were filtrated with filter paper and washed with distilled water until neutral pH. They were bleached by immersing in ethanol for 10 min and dried in an oven at 70 ˚C.

(iv) Deproteinization

This was performed by adding 12.5 M NaOH solution to the dried demineralized shells at a solid/liquid ratio of 1:10 (g/mL). The reaction was carried out under agitation at 80 ºC for 3 h. The solid was filtrated with filter paper and washed with distilled water until it achieved a neutral pH. Then, it was immersed in ethanol for 10 mins for further bleaching, and the resulting chitin was dried in an oven at 70 ˚C

(iv) Deacetylation of chitin: Deacetylation of chitin was measured according to the method described by El Knidri et.al with modifications. The chitin deacetylation reaction to obtain chitosan was carried out by preparing a mixture of chitin and a solution of 50 % NaOH at 100 ºC and 6 h until the chitin was deacetylated to a chitosan. After the reaction, the crude chitosan was washed several times with distilled water to attain a neutral pH and recovered by drying in a dry heat incubator at 50ºC for 12 h.

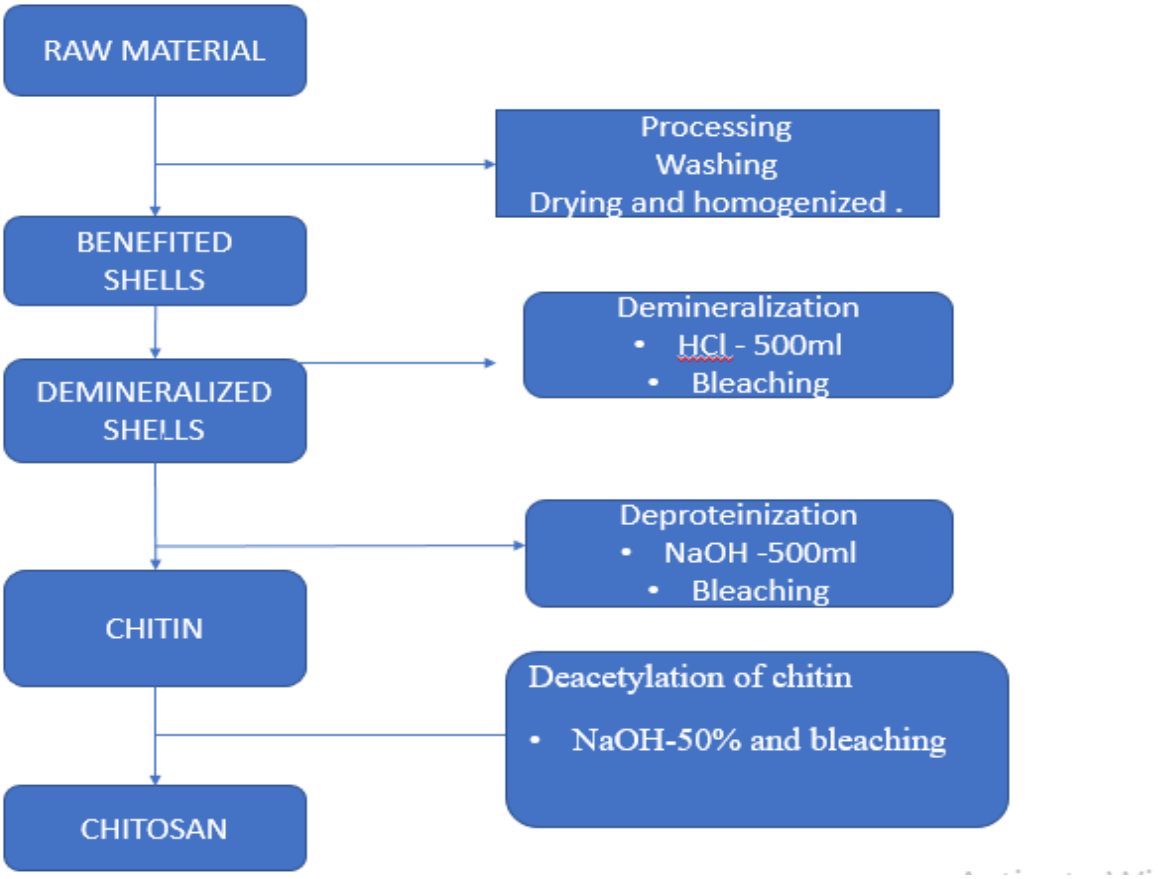

Fig. 3.1Overall chitosan preparation flow chart

(b) Synthesis of Polyaspartic acid from L-aspartic acid:

The synthesis procedures adopted by Bennett, 2005 were followed. L-aspartic acid (4 g) was placed in a 250 ml capacity glass beaker. The beaker was placed on a sand bath such that the sand covered half of the beaker. The bath was heated to a temperature of 250 ^{o}C and the content of the beaker was constantly agitated using a glass rod to prevent it from charring. The process continued as the temperature was maintained until the whole content of the beaker had turned to a tan color. When the heating is complete, the beaker is removed from the sand bath and allowed to cool to room temperature in a cork ring. The cooled solid which is tan or yellowish was placed on filter paper in a filter funnel and washed first with a saturated aqueous solution of $NaHCO_3$ and rinsed with water, secondly, it was washed with 1% HCl

and rinsed with water. The solid is removed from the filter paper and placed in an oven to dry for 30 - 40 mins completing step one.

The dried substance is poured into a dried glass beaker of 500 ml and 250 ml of aqueous NaOHis poured into the 500 ml beaker and stirred until the whole solid is dissolved. The beaker was placed on an electric stove and the solution was brought to a boil. A glass rod was used to stir the solution while boiling to prevent surface tension. The heating continued as the temperature was monitored until more of the liquid evaporated. The beaker is brought down from the electric stove and allowed to cool on a cork ring.

3.2.2 Modifications of Polymers:the polymers used were modified as follows.

3.2.2.1 Modification of Chitosan using nicotinic acid hydriazide

Chitosan was modified using the method stipulated by (Li et al., 2014) with Nicotinic acid hydrazide(NAHD) to improve their inhibition efficiency using formaldehyde as a cross-linking reagent. In this method, chitosan (2g) was added to a 200 ml conical flask containing 10ml of acetic acid and 30ml of distilled water to form a viscous solution. NAHD dissolved in a solution containing ethanol and water at the ratio of 60:40 with constant stirring was introduced into the flask with stirring until a clear solution was formed. Formaldehyde (2 ml) was added to the mixture after 45 mins to cross-link the polymer. The mixture was subjected to a reflux at 80 ^{o}C for 12 h and a creamy white gelly-like product was formed. The product (CTS-NAHD) obtained was washed with 1 M NaOH solution and filtered for neutralization. The product is further washed with distilled water twice, filtered with filter paper, and dried in an oven until the whole water is dried up.

3.2.2.2 Modification of Chitosan with Polyaspartic Acid

The procedures reported by Chen et al., 2018 were followed. In this case, polyaspartic acid (4g) and water 200ml were placed in a glass beaker and the mixture was stirred continuously until complete dissolution of the polymer wasachieved. A mixture containing chitosan sample (2g), 300ml of 2% HCl

solution, and 5ml acetic acid was added into the beaker followed by continuous stirring until complete dissolution was achieved. In addition, an aqueous solution (4 ml) of glutaraldehyde with a mass fraction of 50% was added to dissolve polyaspartic acid. The solution obtained was kept at 40 ^{o}C and its pH was adjusted to 6-7 with hydrochloric acid with stirring. The solution was filtered using anhydrous ethanol and acetone to obtain a solid pale pink product.

3.2.3 Characterization of Polymer Samples: The polymer samples used in this work were characterized using the following techniques

3.2.3.1Fourier-Transform Infrared Spectroscopy (FTIR)

This was used to characterize the synthesized chitosan and polyaspartic acid, the polyaspartic acid-modified chitosan, and Nicotinic acid anhydride-modified chitosan. FTIR spectra were measured on the PerkinElmer Frontier spectrometer by the KBr disk technique. The FTIR instrument was connected to ohmic software which extended from 400 - 4000 cm^{-1}

3.2.3.2Ultraviolent-visible spectroscopy (Uv-vis)

Ultraviolet-visible spectroscopy is an absorption spectroscopy or reflectance spectroscopy in part of the ultraviolet and electromagnetic spectrum. This method is widely used as it is inexpensive and easily implemented in diverse and fundamental applications(Singh et al., 2013)

3.2.4 Corrosion inhibition studies: Anticorrosion studies were carried out using combined weight loss (gravimetric) measurements and electrochemical methodsand the quantitative evaluation of the corrosion inhibition efficiency (IE%) was achieved by adopting the model:

$$\text{IE }\% \left(1 - \frac{W_{Inb}}{W_{blank}}\right) \times 100 \qquad (3.1)$$

Where, W_{Inh} and W_{blank} represent the weight losses obtained with and without the inhibitors.

3.2.4.1 Weight loss measurements

The pre-cleaned and weighed coupons were suspended in beakers containing the test solutions using glass hooks and rods. Tests were conducted under total immersion conditions in 250 ml of unstirred test solutions. To determine weight loss to time, test coupons were retrieved at prescribed time intervals of 24hrs, 72hrs, 120hrs, and 168hrs at room temperature, progressively washed with distilled water, dried in warm air, and reweighed. The weight loss was taken as the difference between the initial and final weight of the coupons. Weight loss measurements were undertaken using a WANT digital weighing balance of 0.001 digits. All the weight results are presented as means of duplicate determinations with standard deviation ranging from 0 - 0.01 g/dm^2.

Temperature consideration (gravimetric approach)

The effect of temperature on the inhibitor was investigated under total immersion of the pre-cleaned coupons in 250ml of the test solution for 3 hours at a temperature range of 40-60^{o}C. The coupons were retrieved after 3 hours, washed with distilled water, dried in warm air, and weighed using the WANTS digital weighing balance.

3.2.4.2 Electrochemical measurements

Electrochemical experiments were conducted in a three-electrode corrosion cell using a ZENNIUM XC complete DC voltammetry corrosion system with a ZAHNER analyzer. A platinum sheet was used as a counter electrode and a saturated calomel electrode (SCE) was used as a reference electrode.

Electrochemical Impedance measurement Spectroscopy (EIS) was performed in aerated and unstirred solutions at the end of 1 h at 25 ± 2^{o}C againstthe reference electrode. The latter was connected via a lugging capillary. Impedance measurements were made at corrosion potentials (E_{corr}) over a frequency range of 100 KHz-0.1 Hz with a signal amplitude perturbation of 10mV.

Potentiodynamic polarization (PDP) studies were carried out in the potential range ± 250 mV versus corrosion potential at a scan rate of 0.3333mVs^{-1}. Each test was run

in triplicate to verify the reproducibility of the data. All experiments were carried out in freshly prepared solution at a constant temperature of 25 ±2^{o}C.In both techniques, the results were monitored and extracted from the computer with the help of the earlier-mentioned software.

3.2.4.3Theoretical Computation

Theoretical quantum chemical computations were performed in the framework of density functional theory (DFT) electronic structure programs as contained in Material Studio 7.0 software to determine the inhibitor effectiveness at the molecular level. In performing the calculations, the electronic structure of the inhibitors and iron (Fe) surface were modeled using DFT electronic structure programs- DMol^{3}. Restricted spin polarization using the DNP basis set and Perdew Wang (PW) local correlation density function were also electronic parameters for the simulation. The electronic properties including HOMO, LUMO, and Fukui functions for electrophilic (F^{-}) and nucleophilic (F^{+}) attack and total electron density were determined. Local reactivity of the inhibitor molecules was assessed from Fukui indices (FI) to establish the adsorption centers or active centers through which the inhibitor molecules would likely interact with the Fe surface.

Molecular dynamics (MD) simulation was performed using Forcite quench molecular dynamics to sample many different low-energy configurations and identify the low-energy minima of the non-covalent interaction between the inhibitor molecules and Fe surface. The calculations were done using a compass force field and a Smart algorithm.

CHAPTER FOUR
RESULTS AND DISCUSSION

4.1 RESULTS: the characterization results, the experimental and theoretical results are reported below

4.1.1 Characterization of the modified and unmodified inhibitor: below is the characterization result of the modified and unmodified inhibitors.

4.1.1.1F-TIR characterization: Fourier–transform infrared spectroscopy was used to characterize the derived inhibitors

Table 4.1.1: FTIR Peaks typical for identifying chitosan preparation

S/N	FTIR peaks	Assignment	Ref
1	3478.68 cm^{-1}	vibrations of -OH bond of the prepared chitosan	(Dimzon & Knepper, 2015)
2	2924.13 cm^{-1}	C–H vibration	(Dong et al., 2001)
3	1656.88 cm^{-1} 1571.05 cm^{-1} 1422.53 cm^{-1} 1378.16 cm^{-1}	The C=O stretching of the amide I band, bending vibrations of the N–H (N-acetylated residues, amide II band), C-H bending, OH bending respectively	(Varma &Vasudevan, 2020)
4	1157.31 cm^{-1}	Anti-symmetric stretching of (C–O–C) bridge	(Varma& Vasudevan, 2020)
5	1075.33^{-1} and 1025.18 cm^{-1}	The skeletal vibration involving C–O stretching	(Ayodele et al., 2018)

(a)

(b)

(c)

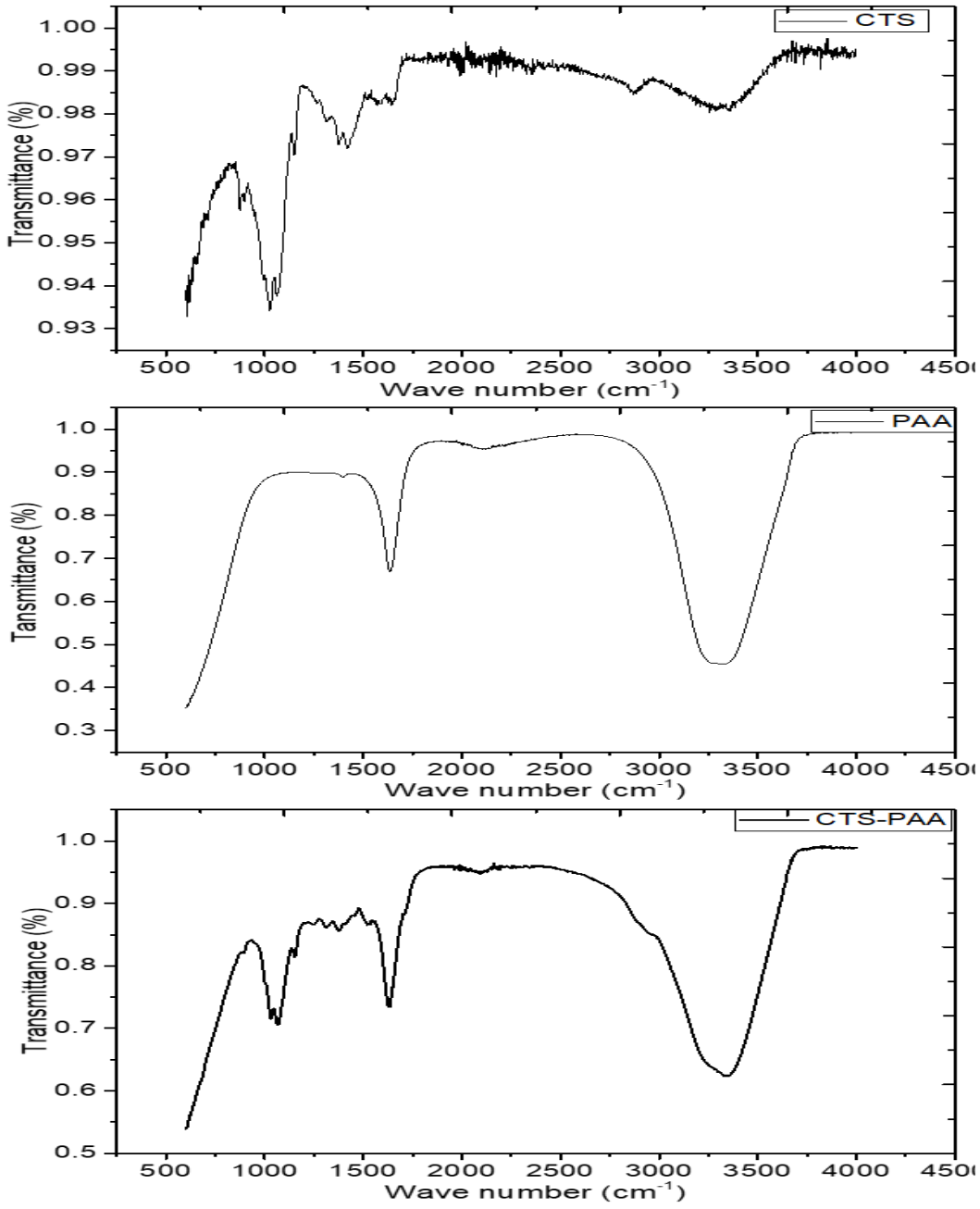

Fig. 4.1.1Comparing the FTIR spectra of CTS (a), PAA (b), and CTS-PAA (c)

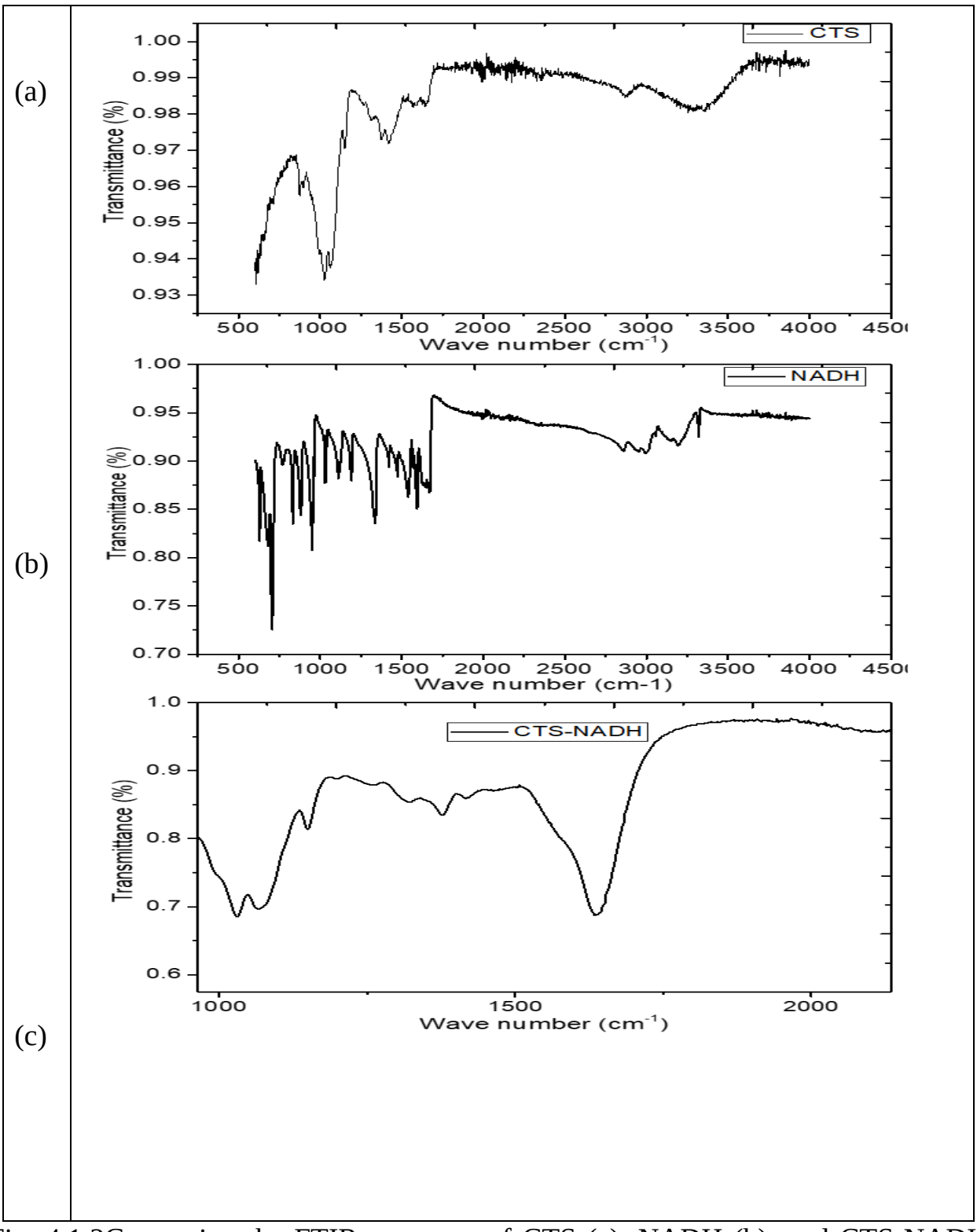

Fig. 4.1.2Comparing the FTIR spectrum of CTS (a), NADH (b), and CTS-NADH (c)

4.1.1.2 Uv-visible: the result below shows Uv-vis characterization of CTS and the modified inhibitors

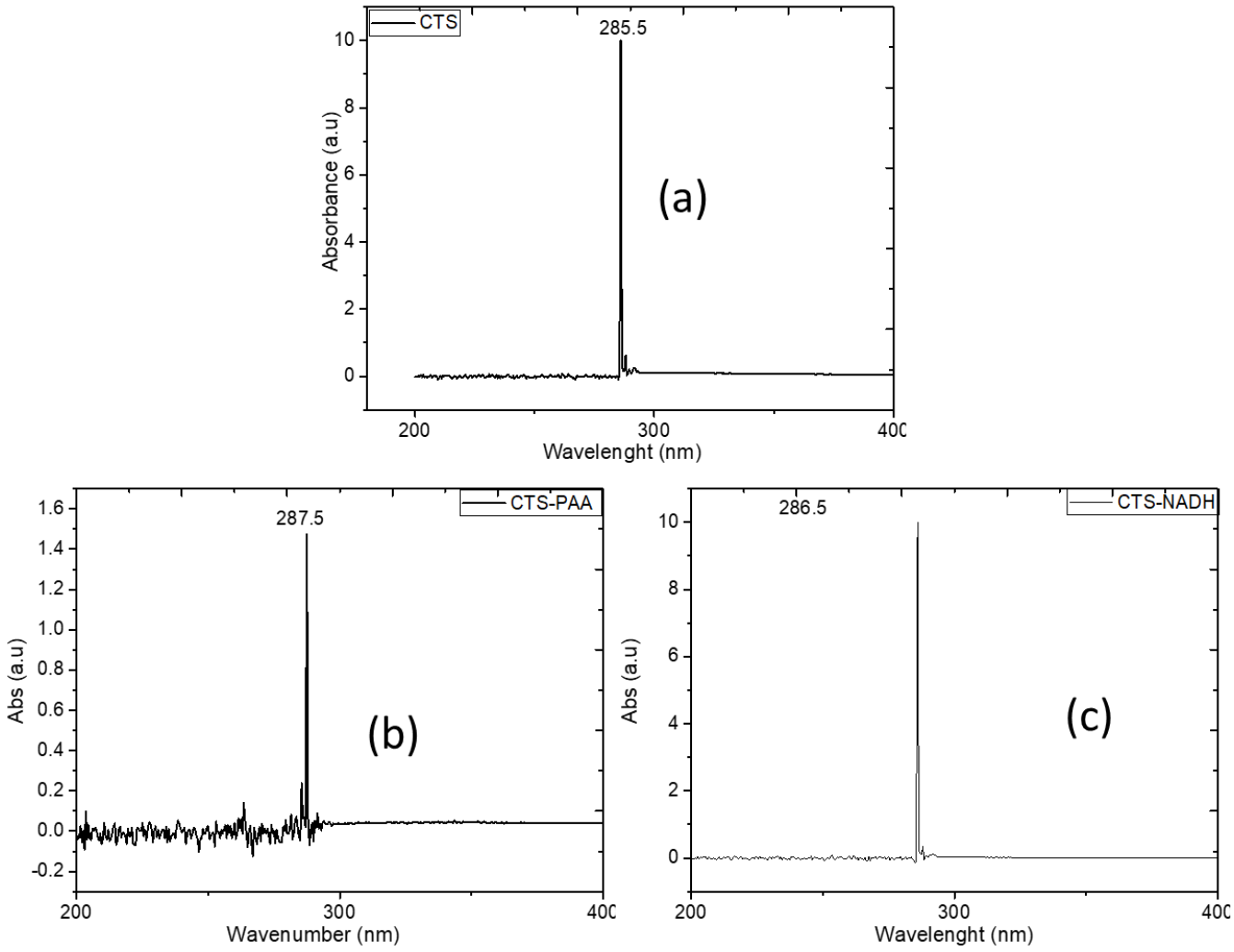

Fig. 4.1.3Uv-vis spectra comparing the spectrum of (a) CTS, with the spectra of (b) CTS-PAA and (c) CTS-NADH

4.1.2 Corrosion inhibition experiment: gravimetric method and electrochemical methods are used for anticorrosion studies

4.1.2.1 Gravimetric (weight loss) measurements: below are the results obtained from the gravimetric experiment

Table 4.1.2: Calculated weight loss, Inhibition Efficiency (%), and Degree of Surface Coverage (Ɵ) for Mild Steel in 1 M HCl in the absence and presence of Polymeric inhibitors from weight loss measurement

Conc.(mg/L)		Weight loss (d/dm^2)				Inhibition Efficiency (%I.E)				Degree of Surface Coverage			
		24 h	72 h	120 h	168 h	24 h	72 h	120 h	168 h	24 h	72 h	120 h	168 h
Blank (HCl)		0.410	1.134	1.738	2.576	—	—	—	—	—	—	—	—
CTS	50	0.108	0.321	0.608	1.064	73.7	71.71	65.0	58.70	0.74	0.72	0.65	0.59
	100	0.119	0.316	0.589	0.980	71.00	72.10	66.1	62.00	0.71	0.72	0.66	0.62
	150	0.142	0.397	0.689	1.148	65.40	65.00	60.42	55.51	0.65	0.65	0.60	0.55
	200	0.104	0.295	0.552	1.185	74.60	73.90	68.20	54.00	0.75	0.74	0.68	0.54
PAA	50	0.214	0.553	1.108	1.551	47.80	51.31	36.20	30.20	0.48	0.51	0.36	0.30
	100	0.103	0.356	0.843	1.371	74.90	68.60	51.49	46.77	0.75	0.69	0.52	0.47
	150	0.137	0.401	0.723	1.580	66.60	64.60	58.90	51.20	0.67	0.65	0.59	0.51
	200	0.099	0.504	0.683	1.185	75.70	55.61	60.81	54.00	0.76	0.56	0.61	0.54
NAHD	50	0.203	0.571	0.921	1.768	50.50	49.60	47.0	31.41	0.51	0.50	0.47	0.31
	100	0.197	0.565	0.904	1.748	51.90	50.20	48.0	32.14	0.52	0.50	0.48	0.32
	150	0.195	0.556	0.896	1.615	52.40	51.0	48.51	37.30	0.52	0.51	0.49	0.37
	200	0.185	0.530	0.820	1.562	54.90	53.31	52.80	39.40	0.55	0.53	0.53	0.39

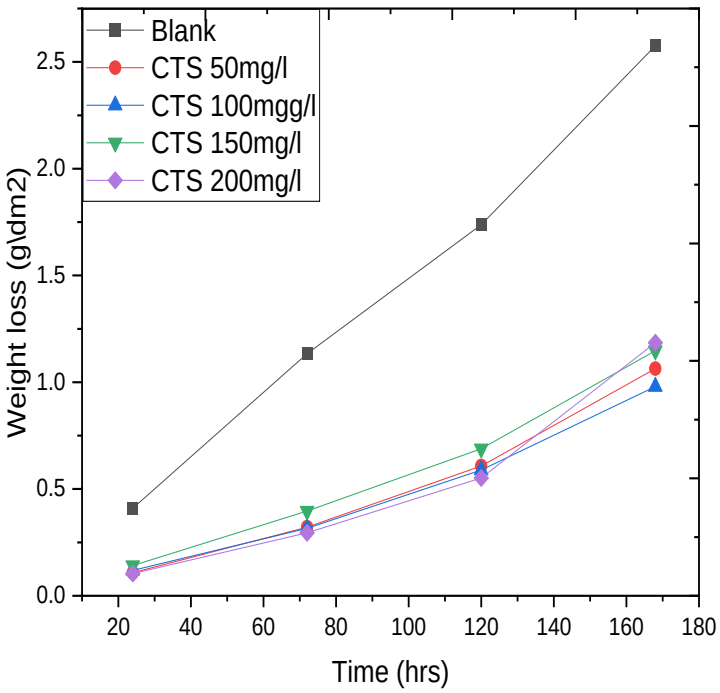

Fig 4.1.4 Plot of weight loss against time for mild steel corrosion in 1 M HCl in the presence and absence of different concentrations of CTS.

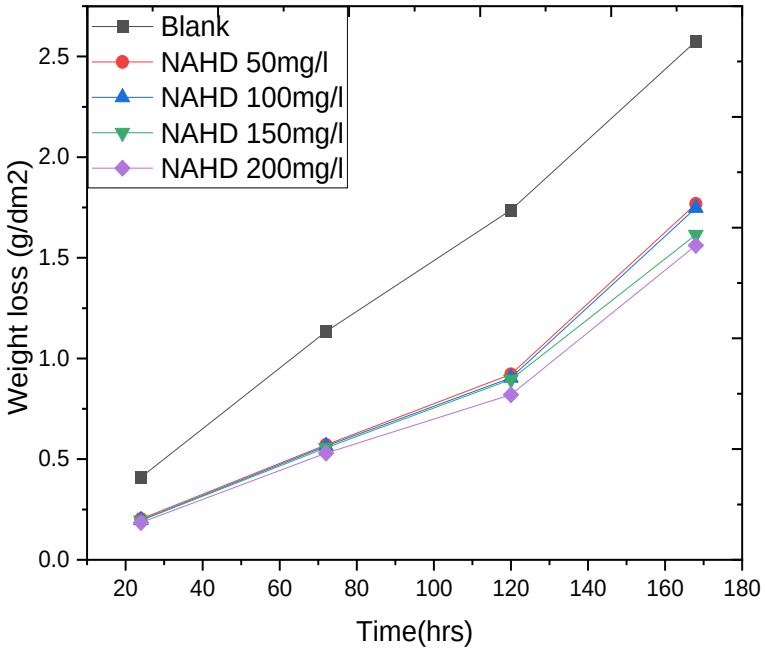

Fig 4.1.5 Plot of weight loss against time for mild steel corrosion in 1 M HCl in the absence and presence of different concentrations of NAHD

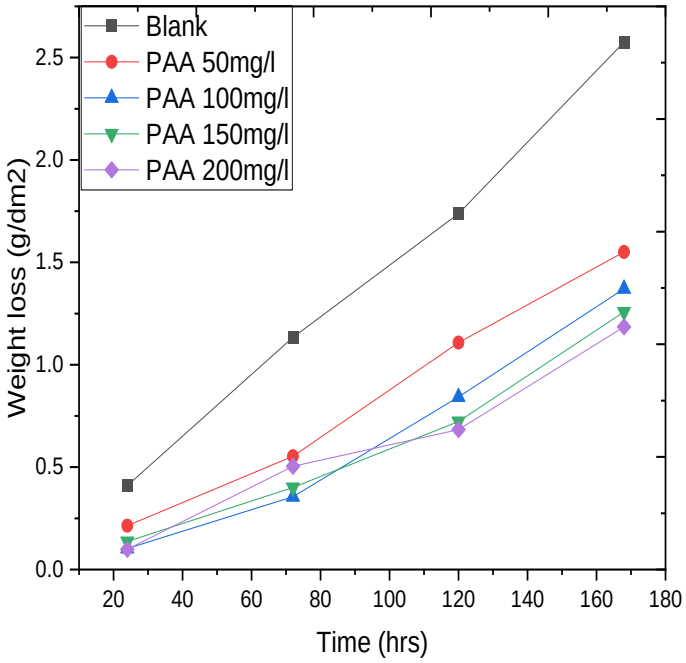

Fig 4.1.6 Plot of weight loss against time for mild steel corrosion in 1 M HCl in the absence and presence of different concentrations of PAA

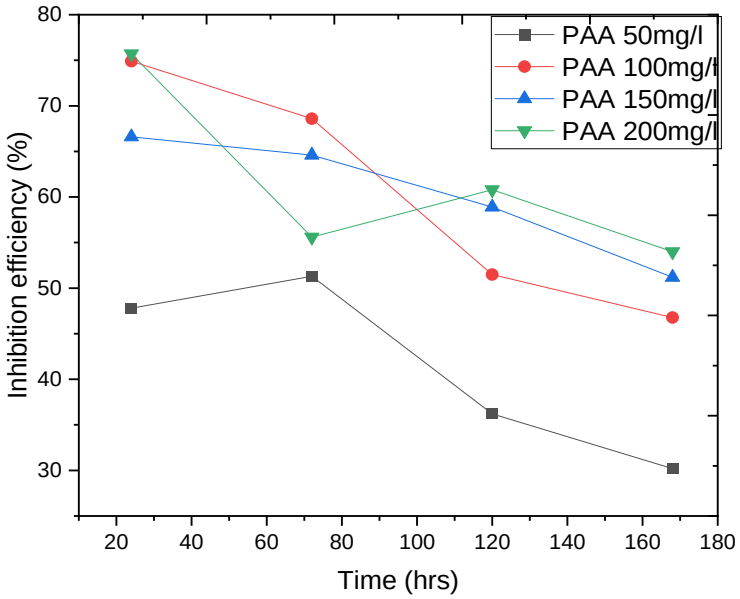

Fig 4.1.7: Plot of inhibition efficiency against inhibitor concentration for mild steel corrosion in 1 M HCl at different times for PAA

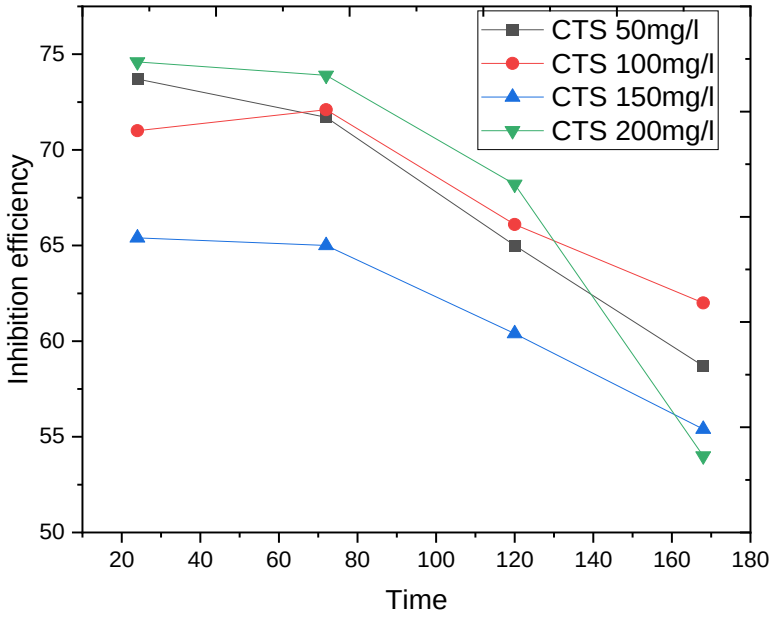

Fig 4.1.8: Plot of inhibition efficiency against time for mild steel corrosion in 1 M HCl at different times for CTS

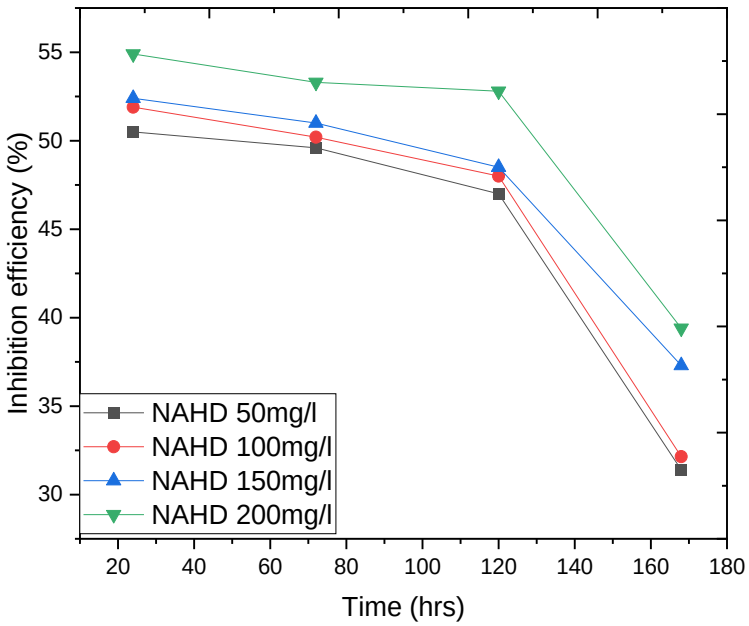

Fig 4.1.9: Plot of inhibition efficiency against inhibitor concentration for mild steel corrosion in 1 M HCl at different times for NAHD

Table 4.1.3: Calculated Weight loss, Inhibition Efficiency (%), and Degree of Surface Coverage (Ɵ) for Mild Steel in 1 M HCl in the absence and presence of the modified polymeric inhibitors from weight loss measurement.

Conc.(mg/L)		Weight loss (d/dm^2)				Inhibition Efficiency (%I.E)				Degree of Surface Coverage			
		24 h	72 h	120 h	168 h	24 h	72 h	120 h	168 h	24 h	72 h	120 h	168 h
Blank (HCl)		0.410	1.134	1.738	2.576	—	—	—	—	—	—	—	—
CTS – NAHD	50	0.098	0.179	0.277	0.422	76.11	84.20	84.10	83.60	0.76	0.84	0.84	0.84
	100	0.108	0.184	0.306	0.389	73.70	83.80	82.40	84.90	0.74	0.84	0.82	0.85
	150	0.069	0.157	0.285	0.372	83.20	86.20	83.60	85.61	0.83	0.86	0.84	0.86
	200	0.072	0.161	0.261	0.345	82.40	85.00	85.00	86.60	0.82	0.85	0.85	0.87
CTS – PAA	50	0.038	0.159	0.392	0.802	90.71	85.98	77.45	68.87	0.91	0.86	0.78	0.69
	100	0.033	0.071	0.102	0.153	91.95	93.74	94.13	94.10	0.92	0.94	0.94	0.94
	150	0.031	0.063	0.093	0.146	92.49	94.40	94.65	94.35	0.93	0.94	0.95	0.94
	200	0.021	0.039	0.070	0.109	94.86	96.56	95.97	95.76	0.95	0.97	0.96	0.96

Fig 4.1.10 Plot of weight loss against time for mild steel corrosion in 1 M HCl in the presence of different concentrations of CTS-NAHD

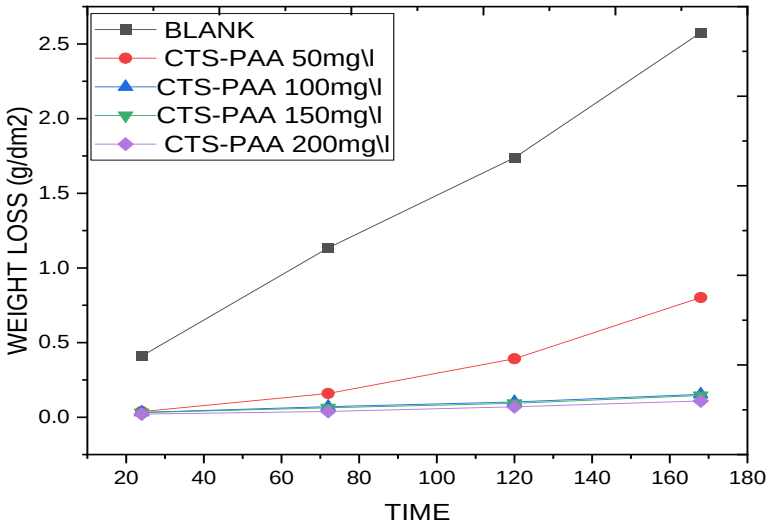

Fig 4.1.11Plot of weight loss against time for mild steel corrosion in 1 M HCl in the presence of different concentrations of CTS-PAA

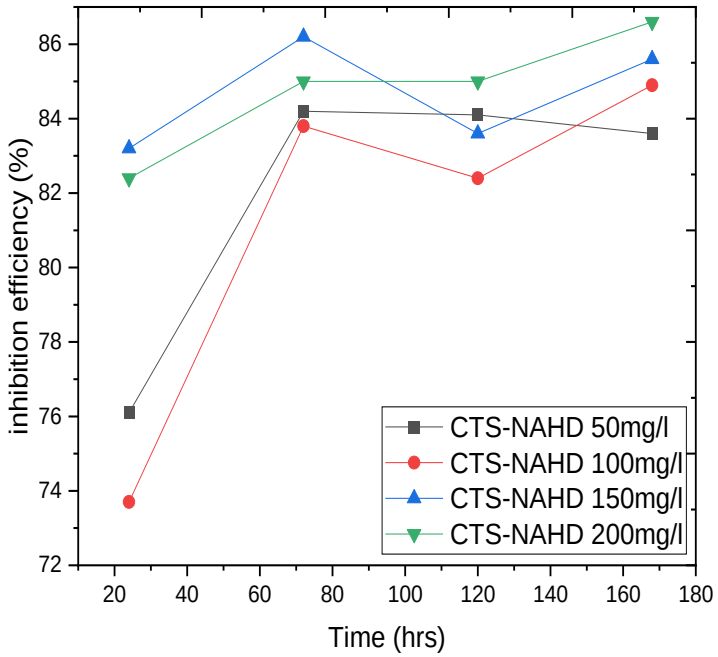

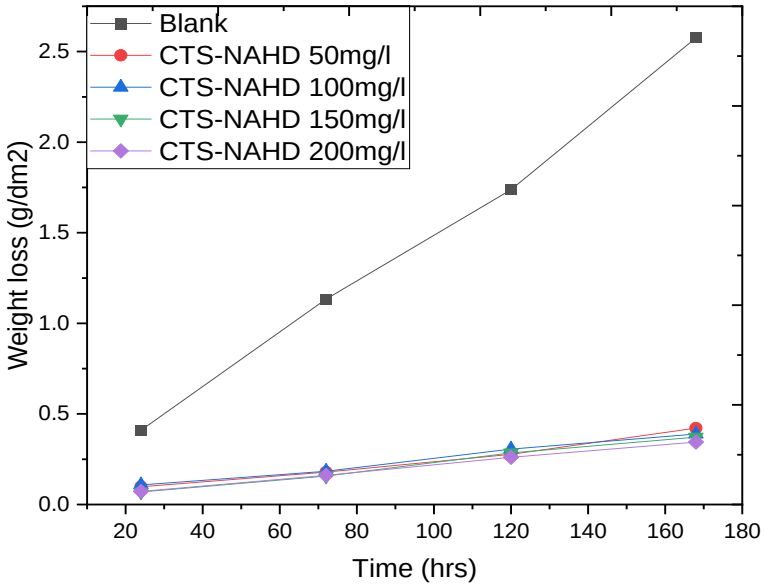

Fig 4.1.12 Plot of inhibition efficiency against time for mild steel corrosion in 1MHCl in the presence of different concentrations of CTS-NAHD

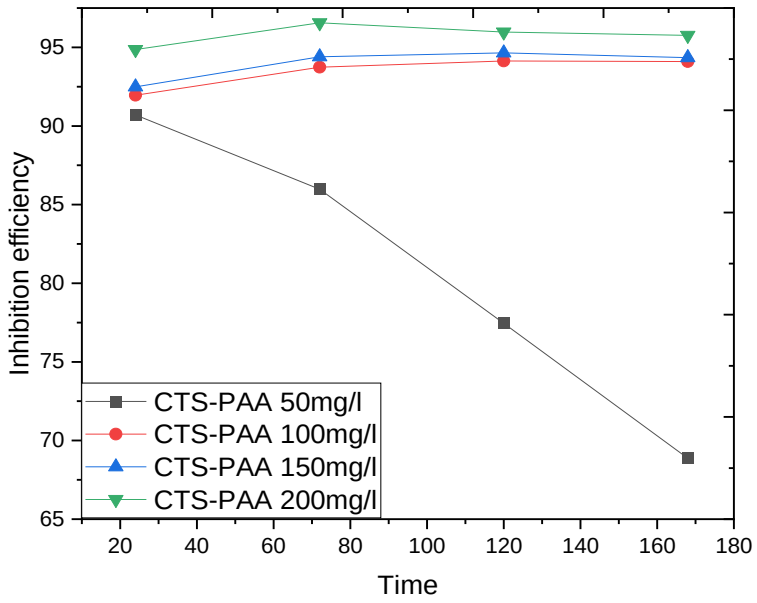

Fig 4.1.13: Plot of inhibition efficiency against time for mild steel corrosion in 1MHCl in the presence of different concentrations of CTS-PAA

4.1.2.2 Electrochemical results:below are the results ofcombined electrochemical methods used in this research work.

4.1.2.2.1 Potentiodynamic polarization (PDP)

Table 4.1.4Polarization fitting data comparing the electrochemical results of mild steel in 1 M HCl without and with different concentrations of CTS, NADH, and the modified CTS (CTS-NADH)

System	E_{coor}(V vs SCE)	I_{coor}(μA/cm^2)	IE%
Blank	-0.4937	342	-
CTS 100 mg/L	-0.5154	144	58
CTS 250 mg/L	-0.5179	109	68
NADH 50 mg/L	-0.5102	157	54
NADH 250 mg/L	-0.5112	114	67
CTS-NADH 50 mg/L	-0.5235	120	65
CTS-NADH 250 mg/ L	-0.5235	57	83

Table 4.1.5Polarization fitting data comparing the electrochemical results of mild steel in 1 M HCl without and with different concentrations of CTS, PAA, and the modified CTS (CTS-PAA).

System	E_{coor}(V vs SCE)	I_{coor} (μA/cm^2)	IE%
Blank	-0.4937	342	-
CTS 100 mg/L	-0.5154	144	58
CTS 250 mg/L	-0.5179	109	68
PAA 50 mg/L	-0.5221	100	71
PAA 250 mg/L	-0.5314	91	73
CTS-PAA 50 mg/L	-0.5356	106	69
CTS-PAA 250 mg/L	-0.5440	55	84

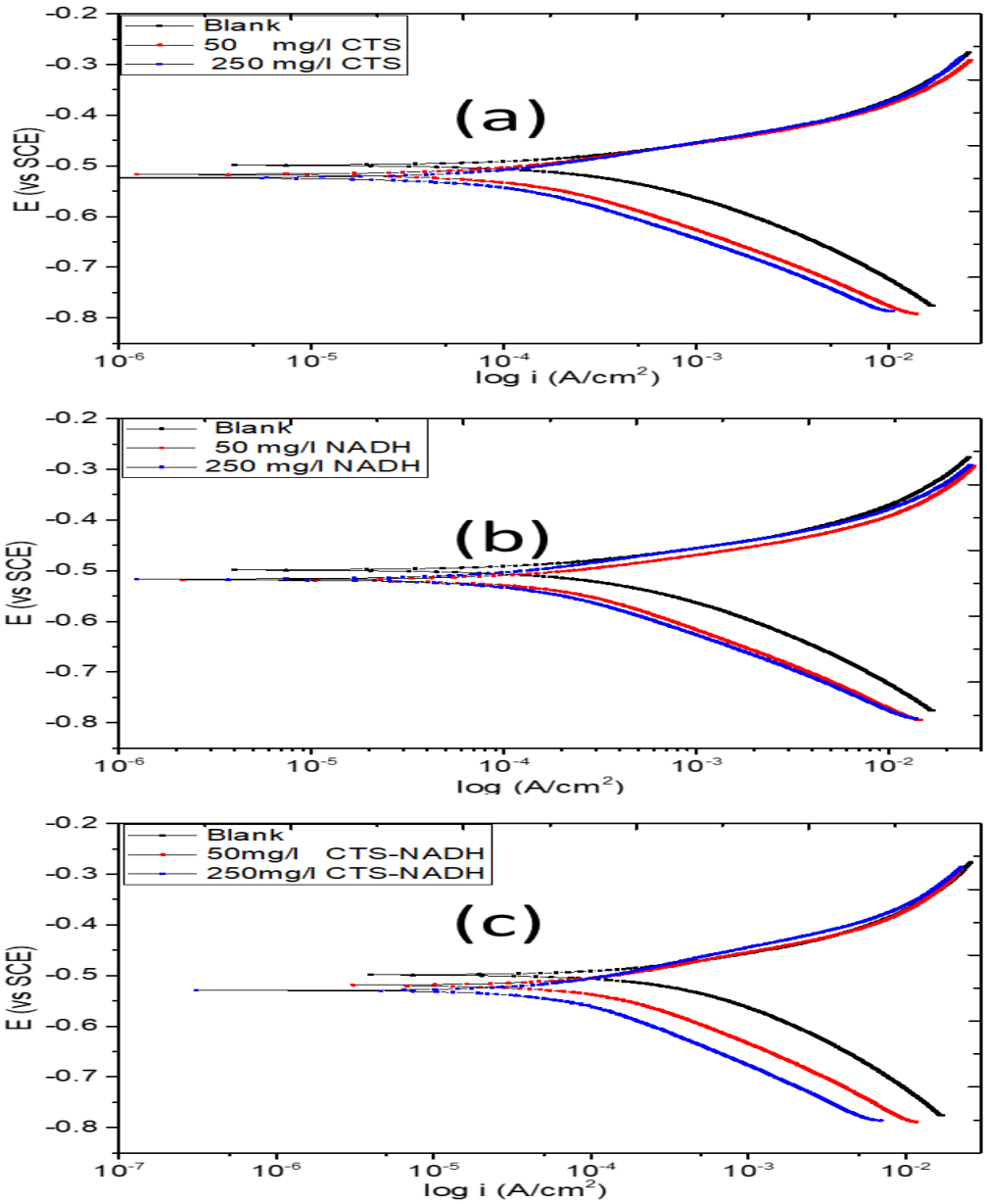

Fig. 4.1.14Polarization curves comparing the electrochemical results of mild steel in 1 M HCl without and with different concentrations of CTS (a), NADH (b), and modified CTS (CTS-NADH) (c).

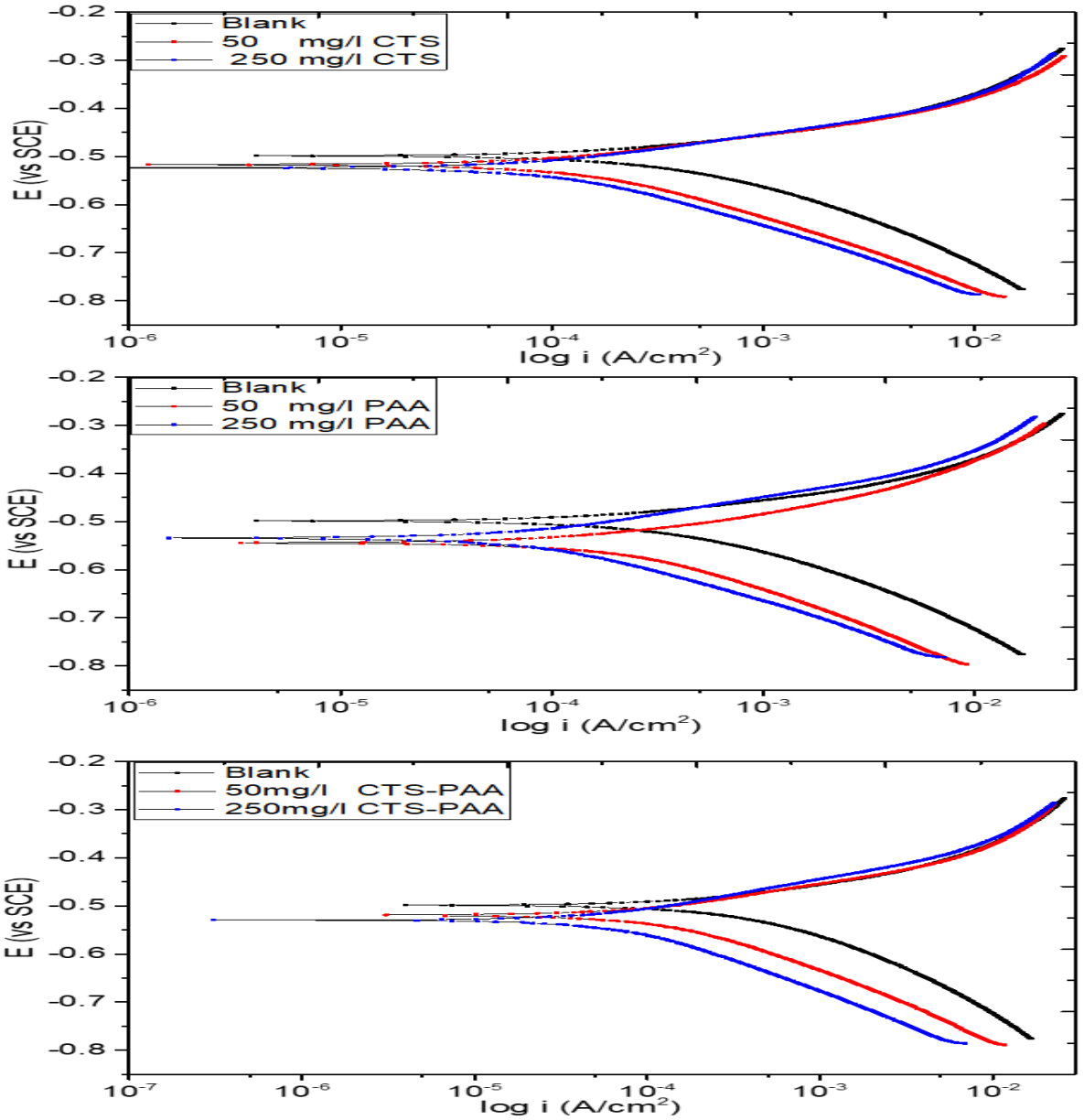

Fig. 4.1.15 Polarization curves comparing the electrochemical results of mild steel in 1 M HCl without and with different concentrations of CTS (a), PAA (b) and the modified CTS (CTS-PAA) (c).

4.1.2.2.2 Electrochemical Impedance Spectroscopy (EIS): the result below shows the EIS results of the inhibitors

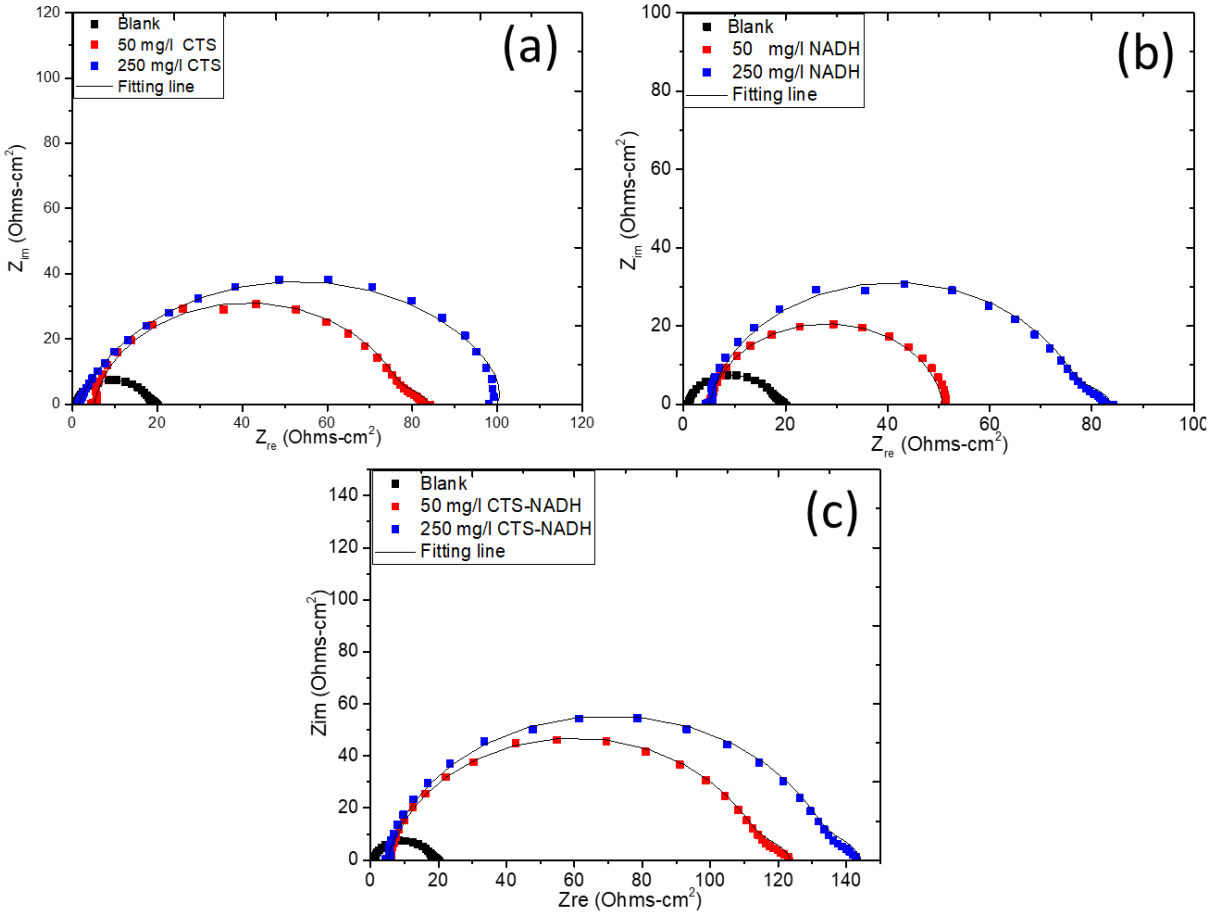

Fig. 4.1.16 Nyquist impedance plots comparing the electrochemical results of mild steel in 1 M HCl without and with different concentrations of CTS (a), NADH (b) and the modified CTS (CTS-NADH) (c).

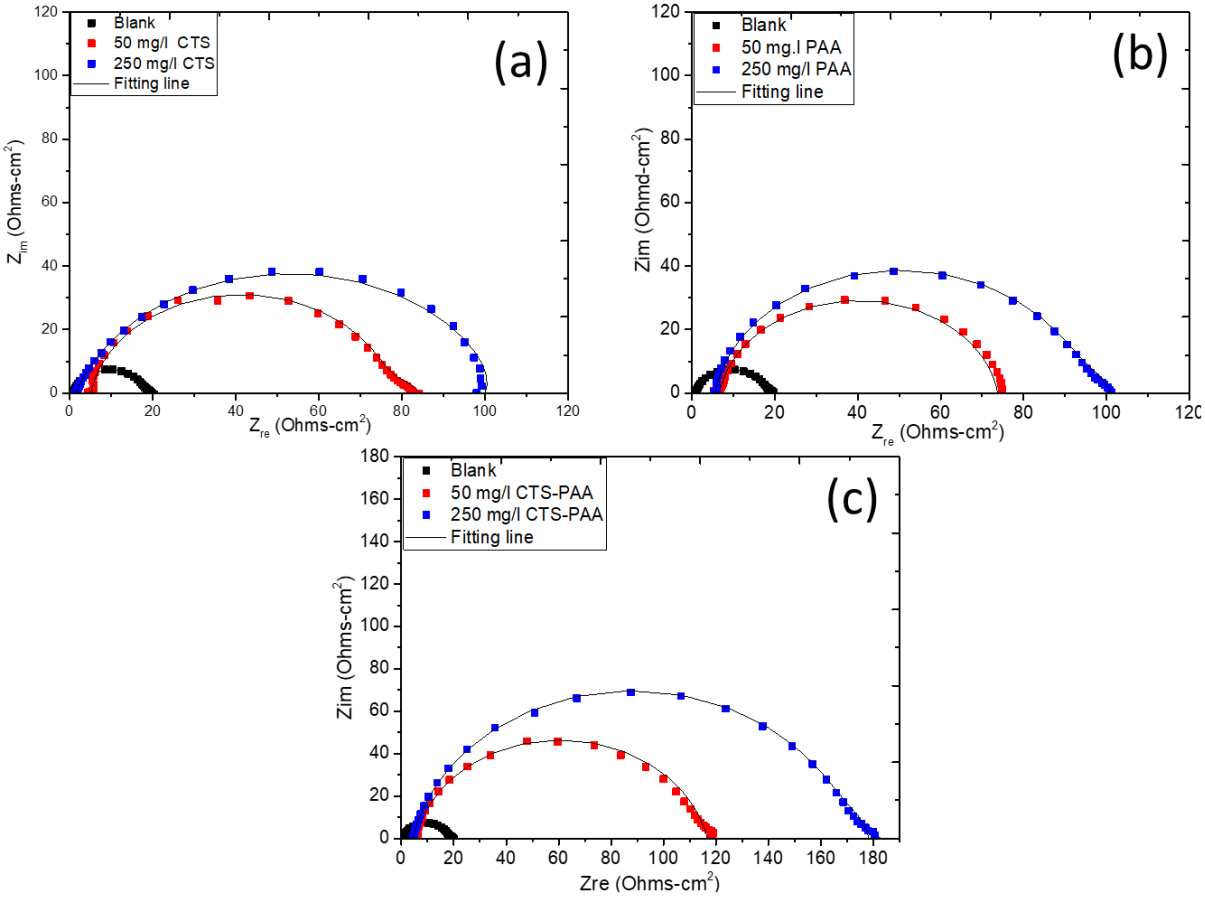

Figure 4.1.17 Nyquist impedance plots comparing the electrochemical results of mild steel in 1 M HCl without and with different concentrations of CTS (a), PAA (b), and the modified CTS (CTS-PAA) (c).

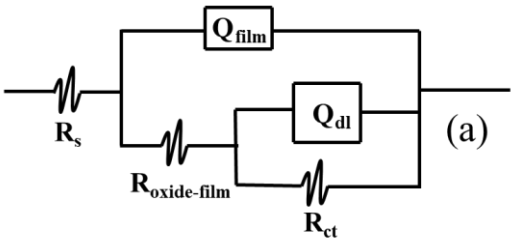

Fig. 4.1.18 Equivalent circuit model describing the impedance behavior of mild steel in 1 M HCl without and with different concentrations of inhibitors

Table 4.1.6 Electrochemical parameters comparing the impedance data for steel in 1 M HCl, NADH, CTS, and the modified CTS (CTS-NADH).

System	**Rs (Ohms-cm2)**	**CPE1 Y_0 ($\pi F cm^{-2} s^{n-1}$)**	**n**	**Rct1 (Ohms-cm2)**	**CPE1 Y_0 ($\pi F cm^{-2} s^{n-1}$)**	**n2**	**Rct2 (Ohms-cm2)**	**Rc_T (Ohms-cm2)**	**IE %**	**X^2 x 10^{-3}**
Blank	1.045	526	0.8982	17.4	216800	0.9348	1.6	19	-	
50 mg/L CTS	5.1	122	0.942	72.0	62230	0.7968	6.0	78	75.6	
250 mg/LCTS	1.4	60	0.8127	96.2	9924	1.000	1.6	98	81	1.1
50 mg/L NADH	5.1	80	0.959	7.0	58	0.8926	39	46	55	0.7
250 mg/L NADH	5.1	122	0.9042	70.0	622	0.7968	6.0	76	75	4.1
50 mg/L CTS-NADH	5.685	96.7	0.9071	108.5	37900	0.8288	9.5	118	83.9	1.2
250 mg/L CTS-NADH	5.026	88.4	0.8984	130.3	4026	0.9253	8.5	139	86.3	3.6

Table 4.1.7 Electrochemical parameters comparing the impedance data for steel in 1 M HCl, CTS, PAA, and the modified CTS (CTS-PAA).

System	Rs (Ohms-cm2)	CPE1 Y_0 ($\pi F cm^{-2} s^{n-1}$)	n	Rct1 (Ohms-cm2)	CPE1 Y_0 ($\pi F cm^{-2} s^{n}$)	n2	Rct2 (Ohms-	Rct_T (Ohms-	IE	X^2 (x 10^{-3})

							cm2)	cm2)		
Blank	1.045	526	0.8982	17.4	216800	0.9348	1.4	19	−	
50 mg/l CTS	5.1	122	0.942	72	62230	0.7968	6.0	78	75.6	
250 mg/l CTS	1.4	60	0.8127	96.2	9924	1	1.6	98	81	1.1
50 mg/l PAA	5.5	12.5	0.9059	1.7	72.9	0.9133	66.5	68	72	1.3
250 mg/l PAA	5.6	10.7	0.9109	89	2829	0.8531	6.5	96	80	1.5
50 mg/l CTS-PAA	5.619	22.7	1	1.9	88.6	0.8139	109.1	111	83	1.7
250 mg/l CTS-PAA	4.462	88	0.8833	168	2881	1	6.0	174	89	0.4

4.1.3. Adsorption consideration:the plots and tables below show the adsorption consideration results of this work.

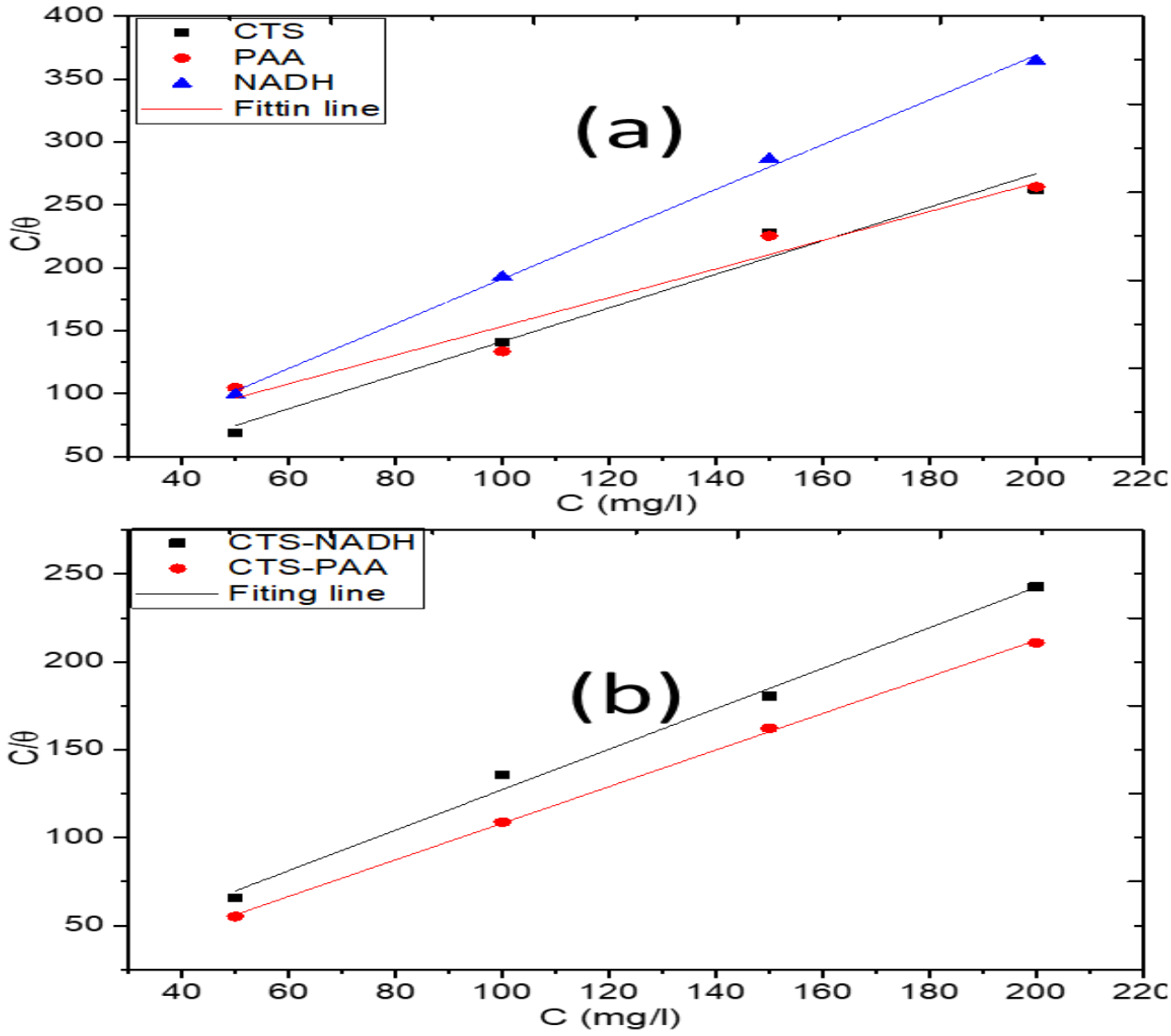

Fig. 4.1.19 Adsorption isotherm plots for the adsorption of CTS, NADH, PAA (a) and the adsorption of CTS-NADH and CTS -PAA (b)

Table 4.1. 8: Linear regression for the adsorption of CTS, PAA, NADH, and the derivatives CTS-NADH and CTS-NADH on mild steel in 1 M HCl

System	Slope	Intercept	K (g/l)	r^2
CTS	1.3352	7.8	128	0.9628
PAA	1.141	39.25	25.5	0.9794
NADH	1.779	13.2	75.6	0.9972
CTS-NADH	1.1512	12.2	82.0	0.9903
CTS-PAA	1.041	4.1	244	0.9992

Table 4.1.9: Corrosion Rate, C_R (mm/yr) and inhibition efficiency (%) for mild steel in 1M HCl in the absence and presence of the different corrosion inhibitors at varying temperatures from weight loss measurement:

Conc. mg/L		**Corrosion rate (mm/yr)**			**Inhibition efficiency (%)**		
		40°C	50°C	60°C	40°C	50°C	60°C
Blank		0.056	0.113	0.145	—	—	—
CTS	50	0.020	0.0461	0.069	64.30	59.30	52.40
	100	0.0191	0.0431	0.0638	66.10	61.90	56.00
	150	0.0183	0.0385	0.0556	67.90	65.50	61.70
	200	0.0174	0.0360	0.0471	69.64	68.10	67.60
PAA	50	0.0310	0.065	0.0851	44.60	42.50	41.40
	100	0.0304	0.0643	0.0836	43.90	43.10	42.30
	150	0.0302	0.0639	0.0830	46.10	43.50	42.80
	200	0.0300	0.0621	0.0811	46.40	45.10	44.10
NAHD	50	0.0271	0.056	0.0751	51.80	50.40	48.30
	100	0.0263	0.0538	0.0722	53.04	52.30	50.20
	150	0.0251	0.0522	0.0689	55.20	53.80	52.50
	200	0.0230	0.051	0.0671	58.90	54.90	53.80
CTS-NAHD	50	0.0171	0.0361	0.061	69.60	68.10	57.90
	100	0.0178	0.0337	0.0531	68.20	70.20	63.40
	150	0.0163	0.0332	0.0500	70.90	70.80	65.50
	200	0.0151	0.0320	0.049	73.20	71.70	66.20
CTS-PAA	50	0.0280	0.0582	0.0782	50.00	48.70	46.20
	100	0.0278	0.0561	0.0776	50.40	50.40	46.50
	150	0.0266	0.0533	0.0732	52.50	52.80	49.50
	200	0.0251	0.0510	0.069	55.40	54.90	52.40

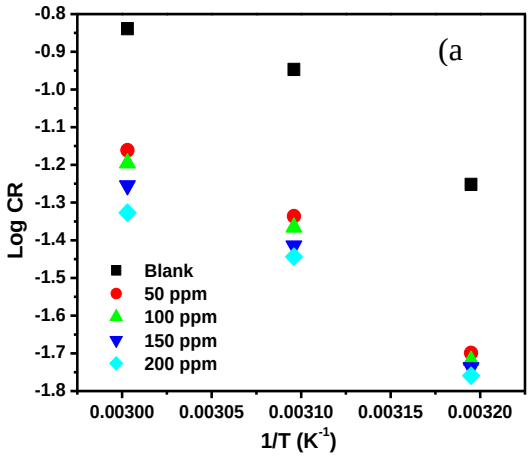
(a
Log CR
1/T (K-1)
Blank
50 ppm
100 ppm
150 ppm
200 ppm

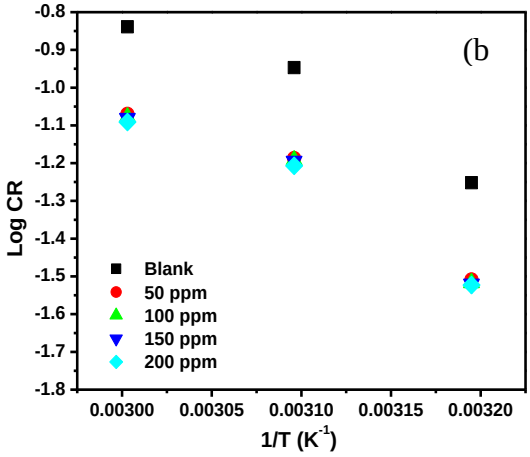
(b
Log CR
1/T (K-1)
Blank
50 ppm
100 ppm
150 ppm
200 ppm

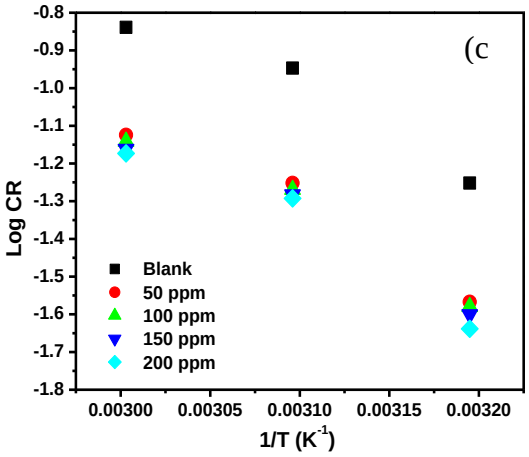
(c
Log CR
1/T (K-1)
Blank
50 ppm
100 ppm
150 ppm
200 ppm

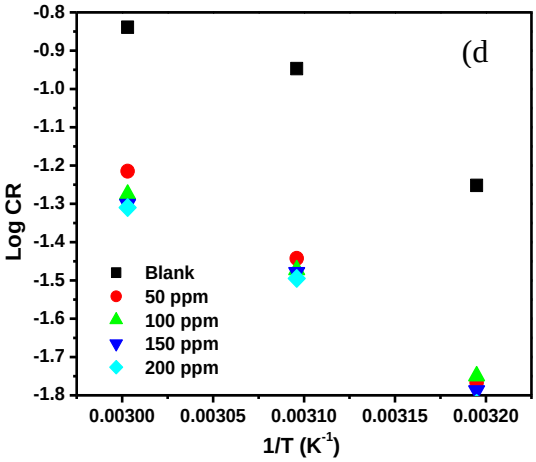
(d
Log CR
1/T (K-1)
Blank
50 ppm
100 ppm
150 ppm
200 ppm

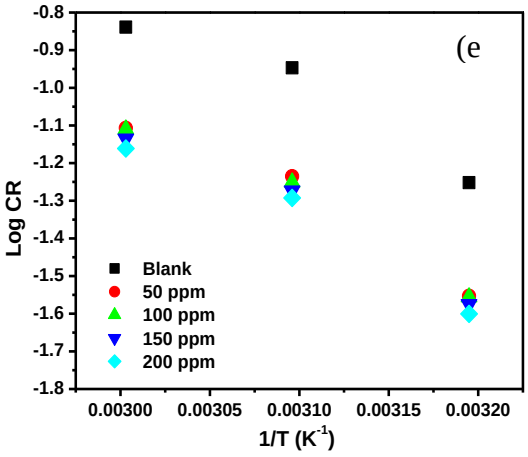
(e
Log CR
1/T (K-1)
Blank
50 ppm
100 ppm
150 ppm
200 ppm

Fig. 4.1.20 Arrhenius plot for carbon steel in 1 M HCl solution in the presence of (a) CTS (b) PAA (c) NAHD (d) CTS-NAHD and (e) CTS-PAA (from different concentrations and temperatures).

Table: 4.1.10 Thermodynamic parameters of the dissolution of carbon steel in 1 M HCl in the absence and presence of different concentrations for CTS, PAA, NAHD, CTS-NAHD, and CTS-PAA at different temperatures.

Inhibitor System		**Intercept**	**Slope**	**E_a (kJ/mol)**	**ΔH (kJ/mol) ΔS**
Blank		5.68889	-2163.15161	41.42	38.73
CTS	50	7.31267	-2812.00716	53.84	51.16
	100	7.05771	-2738.66674	52,44	49.75
	150	6.34761	-2523.1535	48.31	45.63
	200	5.50307	-2263.78811	43.35	40.66
PAA	50	5.85716	-2295.84382	43.96	41.27
	100	5.86366	-2300.19438	44.04	41.36
	150	5.85664	-2298.86268	44.02	41.33
	200	5.73046	-2260.8619	43.29	40.60
NAHD	50	5.86145	-2316.31684	44.35	41.67
	100	5.77882	-2294.76054	43.94	41.25
	150	5.76273	-2295.34623	43.95	41.26
	200	6.17464	-2434.71318	46.62	43.93
CTS-NAHD	50	7.45588	-2882.74143	55.20	52.51
	100	6.17543	-2477.24228	47.43	44.76
	150	6.35579	-2543.084	48.69	46.01
	200	6.73254	-2670.93237	51.14	48.45
CTS-PAA	50	5.93242	-2334.00808	44.69	42.00
	100	5.91696	-2331.43145	44.64	41.95
	150	5.79485	-2299.19825	44.02	41.34
	200	5.76627	-2297.50772	43.99	41.31

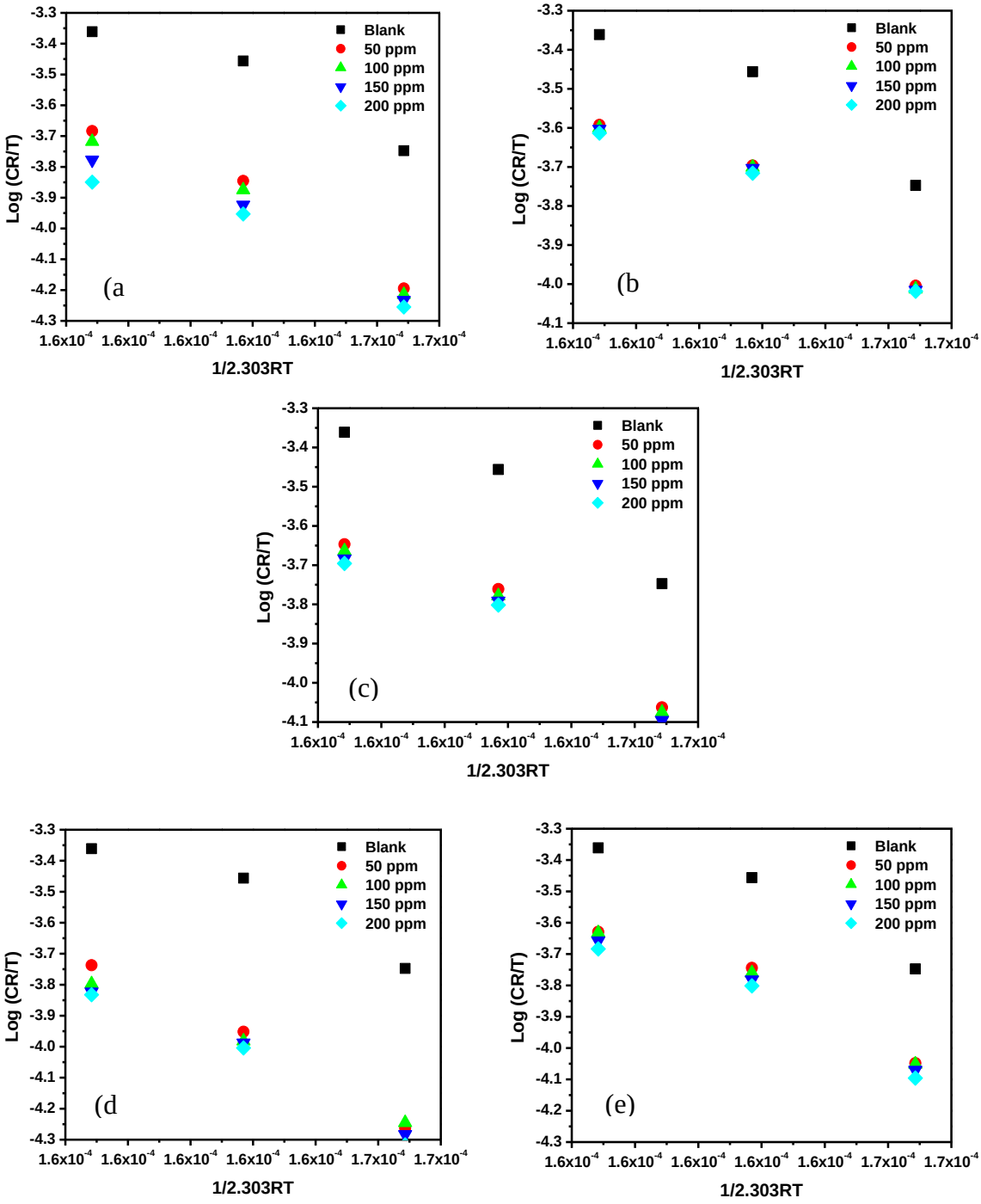

Fig. 4.1.21 Enthalpy plots for carbon steel in 1 M HCl solution in the presence of (a) CTS (b) PAA (c) NAHD (d) CTS-NAHD and (e) CTS-PAA

4.1.4Surface analysis: XPS and SEM wereadoptedto calculate the effect of corrosion on the surface of mild steel.

4.1.4.1 XPS Analysis: below is the XPS result obtained in this research work.

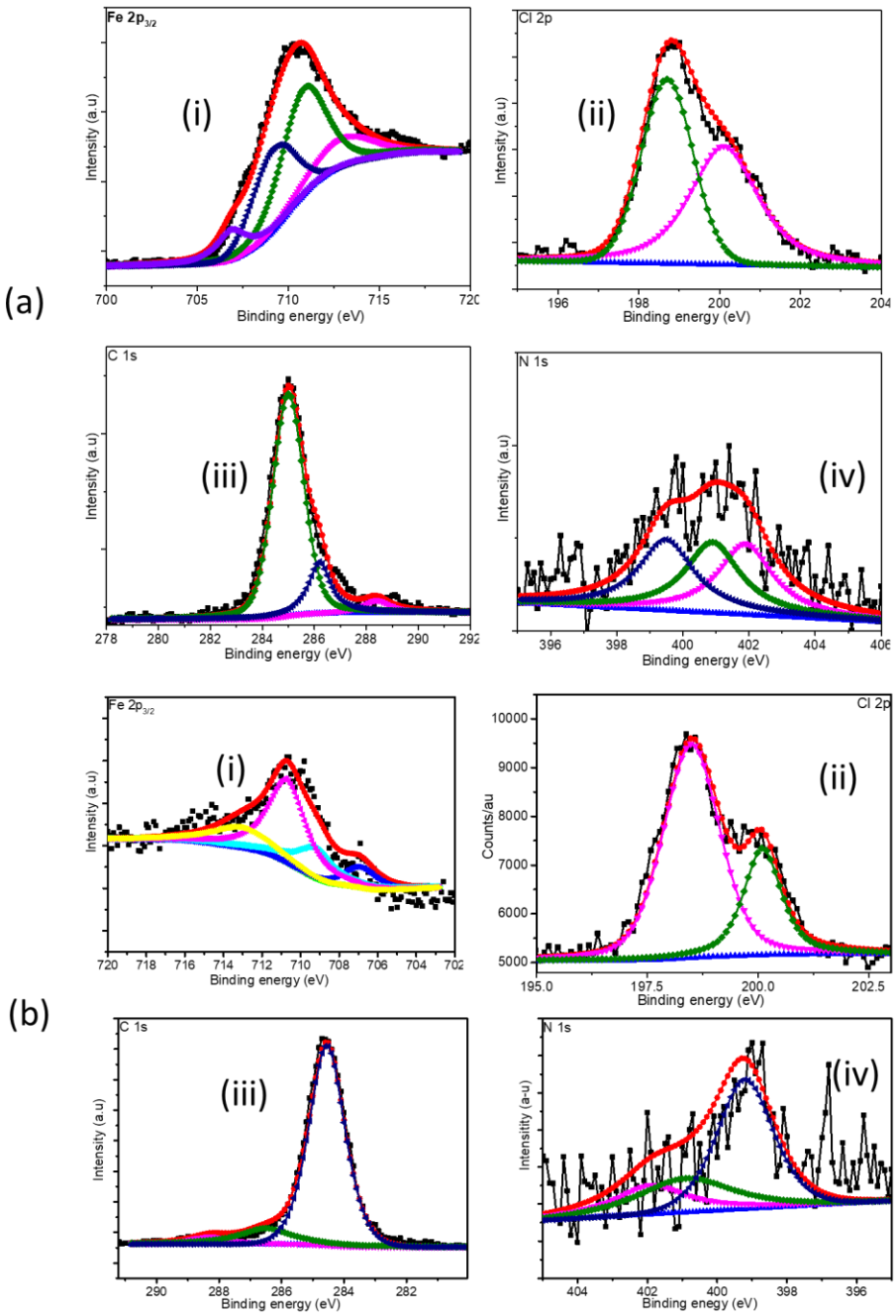

Fig. 4.1.22 XPS deconvoluted profiles for (a) CTS-NADH and (b) CTS-PAA: (i) Fe 2p3/2, (ii) Cl 2p, (iii) C 1s and (iv) N 1s for the exposure of 250 mg/l of the modified natural polymers for mild steel exposed in 1 M HCl after 3h.

4.1.4.2 Scanning electron microscope: the SEM result is shown below

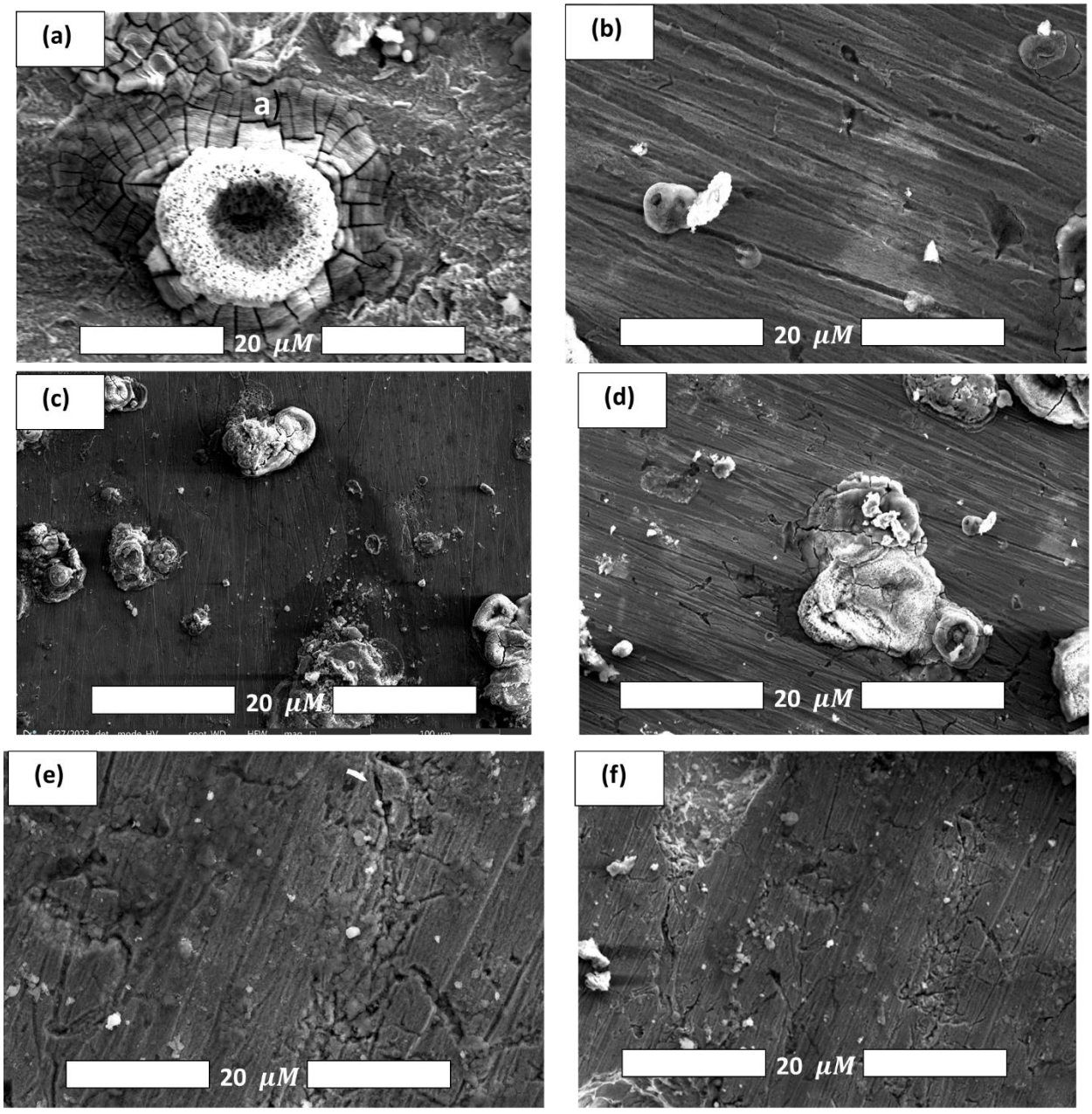

Fig. 4.1.23 SEM images for mild steel in 1 M HCl with (a) blank (b) CTS, (c) NADH, (d) PAA, (e) CTS-NADH and (f) CTS-PAA

4.1.5 Inhibition Mechanism: the proposed inhibition mechanism is stated below

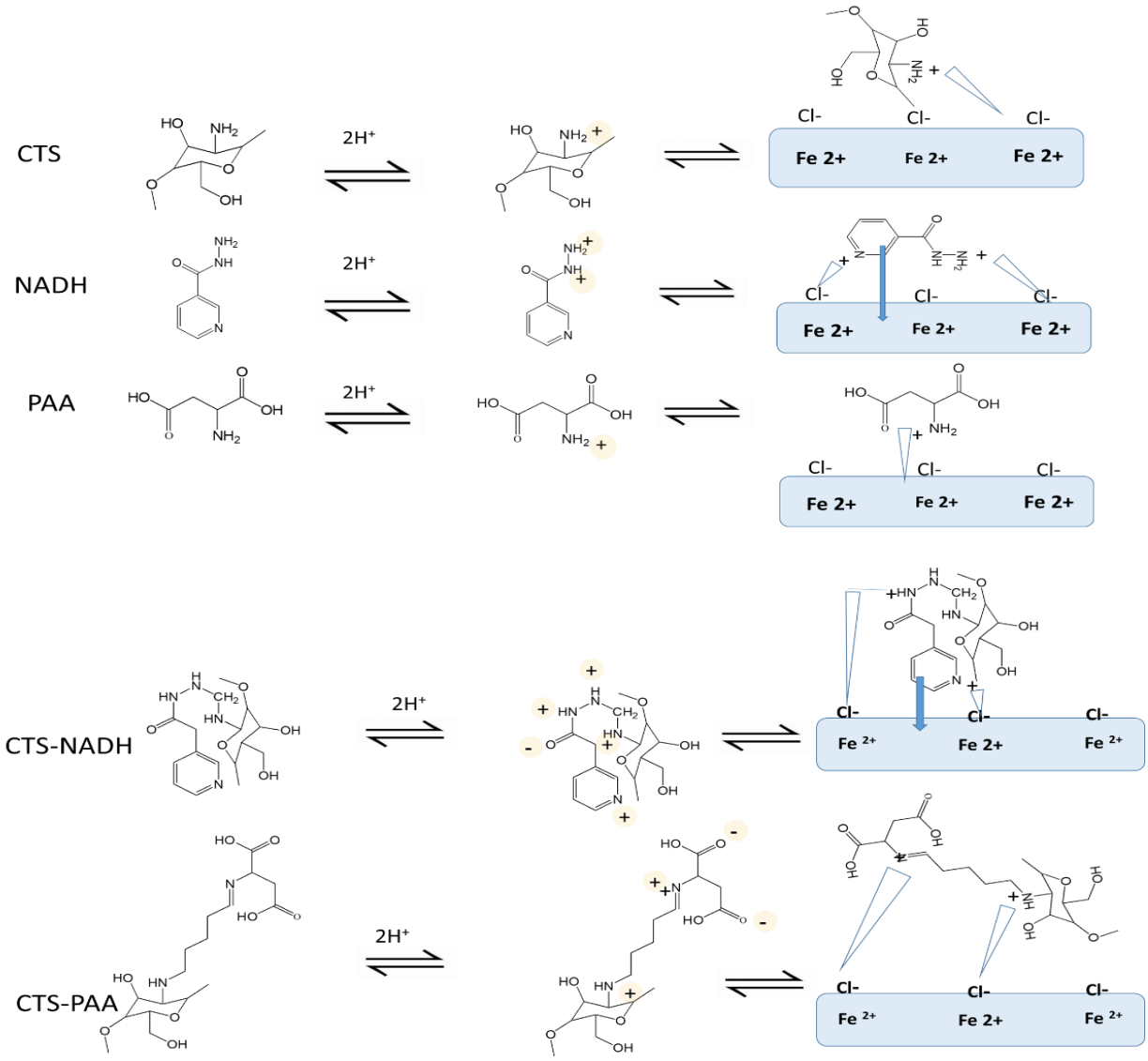

Fig. 4.1.24 Schemes illustrate the protonation leading to the multiplication of the adsorption sites of the modified chitosan polymer with PAA and NADH.

4.1.6Theoretical modeling: DFT and MDS are employed to calculate the electron properties and binding energies of the inhibitor.

4.**1.6.1 Density functional theory (DFT):** Below is the DFT result.

Table 4.1.11 Comparing the Frontier orbital parameters of CTS, NADH, and CTS-NADH

Inhibitor	**E_{HOMO} (eV)**	**E_{LUMO} (eV)**	**ΔE (eV)**	**B.E (KJ/mole)**	**Interaction Energy(KJ/mole)**
CTS	-4.9789	-0.6172	4.3617	-127.252	127.252
NADH	-5.1906	-3.0933	2.0973	-108.973	108.973
CTS-NADH	-5.0772	-2.3774	2.6998	-190.538	190.538

Table 4.1.12 Comparing the frontier orbital parameters of CTS, PAA, and CTS—PAA

Inhibitor	E_{HOMO} (eV)	E_{LUMO}(eV)	ΔE (eV)	N	BE (KJ/mole)	Interaction Energy (KJ/mole)
CTS	-4.9789	-0.6172	4.3617	0.4620	-127.252	127.252
PAA	-4.2215	-2.9061	1.3154	0.9503	-88.744	88.744
CTS-PAA	-4.5593	-3.7029	0.8564	0.8044	-203.697	203.697

CTS	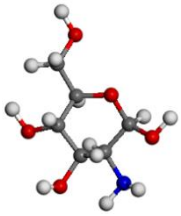	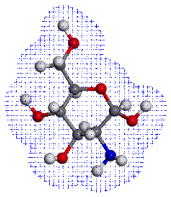	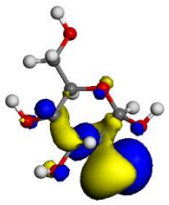
	Optimized structure	**Total Electron density**	**HOMO structure**
	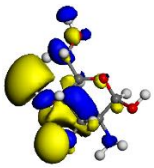	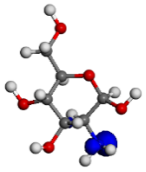	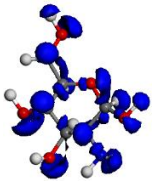
	LUMO structure	**Electrophilic attack**	**Nucleophilic attack**
NADH	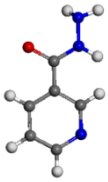	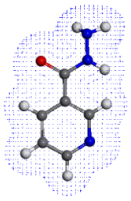	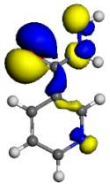
	Optimized structure	**Total Electron density**	**HOMO structure**
	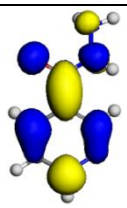	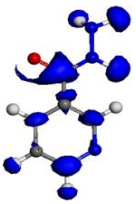	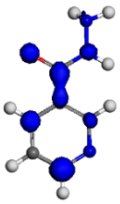
	LUMO structure	**Electrophilic attack**	**Nucleophilic attack**
CTS-NADH	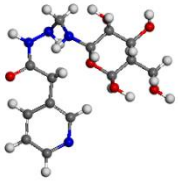	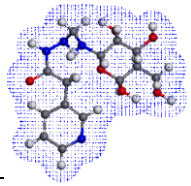	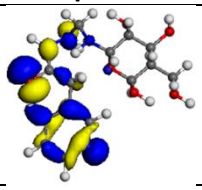
	Optimized structure	**Total Electron density**	**HOMO structure**
	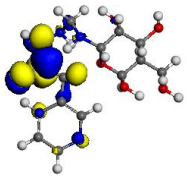	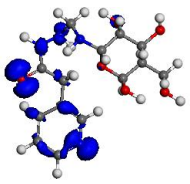	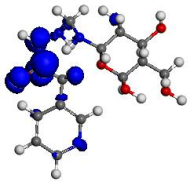

Fig. 4.1. 25 comparing the structural frontal electronic descriptors of (i) CTS, (ii) NADH, and (iii) CTS-NADH: Atom legend [carbon grey; hydrogen-white; oxygenred]. The blue and yellow isosurfaces depict the electron density difference; blue regions show electron accumulation and yellow regions show electron loss.

CTS	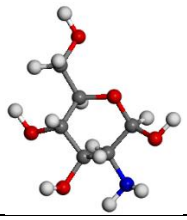	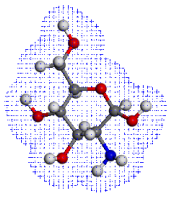	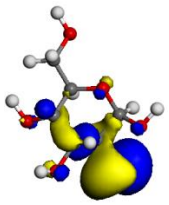
	Optimized structure	**Total Electron density**	**HOMO structure**
	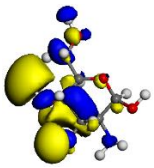	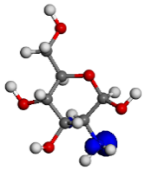	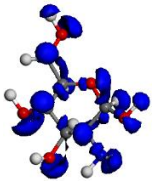
	LUMO structure	**Electrophilic attack**	**Nucleophilic attack**
PAA	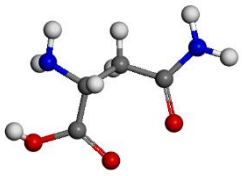	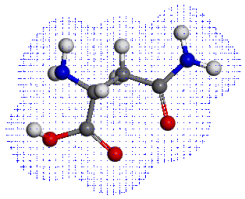	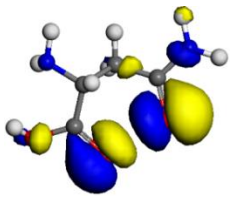
	Optimized structure	**Total Electron density**	**HOMO structure**
	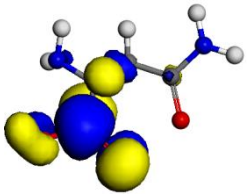	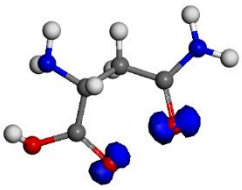	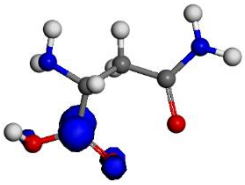
	LUMO structure	**Electrophilic attack**	**Nucleophilic attack**
CTS-PAA	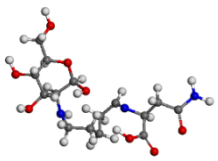	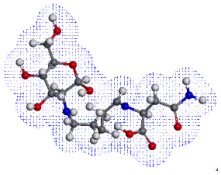	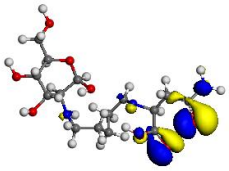
	Optimized structure	**Total Electron density**	**HOMO structure**
	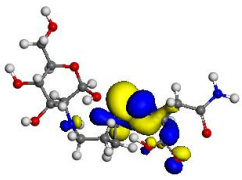	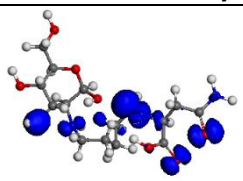	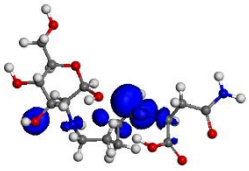
	LUMO structure	**Electrophilic attack**	**Nucleophilic attack**

Figure 4.1.26 compares the structural frontal electronic descriptors of (i) CTS, (ii) PAA, and (iii) CTS-PAA: Atom legend [carbon grey; hydrogen-white; oxygen-red]. The blue and yellow isosurfaces depict the electron density difference; blue regions show electron accumulation and yellow regions show electron loss

4.1.6.2 Molecular dynamic simulation (MDS): the result below shows the MDS results obtained.

CTS	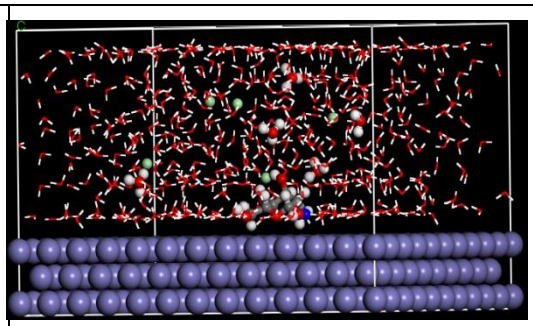	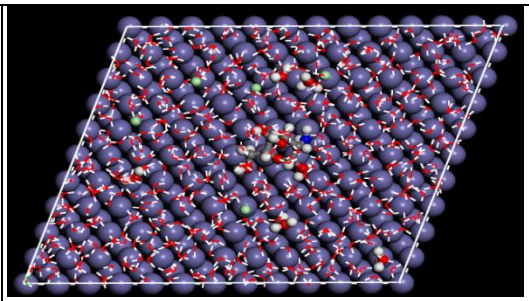
	Side View	**Top View**
NADH	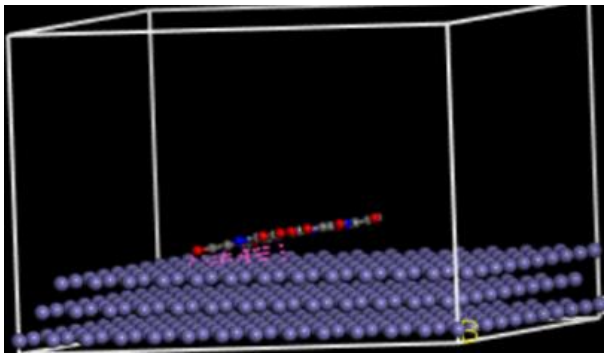	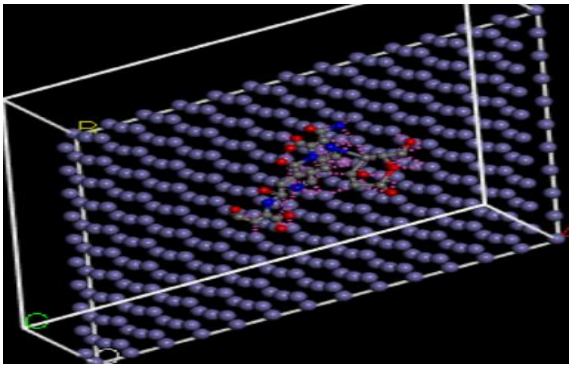
	Side View	**Top View**
CTS-NADH	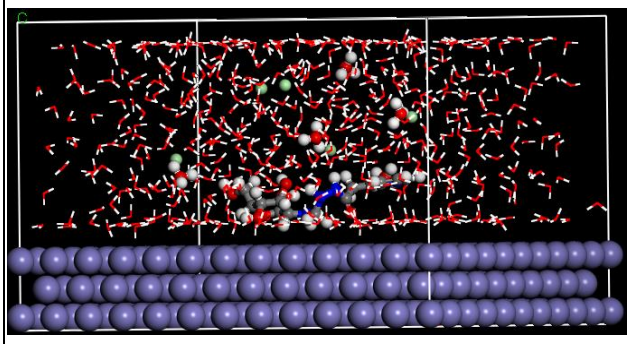	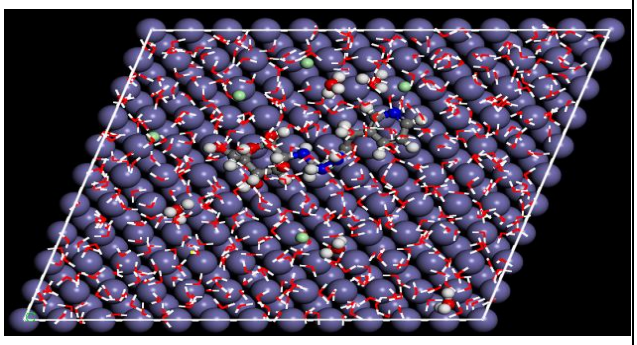
	Side View	**Top View**

Fig. 4.1.27Comparing the Top (i) and side views (ii) of the most stable adsorption orientation during the interactions between metal crystal surface, Fe(110), and (a) CTS, (b) NADH, and (c) CTS-NADH inhibitor molecules in the gas phase

CTS	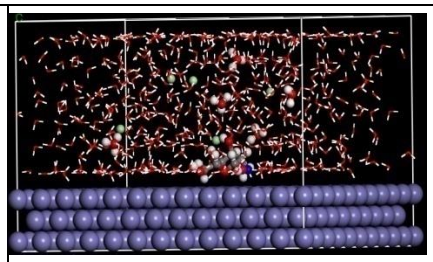	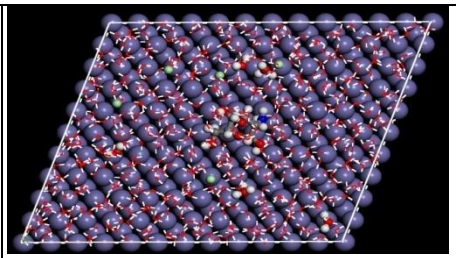
	Side View	**Top View**
PAA	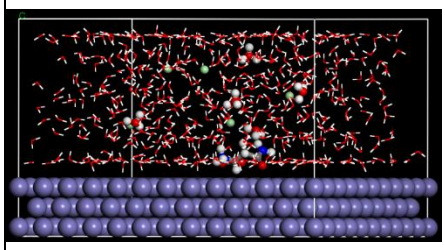	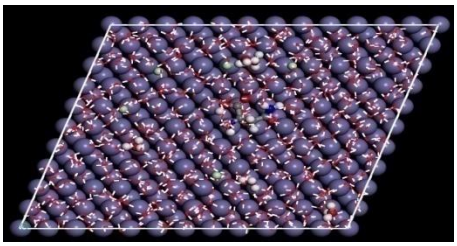
	Side View	**Top View**

CTS - PAA	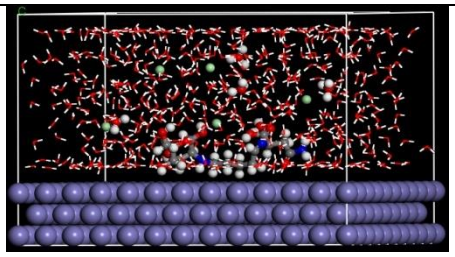	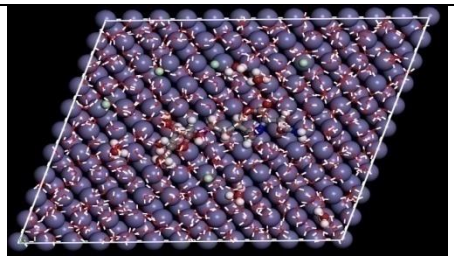
	Side View	**Top View**

Fig. 4.1.28 Comparing the Top (i) and side views (ii) of the most stable adsorption orientation during the interactions between metal crystal surface, Fe (110), and (a) CTS, (b) PAA, and (c) CTS-PAA inhibitor molecules in the gas phase

4.2 DISCUSSION: the F-TIR results of the different inhibitors are discussed below.

4.2.1 F-TIR Characterization. F-TIR was used to characterize the inhibitors.

4.2.1.1 F-TIR Characterization of synthesized Chitosan(CTS): The derived chitosan was characterized in the following manner

(a) Synthesized chitosan

The characteristic peaks identified with the synthetic chitosan were matched with previously prepared chitosan in the literature to confirm its synthesis and purity. The FTIR affords the functional groups specific to chitosan. In Figure 4.1.1 (a) the spectrum for chitosan is shown. FTIR investigations showed a stretching vibration band in the range of 3500 – 1000 cm^{-1} corresponding to NH (primary and secondary) and OH or the intramolecular hydrogen bonds (Queiroz et al., 2015). The peak at 1624 cm^{-1} could be linked to the stretching of the C–N vibration and OH group by bonding (Wolkers et al., 2004), and the adsorption band at 1377 cm^{-1} represents the C–O stretching of the primary alcohol group. The bands at 1100, 1060, and 1024 cm^{-1} indicate the presence of C–O stretching of polysaccharide bonds (Lim & Hudson, 2004; Wolkers et al., 2004). The peaks between (1600–1665) cm^{-1} related to amides seem to be overlapped giving the broad peak indicating a decrease in acetyl groups and hydrogen bonds. Similar observations have been made by Yuan et al. (2011). In this band, the N-acetyl residual groups typical to chitosan 1665 cm−1 (C=O stretching of amide I) are obvious. The C-H symmetric and asymmetric stretching can be seen in 2921 and 2877 cm^{-1} absorption bands at around, respectively. These functional groups are related to the typical polysaccharide (Melo-Silveira et al., 2012) such the carrageenans(Silva et al., 2010) and glucans(Wolkers et al., 2004). The small band around 1550 cm^{-1} corresponds to the N-H bending of amide II (Lim & Hudson, 2004). The peaks for CH_2 bending and CH_3 symmetrical deformations can be seen at 1423 and 1375

cm^{-1}. The band around 1153 cm^{-1} can be ascribed to the asymmetric stretching of the C-O-C Bridge (Vino et al., 2012). All bands are found in the spectra of samples of chitosan reported by others (Song et al., 2013; Vino et al., 2012). Thus, chitosan has been synthesized.

(b) Degree of acetylation:

The degree of acetylation (DD) of CTS was determined by the baseline method based on the FTIR spectrum using Baxter's model: Degree of deacetylation measurement by infrared spectroscopy is based on absorbance ratios of various spectral bands (Fatima, 2020). The ratio of absorbance of amide-I at 1655 cm^{-1} to that of the hydroxyl group at 3450 cm^{-1} in chitosan depends upon the degree of deacetylation in the chitosan (Dimzon & Knepper, 2015). The lower the absorption of the amide-I group, the higher the degree of deacetylation

$$DD = 100 - \left[\frac{A1655}{A3450} \text{ x } \frac{100}{1.33}\right] \quad (4.1)$$

where A1655 and A3450 represent the absorbance of chitosan at the Amide-1 and hydroxyl band respectively. From the calculated results, the degree of acetylation of the prepared CTS was 84 %. Interestingly, the obtained degree of acetylation was similar to the commercial grade of chitosan and even higher than reported in the literature (Dimzon & Knepper, 2015).

4.2.1.2 FTIR of synthesized Polyasparticacid(PAA)

The polyaspartic FTIR data is represented in Figure 4.1.1 b. The characteristic peaks at 3,420 and 1,601 cm^{-1}, can be ascribed to the stretching and bending vibrations of N-H in amide (Chen et al., 2018b). The peak at 1,610 cm-1 is due to the C=O of the carboxylic acid, while the peak at 1,398 cm-1 corresponds to the

strong signal of C-N(Liu et al., 2011; Njoku et al., 2021). The broad adsorption band around 3100 – 3600 cm-1 is due to the stretching vibration of O–H(Wang et al., 2017). The peaksaround 1666 and 1601 cm−1 indicate the strong absorption of –COOH and –CONH(Z. Liu et al., 2011). The peak for C–N is included in the 1400 cm−1. Interestingly, again, the FTIR of the poly-aspartic acid synthesized from aspartic acid exhibited similar peaks to previous data from the literature (Gao et al., 2010; Huang & Kong, 2013).

4.2.1.3 FTIR of synthesized PAA- CTS

The combination of PAA and CTS can be verified from the FTIR of the new compound (PAA-CTS). Inspection of the plots in Figure 4.1.1, many peaks typical to CTS and PAA can be seen in the PAA-CTS. But some few peaks disappeared while some new peaks appeared indicating a chemical reaction leading to the formation of new bonds. For instance, in the PAA-CTS FTIR peaks, new bands at 1643 cm-1 which have been linked to chitosan-polyasparticare obvious. In addition, the peak at 1589 cm-1 of the primary amine became weak, which meant amino had been partly substituted. The above FTIR analysis indicates that the structure of PASP/CS was confirmed (Kumar et al., 2012).

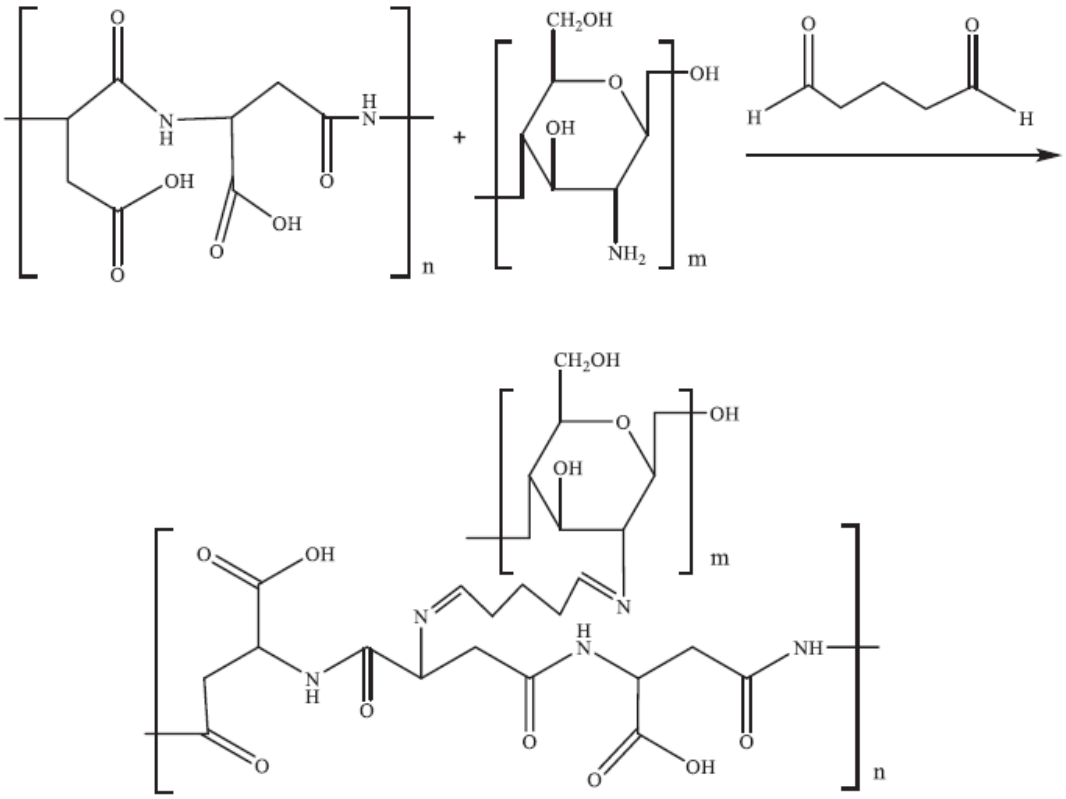

Fig. 4.39 Schematics for the synthesis of chitosan-modified polyaspartic acid.

4.2.1.4 FTIR of NADH

The peak at 3070 – 2819 $cm^{-1}$is related to the vibrational stretching of C-H. The C=O (COO-) asymmetrical stretching band and C=C stretching appeared 1696-1709 cm^{-1} and 1594 cm^{-1}respectively(Jana, 2015; Karabacak & Kurt, 2008). The absorption peak at 1418 cm^{-1} is due to C=N symmetric stretching, the peak at 1325 cm^{-1} is due to C=O symmetrical stretching and the peak at 1303 cm^{-1} has been ascribed to C-N stretching (Jana, 2015; Karabacak & Kurt, 2008; Rai et al., 2006). The stretching peak at 1186 cm^{-1} has been attributed to C-O (COO-)(Jana, 2015; Karabacak & Kurt, 2008; Rai et al., 2006).The band around 2800-3600 cm^{-1} is

usually related to the hydroxyl group of water in the hydrated system manifested from the hydroxyl component symmetric stretch and the asymmetric stretching respectively (Palencia, 2018), although it usually overlaps with the stretching mode of N—H and C—H groups(Njoku, et al., 2021) FTIR spectra for NADH systems are presented in Figure 4.1.2 b. The NADH peak at 1569 cm−1 is due to the N–H of the amide band; (Jose et al., 2021). The peak for C═O vibration is seen at 1669 cm^{-1} and the peak at 1600 cm-1 can be ascribed to the C═N vibration(Jose et al., 2021)(Dege et al., 2014). The corresponding peaks around 3320 cm-1, 3200 cm-1, and 3154 cm-1 are close to the peaks previously ascribed to the vibrations of OH, N—H, and C—H of the pyridine ring, respectively which are typical to the NADH (Dege et al., 2014; Jose et al., 2021; Rai et al., 2006)

4.2.1.5 FTIR of CTS-NADH

At a glance, the formation of CTS-NADH occurs via the imine linkage reaction (see the mechanism of synthesis). The stretching mode obvious at 1649-1664 cm^{-1} has been linked to the stretching of the carbonyl mode in an imide ring with an imine bond (Saini et al., 1993).Aside from this, the overall peaks (Figure 4.1.2 c) seem to be a combination of CTS and NADH individual peaks. Though some peaks disappear and few new ones form. For instance, there is a shift of the peak for the amide group at 1665cm-1 of chitosan (CTS) to 1636 cm^{-1} and the peak at 1569 cm^{-1} for the N–H of the amine band typical of NADH. This forms the band becoming the linkage of NADH and CTS leading to the formation of the new modified compound.

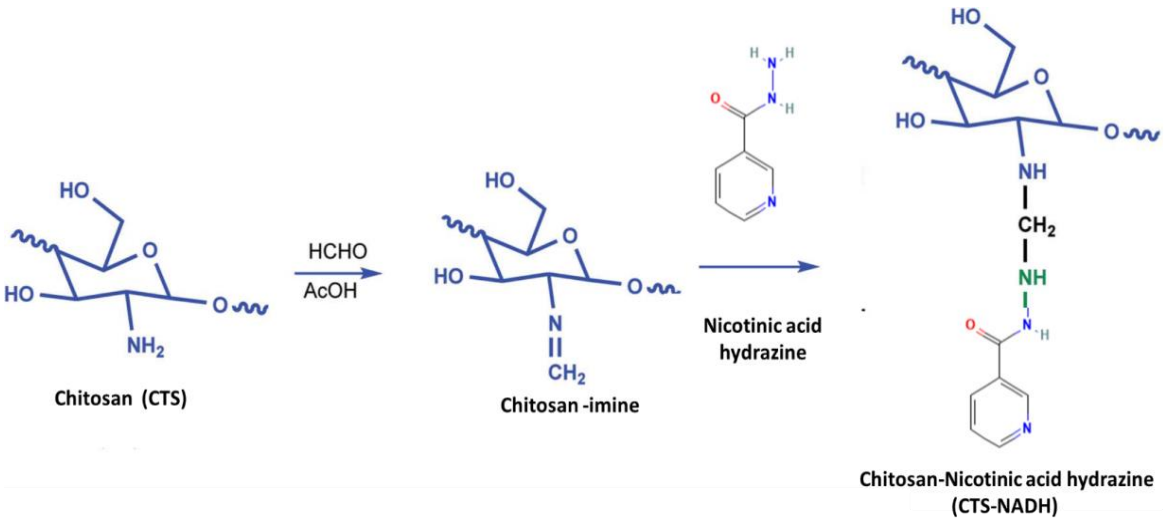

Fig. 4.30 Schematics for the synthesis of chitosan-modified nicotinic acid hydrazide

4.2.1.6 UV-Vis Analysis Results

Uv-Vis of the new CTS derivatives were compared with that of pure CTS to confirm the formation of the new CTS derivative. Figure 4.1.3 compares the Uv-vis spectra of CTS, CTS-NADH and CTS-PAA. In comparison, there was a bathochromic shift (change of spectral band position in the absorption, reflectance, transmittance, or emission spectrum of a molecule to a longer wavelength or higher frequency or energy). This is usually provoked by the increment of conjugation of double and triple bonds and/or groups that contain pi-electrons and hetero atoms(Tong et al., 2020). The spectrum of CTS peaks at 285.5 (nm) while those for CTS-NADH and CTS-PAA peak at 286.5 and 287.5 (nm), respectively. The spectra for the modified CTS are expected to extend beyond these, but since the polymers were dissolved in an acidic medium for dissolution to avoid suspended

particles in the optical pathlength, a lower wavelength might occur(Tong et al., 2020). Also, the wavelengths for NADH and PAA which have been previously identified in the literature at 213/211 nm and 216 (Benković et al., 2016; Zeng et al., 2012), respectively, all disappeared. These are a strong indication of the formation of entirely new derivatives which are now neither CTS nor PAA/NADH. The characterization results (FTIR and uv-vis) confirm the formation of new compounds with more heteroatoms and imine linkage, which are expected to interact with steel more favorably and impact enhanced anticorrosion effect more than the native monomer (CTS) or the functionalizing molecules (PAA and NADH). Hence, the anticorrosion effects of the new compounds will be compared with the individual molecules to confirm our guess.

4.2.2 Corrosion inhibition experiment: The Anticorrosion test was carried out using the following methods

4.2.2.1 Gravimetric (weight loss) measurements

Weight loss is a classical and non-electrochemical technique for the determination of corrosion rates. Gravimetric or weight loss measurement provides more reliable results than electrochemical techniques because the experimental conditions are approached more realistically with the real conditions (Souza *et al*., 2009). However, it has the disadvantage of time-consuming since the coupons have to be immersed for several hours. The anodic dissolution of mild steel coupled with a destabilization of the oxide film by chloride ions from the HCl results in a considerable weight loss when mild steel is immersed in an acidic solution (Njoku et al., 2019). The weight loss of mild steel coupons was evaluated over a total immersion period of 168 hrs in 1 M HCl solution in the presence and absence of chitosan, polyaspartic acid, nicotinic acid hydrazide, chitosan modified with polyaspartic acid and chitosan modified nicotinic acid hydrazide under aerated conditions.

Effect of polymeric inhibitors on mild steel corrosion

The average weight loss and the inhibition efficiency of chitosan (CTS), polyaspartic acid (PAA), and nicotinic acid hydriazide (NAHD) were studied. The calculated results for mild steel corrosion in 1 M HCl without and with different concentrations of polymeric inhibitors Chitosan (CTS), polyaspartic acid (PAA), nicotinic acid hydriazide (NAHD) as a function of time are presented in Table 4.1.2.

Inspection of the experimental results showed that weight loss of mild steel in 1 M HCl solution was highest in the absence of inhibitors while in the presence of inhibitors in the acid environment, the corrosion rate of mild steel decreased with an increase in inhibitor concentration.

Effect of modified polymeric inhibitors on mild steel corrosion

Chitosan was modified using PAA and NAHD respectively to improve their inhibition efficiency. The inhibition efficiency of the modified polymers (CTS-NADH and CTS-PAA) increased with an increase in time which is an indication that the strength of the modified inhibitors increased as a result of the interaction between the molecules of the acid thereby increasing the potency of the solution. The inhibition efficiency of all the polymeric inhibitors investigated for mild steel corrosion was observed to increase with an increase in concentration but the inhibition efficiency of the modified polymer showed higher inhibition efficiency with little or no decrease in inhibition efficiency over time. This inhibitive effect of the polymeric inhibitors could be attributed to the adsorption of inhibitor molecules onto a mild steel surface which forms a barrier or film layer on the metal surface displacing less stable molecules of the acid and thus reducingthedissolution of metal. The order of increment in I.E % at higher inhibitor concentrations is as shown: CTS-PAA > CTS-NAHD > CTS >PAA >NAHD.

4.2.2.2 Electrochemical test: The following electrochemical tests were adopted because corrosion is an electrochemical process.

4.2.2.2.1 Potentiodynamic polarization curves (PDP)

Since corrosion is an electrochemical phenomenon, it is also important to adopt electrochemical approaches to validate the anti-corrosion effects of the various inhibitors. Herein, we adopted the lowest and the highest concentrations of the inhibitors to provide electrochemical evidence of the anticorrosion effects of CTS, the modifying compounds (PAA and NADH), and the grafted/functionalized polymers (CTS-NADH and CTS-PAA). Polarization tests are intended to evaluate the effects of the various inhibitors on the anodic and cathodic corrosion processes. Representative polarization curves for the studied mild steel in 1 M HCl solution without and with different concentrations of the CTS, NADH, and CTS-NADH and CTS, PAA, and CTS-PAA are shown in Figures 4.1.14 and 4.1.15 respectively. Also, the corresponding polarization parameters calculated via the extrapolationofthe linear segments of the anodic and cathodic polarization curves are listed in Tables 4.1.4 and 4.1.5. Although as expected (from the gravimetric data) not to the same degree, the introduction of different inhibitors shifts E_{corr} towards more negative values (in a concentration-dependent manner), as well as reducing both the anodic and cathodic current densities with however pronounced cathodic effect. This suggests a mixed-type inhibition mechanism (Shanmugapriya et al., 2023). The values of the current densities in the absence and presence of different inhibitors calculated from the extrapolation of the linear segments of the cathodic and anodic current arms were used to calculate the inhibition efficiency following the existing model (Njoku et al., 2019; Shanmugapriya et al., 2023):

$$IE\% = \left(1 - \left(\frac{i_{corr,inb}}{i_{corr,0}}\right)\right) \times 100 \qquad (4.3)$$

Where, $i_{corr,inb}$ and $i_{corr,0}$ are the corrosion current densities with and without the inhibitors respectively. From the polarization values, it is conspicuous that although chitosan exhibited good anticorrosion efficacy at both low (50 mg/L) and high (250 mg/L) but < 80 %, modification with NADH and PAA can be seen to improve the inhibition efficiency reaching > 84 % to > 90 % with CTS-NADH and CTS-PAA, respectively. This confirms that the fictionalization of natural polymers can improve their property. NADH and PAA which are smaller molecules with heteroatoms surprisingly showed lower inhibition values (even in the gravimetric data) which can be probably ascribed to the instability effects of the inhibitors in the aggressive acidic solution. However, their grafting into chitosan polymer improved the anticorrosion efficacy of chitosan as well as the stability since IE% was stable over time according to the gravimetric data. The improved IE% exhibited by the functionalized chitosan can be attributed to the presence of additional heteroatoms which constitute the adsorption site in inhibiting species (Chauhan et al., 2019).

4.2.2.2.2 Electrochemical impedance spectroscopy (EIS)

Impedance experiments permit analysis of the kinetics of the interfacial electrochemical processes at the metal/solution interface. Again, to evaluate the protective effects of the various films formed by CTS, NADH, PAA, and the modified CTS compounds: CTS-NADH and CTS-PAA. It is also intended to collaborate the gravimetric and polarization techniques in establishing the anticorrosion effects of the inhibitors and the enhanced anticorrosion effects of the new (modified CTS) compounds achieved via the functionalization with molecules that increase adsorption sites (more heteroatoms). Figure 4.1.16 shows the Nyquist plots comparing the impedance response of mild steel in 1 M HCl without and with different concentrations of CTS, NADH, and CTS-NADH while Figure 4.1.17 shows the Nyquist plots comparing the impedance response of mild steel in 1 M

HCl without and with different concentrations of CTS, PAA and CTS-PAA. The various Nyquist plots largely comprised a large depressed capacitive semicircle in the high-frequency region and perceptible evidence of the formation of another much smaller (almost hidden) capacitive loop at low frequencies. The depressed nature of the Nyquist semicircle with a center under the real axis is characteristic of solid electrodes, which show frequency dispersion of the impedance data (Njoku et al., 2018; Oguzie et al., 2014). The capacitive loop is related to the charge transfer processes complementary with the effect of the double layer capacitance. The diameter of the capacitive loop is related to the interfacial charge transfer resistance (R_{ct}). The magnitude of the charge transfer resistances at both the film and electrode surfaces (R_{ct1} and R_{ct2}) for the mild steel specimen in 1 M HCl improved appreciably in the presence of the different inhibitors in a concentration-dependent manner but the modified compound (CTS-NADH and CTS-PAA) showed higher values. The impedance fitting was achieved using the Zswimp software. The spectra for the various systems fitted very well to the equivalent circuit model $Rs(Q_1(R_{ct1}(Q_2R_{ct2})))$ as shown in Fig. 4.1.18, with minimal error ($chisqaure = 1.0 \times 10^{-3} - 4.0 \times 10^{-4}$). In the equivalent circuit, Rs represents solution resistance, R_{ct2} represents charge transfer resistance at the electrode and outer Helmholtz plan, Rct_1 represents the film resistance, CPE_2 (Q2) and CPE_1 (Q1) denote the constant phase elements representing the double layer and film capacitances respectively(Nwanonenyi et al., 2022; Yaagoob et al., 2023).

The corresponding fitting parameters are listed in Table 4.1.3 and Table 4.1.4. In the tables, n represents the degree of surface inhomogeneity of the interface while R_T represents total impedance resistance. R_T values were estimated as follows: $R_T = R_{ct1} + R_{ct2}$ (and R_{ct1} and R_{ct2} are charge transfer resistances of the film and electrode surfaces respectively).

The inhibition efficiency (IE%) can be estimated from R_T values without ($R_{T,blk}$) and with inhibitor ($R_{T,inb}$) using Eq 4.1.4 The obtained values are listed in tables 4.1.6 and 4.1.7.

$$IE\% = \left(\frac{R_{T,inb} - R_{T,blk}}{R_{T,inb}}\right) X \ \ 100 \qquad (4.4)$$

In the tables (4.1.6-4.1.7), two obvious striking features can be observed upon the introduction of different inhibitors; one is the corresponding increase in the R_T values, and the other, is a decrease in the CPE values. The increase in R_T values and corresponding improvement in inhibition efficiency confirms the corrosion-inhibiting effect of the inhibitors due to the formation of inhibitor films that prevent the ingress of corrosive electrolytes (Cl^- and H^+)(Onyeachu et al., 2023). The observed decrease in CPE values often results from a reduction in dielectric constants and/or an increase in the electric double-layer thickness, both of which are indicators of the replacement of adsorbed water molecules by inhibiting species. Organic species have lower dielectric effects when compared with water molecules, thus their adsorption would lead to the displacement of water molecules on the electrode surface and a consequent decrease in the CPE values (Emori et al., 2023). Here again, the trend of the inhibition efficiencies agrees with the gravimetric and polarization data. Molecules PAA and NADH exhibited weak values compared to CTS-PAA > CTS -NADH. These modified natural polymers are therefore a better choice for corrosion protection of mild steel in 1 M HCl compared to both the synthesized chitosan (natural polymer) or nontoxic polymer (PAA) / a naturally derived compound (NADH). EIS confirmed that the inhibitors could adsorbed on the electrolyte/steel interface to achieve protection since double-layer capacitance values appreciably decreased in the inhibited system

4.2.3. Adsorption consideration: The adsorption of these inhibitors on the surface of mild steel followed,

4.2.3.1 Langmuir adsorption isotherm.

Adsorption isotherm fitting can be employed to establish that the corrosion inhibition exhibited by organic molecules is due to the adsorption of the molecules on the substrate (mild steel) in the studied media (acidic solution system) forming surface coverage of inhibitor film. Langmuir adsorption isotherm provides the optimal regression. In this plot, the relationship between the degree of surface coverage (θ) (obtained from the relation IE%= θ x 100) and the inhibitor concentration (expressed in mg/l) were employed to fit the experimental data to the Langmuir adsorption isotherm model(Ouici et al., 2016; Saha et al., 2016)

$$C / \theta = 1/ K + C \quad (4.5)$$

Where K is the equilibrium constant of the adsorption process and C is the concentration of the inhibitors. The obtained slopes, intercepts, and goodness of fit parameters (r^2) for all the molecules are listed in Table 4.1.8. A close look at the fitting plots in Figure 4.1.19 and the parameters in Table 4.1.8 show that the goodness of fit in all systems approximate unity indicating conformation to Langmuir isotherm. Also, near-unity slopes indicating minimal interaction in the adsorption layer were obtained in all the systems. Nonetheless, the slight deviation of the slopes from unity can be attributed to the existence of mild interactions between adsorbed species on the surface and/ or changes in the adsorption energies as the surface coverage increases (Njoku et al., 2021, Okafor, et al., 2021).

The equilibrium constant), K_{ads} represents the rate of adsorption of the adsorbents on the adsorbent. The values increase in the modified compounds with CTS—PAA exhibiting the highest values. This adsorption isotherm parameter confirms that the anticorrosion effects recorded by the various inhibiting agents are due to their

adsorption on the steel surface thereby blocking access to water and other corrosive agents as predicted via electrochemical methods.

4.2.3.2 Thermodynamic Considerations

The thermal influence on the corrosionproperties of mild steel in 1.0 M HCl without and with the various inhibitive additives was evaluated. This is intended to provide the thermodynamic parameters associated with the inhibition process of both the modifying agents (PAA, CTS, and NADH) and the modified polymers (CTS-NADH and CTS-PAA). The temperature range was 313–333 K. In Table 4.1.9, it is clear that the inhibition efficiency increases with increasing inhibitor concentration but decreases with increasing temperature with CTS-NADH > CTS > NADH > CTS-PAA> PAA. The performance of CTS (more than the modified CTS-PAA) could be related to the effect of temperature on its solubility. Corrosion rate is related to weight loss following the model (Ali & Fulazzaky, 2020);

$$C_r = \frac{87{,}6\ W_L}{A t \rho} \tag{4.6}$$

Where C_r is the corrosion rate (in mm/y), W_L is the weight loss (mg), and t is the immersion time (h), ρ is the density of the steel specimen (in g/cm^3). The relationship between corrosion rate (Cr), temperature (t), and activation energy (E_a) is expressed by the Arrhenius equation in Eq. (4.6)(Ben, 2017):

$$\log (CR) = \ LogA - \frac{E_a}{2.303RT} \tag{4.7}$$

Where A is the Arrhenius pre-exponential constant, T is the absolute temperature (K) and R is the universal gas constant (8.314 J/mol.K).

A plot of Log CR against 1/T gives a straight line from which the E_a can be deduced from the slope. The Arrhenius plots obtained for all tested corrosion inhibitor systems are presented in Fig. 4.1.20 (a-e), respectively for CTS, PAA,

NAHD, CTS-NAHD, and CTS-PAA. The slopes extrapolated from all the individual plots in Figure 4.1.20 have been utilized to calculate the E_a values detailed in Table 4.1.10. The E_a values deduced in the presence of an inhibitor are higher than for the blank solution. This implies strong adsorption of the inhibitor molecules at the metal surface that creates a barrier on the steel surface (Hamdy & El-Gendy, 2013). When compared again, it is observed that a sharp increase in the E_a occurs in the presence of 50 ppm CTS, after which the E_a value decreases steadily and continually with an increase in CTS concentration. Such may signify rapid adsorption of CTS molecules at lower doses (due to abundant active sites available for adsorption). Afterwards, at higher concentrations, interactions between inhibitor molecules could arise which makes their adsorption tend to form multilayers of inhibitor films at lower activation energies. The Ea changes concerning inhibitor concentration showed no defined trend.

An alternative form of the Arrhenius equation is the transition state equation described in Eq. (4.8), which can permit the calculation of enthalpy ΔH and entropy ΔS of the interaction process.

$$\log\left(\frac{\mathrm{CR}}{\mathrm{T}}\right) = \left[\log\left(\frac{\mathrm{R}}{\mathrm{hN}}\right) + \left(\frac{\Delta \mathrm{S}}{2.303\mathrm{R}}\right)\right] - \frac{\Delta \mathrm{H}}{2.303\mathrm{RT}} \qquad (4.8)$$

It relates the enthalpy of the reaction with the corrosion rate and temperature. A plot of log CR/T) against (1/2.303RT) gives a straight line with a slope equal to – ΔH (kJ/mol). Hence, ΔH can be calculated from the slope and ΔS from the intercept. The plots are displayed in Figure 4.1.21, while the values slope and enthalpy (H) extrapolated from the plots are included in Table 4.1.10. Positive values are obtained for the ΔH values in the presence of inhibitor systems, and the values are greater than those exhibited by the steel in the blank solution. The positive H values increase with inhibitor concentration, The Ea values are greater than the ΔH values, indicating that the corrosion process involved electrochemical

reactions that led to the release of gaseous products which is archetypal to acidic systems (especially hydrogen evolution reaction)(Rezaierod et al., 2014).

4.2.4 Surface analysis: The inhibitive effects of these inhibitors were studied using

4.2.4.1 XPS Analysis

To confirm the mechanism, XPS analysis of the adsorption of the modified compounds has been carried. This test can reveal the nature of chemical bonding existing on the steel solution interface. For instance, generally, the dissolution of steel produces Fe^{2+} ($Fe \rightarrow Fe^{2+} + 2e^{-}$) which can further oxidize to Fe^{3+}.In HCl, chloride (Cl^{-}) and water molecules $(H_2O)_{ads}$ pre-adsorption on the steel surface will give $FeCl_x$andFeOOH. On the other hand, in the presence of organic molecules, the protonation of organic molecules produces (—NH_2^+) while binding energy peaks relating to the adsorption of organic species such as Fe—N, Fe—NH_2^+, C═C/C═O bonds can be found. Interestingly, with the help of sophisticated XPS analysis, these peaks can be identified to confirm the adsorption mechanism. Figure 4.1.6 and 4.1.7 presents the XPS data for the interaction of CTS-NADH and CTS-PAA, respectively with the steel surface in 1 M HCl. Inspection of the Figures reveals the peaks for the various bonds at the steel surface. These correctly confirm the proposed mechanism. The deconvolution of the Fe peak produces a binding energy peak at 706.9 eV which is related to the bulk steel (Fe^0), the peak at 709.2 eV is due to iron (II) state (Fe^{2+}) compounds, while the peak at 710 eV and 713 eV are for iron (III) (Fe^{3+}) state compounds and the associated satellite respectively(Krishna & Philip, 2022).The pre-adsorption of chlorides on the steel can be verified from the Cl 2p deconvoluted peaks. The Cl 2p deconvoluted peaks at 197 eV and 199.5 eV have been ascribed to metallic chlorides (FeClx) (Njoku et al., 2018). The interaction/adsorption of organic species from CTS, NADH, and

PAA can be best confirmed by considering binding energy peaks relating to nitrogen (N) and carbon adsorptions (C). The peak for N is deconvoluted into binding energy peaks at 399.2 eV, 400.9 eV, and 401.9 eV which are ascribed to C−N, coordinated nitrogen with the steel surface (N-Fe)(Loto& Loto, 2016) and the protonated nitrogen. The carbon (C 1s) peak was deconvoluted into three other peaks belonging to the different structural moieties of the modified polymers (CTS-NADH and CTS-PAA). The prominent peak at 284.5 eV is ascribed to C−C, and C=C or C−H while the peak at 286.4 is related to the carbon atoms bonded with nitrogen in the form of C−N and C=N(Loto& Loto, 2016). Finally, the peak confirming protonation can be verified at 288.4 which is ascribed to a protonated carbon peak (C=N+)(Loto& Loto, 2016; Njoku et al., 2021). The presence of these peaks confirms that the interaction/adsorption of the modified chitosan polymer compound is responsible for the anticorrosion effect recorded experimentally and agrees with the proposed mechanism of inhibition.

4.2.4.2 SEM analysis

SEM (scanning electron microscopy) provides evidence of corrosion protection at the microscopic levels. Excellent corrosion-inhibiting agents will maintain a smooth surface devoid of voids and corrosion products; while weak or poor agents only offer minimized reduction of corrosion products and/or micro defects due to corrosion aggression. Meanwhile, an uninhibited system will be laden with both corrosion products and defects indicating unhindered corrosion action. The images comparing the surface microstructure of the steel exposed in both the inhibited and uninhibited system after 24 h exposure time are presented in Figure 4.1.21. The steel surface exposed in the uninhibited solution revealsavery rough surface with lots of corrosion products, while the steel surface exposed in the inhibited system revealsasmooth surface devoid of corrosion products which indicates corrosion inhibition action. However, the difference in the corrosion protection ability

amongst the inhibitors is obvious with the modified polymers (CTS-NADH and CTS-PAA) offering the best protection compared with NADH, PAA, and CTS (see Figure 4.1.21).

4.2.5 Inhibition Mechanism

Generally, acids corrode steel following ($Fe \rightarrow Fe^{2+} + 2e^-$) making the surface to be positively charged. Therefore, in the presence of chlorides (HCl), Cl^- which is negatively charged can be attracted to the surface by electrostatic attraction thereby recharging the steel surface to negatively chargedas illustrated in the scheme in Figure 4.1.22. Herein the steel corrodes following the notorious equation:

$$Fe[(H_2O)_nCl^-]_{ads} \leftrightarrow Fe[(H_2O)_n\,Cl]_{ads} + e^- \quad (4.6)$$

$$Fe[(H_2O)_n\,Cl]_{ads} \rightarrow Fe\left[(H_2O)_nCl^+\right] + e^- \quad (4.7)$$

$$Fe\left[(H_2O)_nCl^+\right] \leftrightarrow Fe^{2+} + Cl^- \quad (4.8).$$

Interestingly, organic molecules protonate (become positively charged) at nitrogen functional groups as illustrated in the scheme in Figure 4.1.22. The implication of these is that electrostatic interaction can provoke the adsorption of these molecules on the steel surface thereby displacing water molecules and other corrosive species according to the model:

$$(Org.mol)_{(aqueous)} + xH_2O_{(ads)} \leftrightarrow (Org.mol)_{(ads)} + xH_2O_{(aqueous)} \quad (4.9)$$

Where $(Org.mol)_{(aqueous)}$ represent organic molecules in solution and$xH_2O_{(ads)}$sent the previously adsorbed water molecules on the steel surface and vice versa. Therefore, the more the number of heteroatoms, the more the adsorption sites present. Again, this is the motivation for the grafting of the smaller molecules with additional heteroatom (PAA and NADH) into the natural chitosan polymer (CTS) to multiply the number of adsorptive sites in the polymer with a possible consequential improvement in the anti-corrosion effect. As obvious in the

scheme describing the mechanism of adsorption of the various molecules, modification of CTS with NADH and PAA via grafting with formaldehyde and glutaraldehyde increased the number of adsorptive sites in the new (functionalized chitosan) compounds. From the literature, this usually manifestsin increased binding and interaction energies of the molecule's adsorption on steel leading to improved corrosion inhibition efficiency. The scheme in Figure 4.1.22 affords mechanistic insights into the protonation of the inhibitor compounds and their adsorption on the steel surface.

4.2.6 Theoretical Consideration: Material Studio 7.0 software was used to calculate the following theoretical models

4.2.6. 1 DFT calculations

The DFT calculations were carried out herein to provide insights into the structural and/or electronic properties of the various inhibiting compounds, particularly since the structural and electronic properties of organic compounds have previously correlated with their inhibiting capabilities (Singh et al., 2013; Zhang et al., 2016) The interactive adsorption of organic compounds on metallic surface occurs principally through donor-acceptor reactions, thus, the highest occupied frontier molecular orbital (HOMO) in a compound depicts the electron-donating ability of the organic molecule and the lowest unoccupied frontier molecular orbital (LUMO) which represents the ability of the compound to accept an electron are the two most important indices for predicting the reactivity of a chemical species (Emori et al., 2023; Njoku et al., 2018). Figure 4.1.23 depicts the representative snapshots revealing the distribution of HOMO and LUMO as well the Fukui reactive centers on CTS, NADH, and CTS-NADH new compound, while Figure 4.1.24 depicts the representative snapshots revealing the distribution of HOMO and LUMO as well the Fukui reactive centers on PAA and CTS-PAA new

compound. Tables 4.1.9 and 4.1.10 collated the corresponding calculated quantum chemical calculation parameters such as; E_{HOMO}, E_{LUMO}, ΔE, and ΔN.

The electron affinity (EA) and ionization potential (IP) which are relevant to estimate ΔN can be deduced from *E*HOMO and $E_{LUMO}$by the Equations (4.10) and (4.11)(Lgaz et al., 2017):

$$IP = - E_{HOMO} \quad (4.10)$$

$$EA = - E_{LUMO} \quad (4.11)$$

Mulliken electronegativity (χ) and Absolute hardness (η) can be approximated using(Martinez, 2003):

$$\chi = \frac{IP+EA}{2} \quad (4.12)$$

$$\eta = \frac{IP-EA}{2} \quad (4.13)$$

The number of transferred electrons (ΔN) is calculated by application of the Pearson method using the equation(Martinez, 2003):

$$\Delta N = \frac{\chi_{Fe}-\chi_{inh}}{2(\eta_{Fe}+\eta_{inh})} \quad (4.14)$$

Where χ_{Fe} and χ_{inh}denote the absolute electronegativity of iron and inhibitor molecule η_{Fe} and η_{inh} denote the absolute hardness of iron and the inhibitor molecule respectively. A theoretical value of χ_{Fe} = 7 eV and η_{Fe} = 0 (since for bulk metallic atoms $I = A$) was considered to calculate the ΔN values (Shokry, 2014). Recently, it was reported that the value of χ_{Fe}= 7 eV is theoretically not acceptable since electron-electron interactions were not considered, only free electron gas Fermi energy of iron was considered (Shokry, 2014). Hence, researchers, now, are usingthework function (ϕ) of the metal surface instead of χ_{Fe}, as it is a more appropriate measure for its electronegativity. Thus, Equation 4.6 is rewritten as follows:

$$\Delta N = \frac{\phi-\chi_{inh}}{2(\eta_{Fe}+\eta_{inh})} \quad (4.15)$$

Where ϕ denotes the work function. The obtained DFT derived ϕ values for Fe (100), Fe (110), and Fe (111) surfaces have been reported to be; 3.91, 4.82, and 3.88 eV, respectively(Lgaz et al., 2017; Martinez, 2003; Njoku et al., 2018; Shokry, 2014). However, here, we only considered the Fe (110) surface due to its higher stabilization energy and packed surface. The compounds with high E_{HOMO} are likely going to have a higher tendency to donate electrons to an electron-deficient site of the electrode surface, whereas the compounds with lower $E_{LUMO,}$ on the second hand,havea greater tendency to accept electrons from the electrode matrix (the vacant d-orbitals of the transition metals like iron) using anti-bonding orbitals to form feed-back bonds (Obot et al., 2015). The energy difference between the HOMO and the LUMO (ΔE) gives another insight into the reactivity of inhibitor molecules. This important quantum parameter can give significant information about the stability index and molecule–metal interaction. The Lower the ΔE value is, the better will be its inhibition efficiency. The smaller the value of ΔE, the higher the reactivity of the molecule since the molecule would become easily polarizable (soft)(Kumar et al., 2013). Close inspection of the data in Table 4.1.9 and 4.1.10, it can be seen that the modified CTS derivatives (CTS-NADH and CTS-PAA) exhibited ΔE and lower ΔN values compared with CTS, NADH, and PAA single inhibitor compounds. These outs rightly supported the objective of the modification of the natural polymer (CTS) for increased performance. Lower ΔE values indicate that modified CTS can afford higher interaction energies with the steel surface and consequently, higher inhibiting abilities (IE %). Going further, ΔN is related to reactivity by the relation: $\Delta N > 0$, indicates a high disposition to transfer or release electrons, while $\Delta N < 0$ indicatesalow disposition to transfer or release electrons (Njoku et al., 2018; Oguzie et al., 2014). The use of Fukui analysis to estimate the adsorption centers of inhibitors has been widely reported. In Figures 4.1.23 and 4.1.24, the electron-rich centers (f-) and deficient

sites (f^+) are revealed by Fukui functions. Also, the HOMO and LUMO isosurfaces can be seen to saturate more in the modified compounds due to the extensive presence of heteroatoms which are the pi-electron carriers in an organic compound. The modification of CTS with NADH and PAA improve the overall electronic properties. They become more suited for effective adsorption of Fe surface.

4.2.6.2 Molecular dynamics simulation (MDS)

Recently, to well understand and predict the behavior of the corrosion inhibition process, considerable attention has been paid to the use of Molecular Dynamic (MD) simulations(Njoku, et al., 2021). The results of the various frontier electronic and structural parameters of the different compounds obtained via DFT calculations revealed only slightly different degrees of dispositions to the adsorptive abilities with the modified derivative providing better parameters. To correlate the frontal orbital parameters with binding energy between the inhibitor compounds, MDS was carried. This is to probe the nature of the interactive strengths of the various tested inhibitor compounds with the steel surface to ascertain the stability and the adsorption strengths of the compounds(Njoku, et al., 2021; Nwanonenyi et al., 2022). The motivation for this is to offer a clearer theoretical basis for previous experimentally recorded inhibition efficacy of these inhibitors, particularly since metal/adsorbate interaction energies have also been correctly correlated with corrosion mitigating efficacy(Maduabuchi et al., 2020; Njoku et al., 2019). Tables 4.1.9 and 4.1.10 present the interactive and binding energies of the inhibiting compounds. The higher the interaction / binding energies the higher the ability of the inhibitors to adsorb firmly and/ or form a compact protective barrier film on the metal surface(Oguzie et al., 2014). Again, on average, CTS-NADH and CTS-PAA modified natural polymers which provided better frontier electronic properties have higher interaction energies compared with the individual/unmodified CTS, NADH, and PAA. The theoretical results are in

perfect agreement with the experimental data presented and certify the objective of the synthesis of the new compounds. This shows that the modified compounds might likely have the best inhibiting efficiency (protective efficacy). The resulting low-energy adsorption structures (side and top views) for the various organic compounds are presented in Figure 4.1.25 and 4.1.26 for CTS-NADH and CTS-PAA respectively.

Interestingly, the compounds adopt a near-flat orientation on the Fe (110) surface (Figure 4.1.25 and 4.1.26 respectively). This sort of orientation usually results in the formation of a strong coordinate bonds and back-bonding formation between the inhibitors molecules and the Fe (110) surface which providesalarger blocking area by the inhibitors preventing the surface from corrosion(Oguzie et al., 2014). From the adsorption configuration of the two inhibitors, it can be seen that the larger the molecules are the better surface coverage of the surface of the metal. As anticipated both higher positive binding energy (B.E) and higher negative interaction energies were recorded with the modified polymers exhibiting better results. High B.E means favorable specific interaction while high negative interaction energy reflects sustainable interaction reaction. Therefore, CTS-NADH and CTS-PAA show a stronger tendency to adsorb on the steel surface and should provide higher corrosion protection (Nwanonenyi et al., 2022). Hence, theoretical results support the experimental data.

CHAPTER FIVE

CONCLUSION AND RECOMMENDATIONS

5.1 Conclusion

1. Chitosan was prepared from oyster shells through deacetylation of chitin.
2. FT-IR and UV-visible were used to confirm successful derivation and modification of the naturally derived chitosan (CTS) with poly-aspartic acid and nicotinic acid hydrazide.
3. Moderate anticorrosion properties of CTS were improved by grafting CTS with PAA and NAHD as revealed by gravimetric, electrochemical, and spectroscopictechniques.
4. The adsorption of the modified CTS on the surface of mild steel was verified with XPS and the adsorption process obeyed Langmuir's adsorption isotherm.
5. Theoretical modeling (DFT & MDS) was employed to calculate the electron properties and adsorption energies of the inhibitors. The theoretical results agree with the experimental result

5.1.1 Contribution to Knowledge

In my research, I found out that chitosan has not been modified with Nicotinic acid hydrazide for corrosion inhibition on mild steel or any other steel in an acid environment. Hence, the following contributions are made:

(a) The grafting of chitosan sourced from waste agricultural products with NADH and PAA improved its anticorrosion properties by increasing the number of heteroatoms present in the compound.

(b) The inhibition efficiency of chitosan increased from 70% to 93% therefore, it can successfully be applied in solving the problem of corrosion on engineering materials

5.2 Recommendations

The following recommendations are made for future researchers who may wish to carry out further study on the use of natural and modified natural polymers as inhibitors for mild steel corrosion inhibition:

i). The modification of more natural polymers with molecules containing extensive heteroatoms and double bonds in conjugation (nitrogen, sulfur, phosphorus, aromatic rings,etc) should be encouraged until compounds that can out-perform chromate-based inhibitors for corrosion control in varied systems are achieved.

ii). The use of biodegradable, renewable, and eco-friendly, polymers should be traversed as possible corrosion inhibitors as they are nontoxic to man and its environment.

iii). The use of polymer blends and composites in controlling the corrosion of metals should be explored as possible corrosion inhibitors.

REFERENCE

Ali, N., & Fulazzaky, M. A. (2020). The empirical prediction of weight change and corrosion rate of low-carbon steel. *Heliyon*, *6*(9), e05050–e05050. https://doi.org/10.1016/j.heliyon.2020.e05050

Alvarenga, R. A. F. de, Galindro, B. M., Helpa, C. de F., & Soares, S. R. (2012). The recycling of oyster shells: An environmental analysis using Life Cycle Assessment. *Journal of Environmental Management*, *106*, 102–109. https://doi.org/https://doi.org/10.1016/j.jenvman.2012.04.017

Ansari, K. R., & Quraishi, M. A. (2015). Effect of three component (aniline–formaldehyde and piperazine) polymer on mild steel corrosion in hydrochloric acid medium. *Journal of the Association of Arab Universities for Basic and Applied Sciences*, *18*, 12–18. https://doi.org/https://doi.org/10.1016/j.jaubas.2014.04.001

Assem, R., & Fouda, A. S. (2019). *Evaluation of Cationic Surfactant Benzalkonium Chloride as an inhibitor of Corrosion of Steel in the presence of Hydrochloric Acid Solution*.

Ayodele, O., Okoronkwo, A. E., Oluwasina, O. O., & Abe, T. O. (2018). Utilization of blue crab shells for the synthesis of chitosan nanoparticles and their characterization. *Songklanakarin Journal of Science and Technology*, *40*(5), 1039–1042. https://doi.org/10.14456/sjst-psu.2018.128

Ben Aoun, S. (2017). On the corrosion inhibition of carbon steel in 1 M HCl with a pyridinium-ionic liquid: Chemical, thermodynamic, kinetic and electrochemical studies. *RSC Advances*, *7*(58), 36688–36696. https://doi.org/10.1039/c7ra04084a

Benković, T., Kontrec, D., Tomišić, V., Budimir, A., & Galić, N. (2016).Acid–Base Properties and Kinetics of Hydrolysis of Aroylhydrazones Derived from

Nicotinic Acid Hydrazide. *Journal of Solution Chemistry*, *45*(8), 1227–1245. https://doi.org/10.1007/s10953-016-0504-8

Bennett, G. D. (2005). *A Green Polymerization of Aspartic Acid for the Undergraduate Organic Laboratory*. J.Chem.Educ 2005,*82*(9), 1380. http://doi.org/10.1021/ed082p1380.

Chai, C., Xu, Y., Xu, Y., Liu, S., & Zhang, L. (2020). *Dopamine-modified polyaspartic acid as a green corrosion inhibitor for mild steel in acid solution European polymer journal volume137, https://doi.org/10.1016/j.eurpolymj*.

Chauhan, D. S., Quraishi, M. A., Sorour, A. A., Saha, S. K., & Banerjee, P. (2019). Triazole-modified chitosan: A biomacromolecule as a new environmentally benign corrosion inhibitor for carbon steel in a hydrochloric acid solution. *RSC Advances*, *9*(26), 14990–15003. https://doi.org/10.1039/c9ra00986h

Chen, T., Zeng, D., & Zhou, S. (2018a). Study of polyaspartic acid and chitosan complex corrosion inhibition and mechanisms. *Polish Journal of Environmental Studies*, *27*(4), 1441–1448. https://doi.org/10.15244/pjoes/78245

Chen, T., Zeng, D., & Zhou, S. (2018b). *Study of Polyaspartic Acid and Chitosan Complex Corrosion Inhibition and Mechanisms*. *27*(4), 1441–1448. https://doi.org/10.15244/pjoes/78245

Chugh, B., Singh, A. K., Poddar, D., Thakur, S., Pani, B., & Jain, P. (2020). Relation of a degree of substitution and metal protecting ability of cinnamaldehyde modified chitosan.*CarbohydratePolymers*,*234*(June).https://doi.org/10.1016/j.carbpol.2020.115945

Cui, R., Gu, N., & Li, C. (2011). *Polyaspartic acid is a green corrosion inhibitor for carbon steel*. *4*, 362–369. https://doi.org/10.1002/maco.200905511

Dang, N., Wei, Y. H., Hou, L. F., Li, Y. G., & Guo, C. L. (2015). Investigation of

the inhibition effect of the environmentally friendly inhibitor sodium alginate on magnesium alloy in sodium chloride solution. *Materials and Corrosion*, *66*(11), 1354–1362. https://doi.org/10.1002/maco.201408141

Dege, N., Şenyüz, N., Bati, H., Günay, N., Avci, D., Tamer, Ö., & Atalay, Y. (2014). The synthesis, characterization, and theoretical study on nicotinic acid [1-(2,3-dihydroxyphenyl)methylidene]hydrazide. *Spectrochimica Acta - Part A: Molecular and Biomolecular Spectroscopy*, *120*, 323–331. https://doi.org/10.1016/j.saa.2013.10.030

Dimzon, I. K. D., & Knepper, T. P. (2015). Degree of deacetylation of chitosan by infrared spectroscopy and partial least squares. *International Journal of Biological Macromolecules*, *72*, 939–945. https://doi.org/10.1016/j.ijbiomac.2014.09.050

Dong, Y., Xu, C., Wang, J., Wang, M., Wu, Y., & Ruan, Y. (2001). Determination of degree of substitution for N-acylated chitosan using IR spectra. *Science in China Series B: Chemistry*, *44*(2), 216–224. https://doi.org/10.1007/BF02879541

El-deeb, M. M., Ads, E. N., & Humaidi, J. R. (2018). *Evaluation of the Modified Extracted Lignin from Wheat Straw as Corrosion Inhibitors for Aluminum in Alkaline Solution*.Int.J.Electrochem.Sci.,*13*, 4123–4138. https://doi.org/10.20964/2018.05.49

El, K., Singh, D., Quraishi, M. A., Bazzi, L., & Hilali, M. (2020). *Cinnamaldehyde-modified chitosan as a bio-derived corrosion inhibitor for acid pickling of copper : Microwave synthesis , experimental and computational study*. *International Journal of Biological Macromolecules 164*, 3709–3717.

Emori, W., Louis, H., Okonkwo, P. C., Njoku, D. I., Edet, H. O., Okafor, P. C., & Cheng, C.-R. (2023). Dispersive adsorption and anticorrosion properties of

natural capsaicin on Q235 steel in mixed H2SO4 and NaCl environment: Characterization, experimental and theoretical studies. *Sustainable Chemistry and Pharmacy*, *32*, 101042. https://doi.org/https://doi.org/10.1016/j.scp.2023.101042

Farhadian, A., Assar Kashani, S., Rahimi, A., Oguzie, E. E., Javidparvar, A. A., Nwanonenyi, S. C., Yousefzadeh, S., & Nabid, M. R. (2021). Modified hydroxyethyl cellulose as a highly efficient eco-friendly inhibitor for suppression of mild steel corrosion in a 15% HCl solution at elevated temperatures. *Journal of Molecular Liquids*, *338*, 116607. https://doi.org/https://doi.org/10.1016/j.molliq.2021.116607

Fatima, B. (2020). *Quantitative Analysis by IR: Determination of Chitin/Chitosan DD* (M. Khan, G. M. do Nascimento, & M. El-Azazy (eds.); p. Ch. 7-Ch. 7). IntechOpen. https://doi.org/10.5772/intechopen.89708

Fekry, A. M., & Mohamed, R. R. (2010). Acetyl thiourea chitosan is an eco-friendly inhibitor for mild steel in a sulphuric acid medium. *Electrochimica Acta*, *55*(6), 1933–1939. https://doi.org/10.1016/j.electacta.2009.11.011

Gao, C., Zhao, X., Dong, X., & Wang, S. (2020). *Construction of eco-friendly corrosion inhibitor lignin derivative with excellent corrosion-resistant behavior in hydrochloric acid solution Corrosion test*. *May*, 1–10. https://doi.org/10.1002/maco.202011799

Gao, Y., Wang, Y., Liu, Z., & Li, H. (2010). Synthesis, scale, and corrosion inhibition of modified polyaspartic acid. *Asian Journal of Chemistry*, *22*(2), 1495–1502. file:///C:/Users/DEMIAN/Desktop/my wife project 2022/Demian Ciata/AJC-22-2-97.pdf

Hamdy, A., & El-Gendy, N. S. (2013). Thermodynamic, adsorption, and electrochemical studies for corrosion inhibition of carbon steel by henna extract in acid medium. *Egyptian Journal of Petroleum*, *22*(1), 17–25.

https://doi.org/https://doi.org/10.1016/j.ejpe.2012.06.002

Huang, K., & Kong, L. (2013). Preparation and characterization of poly(aspartic acid) derivatives as biodegradable water treatment agents. *Asian Journal of Chemistry*, *25*(18), 10233–10237. https://doi.org/10.14233/ajchem.2013.15243A

Jana, S. (2015). Spectroscopic Characterization of Disulfiram and Nicotinic Acid after Biofield Treatment. *Journal of Analytical & Bioanalytical Techniques*, *6*(5). https://doi.org/10.4172/2155-9872.1000265

Jmiai, A., Ibrahimi, B. El, Tara, A., Issami, S. El, Jbara, O., Bazzi, L., Ibrahimi, B. El, Tara, A., Issami, S. El, Jbara, O., & Bazzi, L. (2017). *Accepted Manuscript*. https://doi.org/10.1016/j.molstruc.2017.12.060

Jose, J., Subramanian, V., Shaji, S., & Sreeja, P. B. (2021). An electrochemical sensor for nanomolar detection of caffeine based on nicotinic acid hydrazide anchored on graphene oxide (NAHGO). *Scientific Reports*, *11*(1), 1–12. https://doi.org/10.1038/s41598-021-89427-6

Karabacak, M., & Kurt, M. (2008). Comparison of experimental and density functional study on the molecular structure, infrared and Raman spectra, and vibrational assignments of 6-chloronicotinic acid. *Spectrochimica Acta. Part A, Molecular and Biomolecular Spectroscopy*, *71*(3), 876–883. https://doi.org/10.1016/j.saa.2008.02.014

Kilmartin, P. A., Trier, L., & Wright, G. A. (2002). *Corrosion inhibition of polyaniline and poly (o -methoxyaniline) on stainless steels*. *131*, 99–109.

Koch, G. (2017). 1 - Cost of corrosion. In A. M. B. T.-T. in O. and G. C. R. and T. El-Sherik (Ed.), *Woodhead Publishing Series in Energy* (pp. 3–30). Woodhead Publishing. https://doi.org/https://doi.org/10.1016/B978-0-08-101105-8.00001-2

Krishna, D. N. G., & Philip, J. (2022). Review on surface-characterization

applications of X-ray photoelectron spectroscopy (XPS): Recent developments and challenges. *Applied Surface Science Advances*, *12*, 100332. https://doi.org/https://doi.org/10.1016/j.apsadv.2022.100332

Kumar, Santosh, Koh, J., Kim, H., Gupta, M. K., & Dutta, P. K. (2012). New chitosan–thymine conjugate: Synthesis, characterization, and biological activity. *International Journal of Biological Macromolecules*, *50*(3), 493–502. https://doi.org/https://doi.org/10.1016/j.ijbiomac.2012.01.015

Kumar, Sumit, Sharma, D., Yadav, P., & Yadav, M. (2013). Experimental and Quantum Chemical Studies on Corrosion Inhibition Effect of Synthesized Organic Compounds on N80 Steel in Hydrochloric Acid. *Industrial & Engineering Chemistry Research*, *52*(39), 14019–14029. https://doi.org/10.1021/ie401308v

Lahrour, S., Benmoussat, A., Bouras, B., Mansri, A., Tannouga, L., & Marzorati, S. (2019). Glycerin-Grafted starch as corrosion inhibitor of C-Mn steel in 1 M HCl solution. *Applied Sciences (Switzerland)*, *9*(21), 1–18. https://doi.org/10.3390/app9214684

Lgaz, H., Salghi, R., Jodeh, S., & Hammouti, B. (2017). Effect of clozapine on inhibition of mild steel corrosion in 1.0M HCl medium. *Journal of Molecular Liquids*, *225*, 271–280. https://doi.org/https://doi.org/10.1016/j.molliq.2016.11.039

Li, M., Xu, J., Li, R., Wang, D., Li, T., Yuan, M., & Wang, J. (2014). *Journal of Colloid and Interface Science Simple preparation of aminothiourea-modified chitosan as a corrosion inhibitor and heavy metal ion adsorbent*. *417*, 131–136.

Lim, S.-H., & Hudson, S. M. (2004). Synthesis and antimicrobial activity of a water-soluble chitosan derivative with a fiber-reactive group. *Carbohydrate Research*, *339*(2), 313–319. https://doi.org/10.1016/j.carres.2003.10.024

Liu, M., Xia, D., Singh, A., & Lin, Y. (2021). Analysis of the Anti-Corrosion Performance of Dextrin and Its Graft Copolymer on J55 Steel in Acid Solution. *Processes*, *9*(9), 1642. https://doi.org/10.3390/pr9091642

Liu, Z., Sun, Y., Zhou, X., Wu, T., Tian, Y., & Wang, Y. (2011). Synthesis and scale inhibitor performance of polyaspartic acid. *Journal of Environmental Sciences*, *23*, S153–S155. https://doi.org/https://doi.org/10.1016/S1001-0742(11)61100-5

Loto, C. A., & Loto, R. T. (2016). Corrosion inhibition effect of Allium Cepa extracts on mild steel in H 2 SO 4. *Der Pharma Chemica*, *8*(20), 272–281. file:///C:/Users/DEMIAN/Desktop/NTA NHDH manuscript/References/Synergistic-effect-of-polyaspartic-acid-and-iodide-ion-on-co_2013_Corrosion-.pdf

Maduabuchi, C. A., Njoku, D. I., Anthony, O. I., Nwanonenyi, S. C., Akalezi, C., Blessing, A., & Oguzie, E. E. (2020). Experimental and Theoretical Studies on the Protective Effect of a Biomass Corrosion Inhibitor (vigna radiata) on Mild Steel in Acidic Medium. *Electroanalysis*, *32*(12), 3117–3130. https://doi.org/10.1002/elan.202060378

Manickavasagam, R., Karthik, K. J., Paramasivam, M., & Iyer, S. V. (2002). *Reviewed articles Poly (styrene sulphonic acid) -doped polyaniline as an inhibitor for the corrosion of mild steel in hydrochloric acid*. Central Electrochemical Research Institute.*49*(1), 19–26. https://doi.org/10.1108/00035590210413566

Martinez, S. (2003). Inhibitory mechanism of mimosa tannin using molecular modeling and substitutional adsorption isotherms. *Materials Chemistry and Physics*, *77*(1), 97–102. https://doi.org/10.1016/S0254-0584(01)00569-7

Melo-Silveira, R. F., Fidelis, G. P., Costa, M. S. S. P., Telles, C. B. S., Dantas-Santos, N., de Oliveira Elias, S., Ribeiro, V. B., Barth, A. L., Macedo, A. J.,

Leite, E. L., & Rocha, H. A. O. (2012). In vitro antioxidant, anticoagulant and antimicrobial activity and in inhibition of cancer cell proliferation by xylan extracted from corn cobs. *International Journal of Molecular Sciences*, *13*(1), 409–426. https://doi.org/10.3390/ijms13010409

Milewska, A., Ciejka, J., Kaminski, K., Karewicz, A., Bielska, D., Zeglen, S., Karolak, W., Nowakowska, M., Potempa, J., Bosch, B. J., Pyrc, K., & Szczubialka, K. (2013). Novel polymeric inhibitors of HCoV-NL63. *Antiviral Research*, *97*(2), 112–121. https://doi.org/https://doi.org/10.1016/j.antiviral.2012.11.006

Mobin, M., Rizvi, M., Olasunkanmi, L. O., & Ebenso, E. E. (2017). *Biopolymer from Tragacanth Gum as a Green Corrosion Inhibitor for Carbon Steel in 1 M HCl Solution*. ACS Omega 2,7,3997-4008 https://doi.org/10.1021/acsomega.7b00436

Moraga, G. A., Silva, G. G., Matencio, T., & Paniago, R. M. (2006). Poly(2,5-dimethoxy aniline)/fluoropolymer blend coatings to corrosion inhibition on stainless steel. *Synthetic Metals*, *156*(16–17), 1036–1042. https://doi.org/10.1016/j.synthmet.2006.06.026

Njoku, D. I., Li, B., Khan, M. S., Chinonso, U. P., Njoku, C. N., Onyeachu, I. B., & Li, Y. (2021). Quadruple-action coatings provided by doping epoxy with inhibitor-laden clay nanotubes functionalized with layer-by-layer of cross-bridged chitosan and anionic polyelectrolytes. *Progress in Organic Coatings*, *157*, 106312. https://doi.org/https://doi.org/10.1016/j.porgcoat.2021.106312

Njoku, D. I., Li, Y., Lgaz, H., & Oguzie, E. E. (2018a). Dispersive adsorption of Xylopia aethiopica constituents on carbon steel in acid-chloride medium: A combined experimental and theoretical approach. *Journal of Molecular Liquids*, *249*, 371–388. https://doi.org/10.1016/j.molliq.2017.11.051

Njoku, D. I., Li, Y., Lgaz, H., & Oguzie, E. E. (2018b). Dispersive adsorption of

Xylopia aethiopica constituents on carbon steel in acid-chloride medium: A combined experimental and theoretical approach. *Journal of Molecular Liquids*, *249*, 371–388.

Njoku, D. I., Njoku, C. N., Lgaz, H., Okafor, P. C., Oguzie, E. E., & Li, Y. (2021). Corrosion protection of Q235 steel in acidic-chloride media using seed extracts of Piper guineense. *Journal of Molecular Liquids*, *330*, 115619. https://doi.org/https://doi.org/10.1016/j.molliq.2021.115619

Njoku, D. I., Okafor, P. C., Lgaz, H., Uwakwe, K. J., Oguzie, E. E., & Li, Y. (2021). Outstanding anti-corrosion and adsorption properties of 2-amino-6-methoxybenzothiazole on Q235 and X70 carbon steels: Effect of time, XPS, electrochemical and theoretical considerations. *Journal of Molecular Liquids*, *324*, 114663. https://doi.org/https://doi.org/10.1016/j.molliq.2020.114663

Njoku, D. I., Onuoha, G. N., Oguzie, E. E., Oguzie, K. L., Egbedina, A. A., & Alshawabkeh, A. N. (2019). Nicotiana tabacum leaf extract protects aluminum alloy AA3003 from acid attack. *Arabian Journal of Chemistry*, *12*(8), 4466–4478. https://doi.org/https://doi.org/10.1016/j.arabjc.2016.07.017

Nwanonenyi, S., Arukalam, I. O., Obasi, H., Ezeamaku, U., Chukwujike Nwuzor, I., Arinzechukwu Maduabuchi, C., & Ochiagha Innocent, E. (2017). *Corrosion Inhibitive Behavior and Adsorption of Millet (Panicum miliaceum) Starch on Mild Steel in Hydrochloric Acid Environment*.

Nwanonenyi, S. C., Obasi, H. C., Udochukwu, M., Chidiebere, M. A., Njoku, D. I., & Oguzie, E. (2022). Protection by a polymer composite on carbon steel surface in 1.0 M HCl environment: a combined experimental and theoretical approach. *Brazilian Journal of Chemical Engineering*, *39*(1), 159–173. https://doi.org/10.1007/s43153-021-00187-2

Obot, I. B., Macdonald, D. D., & Gasem, Z. M. (2015). Density functional theory (DFT) as a powerful tool for designing new organic corrosion inhibitors. Part

1: An overview. *Corrosion Science*, *99*, 1–30. https://doi.org/https://doi.org/10.1016/j.corsci.2015.01.037

Obot, I. B., Onyeachu, I. B., & Kumar, A. M. (2017). Sodium alginate: A promising biopolymer for corrosion protection of API X60 high-strength carbon steel in saline medium. *Carbohydrate Polymers*, *178*, 200–208. https://doi.org/https://doi.org/10.1016/j.carbpol.2017.09.049

Ochoa, N., Bello, M., Sancristóbal, J., Balsamo, V., Albornoz, A., & Brito, J. L. (2013). Modified cassava starches as potential corrosion inhibitors for sustainable development. *Materials Research*, *16*(6), 1209–1219. https://doi.org/10.1590/S1516-14392013005000126

Oguzie, E. E., Njoku, D. I., Chidebere, M. A., Ogukwe, C. E., Onuoha, G. N., Oguzie, K. L., & Ibisi, N. (2014). Characterization and Experimental and Computational Assessment of *Kola nitida* Extract for Corrosion Inhibiting Efficacy. *Industrial & Engineering Chemistry Research*, *53*(14), 5886–5894. https://doi.org/10.1021/ie404273f

Olusiji, Ayoade Adeyanju&Layioye Ola Oyekunle (2019) Experimental Investigation of the Effects of Different Environmental Conditions on Pipelines Corrosion RatesSPE Nigeria Annual International Conference and Exhibition SPE Nigeria Annual International Conference and Exhibition https://doi.org/10.2118/198708-MS

Onyeachu, I. B., Njoku, D. I., Nwanonenyi, S. C., Ahanotu, C. C., & Etiowo, K. M. (2023). Investigation into the adsorption and inhibition properties of sodium octanoate against CO2 corrosion of C1018 carbon steel under static and hydrodynamic conditions. *Scientific African*, *20*, e01603–e01603. https://doi.org/10.1016/j.sciaf.2023.e01603

Ouici, H. B., Benali, O., & Guendouzi, A. (2016). Experimental and quantum

chemical studies on the corrosion inhibition effect of synthesized pyrazole derivatives on mild steel in hydrochloric acid. *Research on Chemical Intermediates*, *42*(9), 7085–7109. https://doi.org/10.1007/s11164-016-2520-0

Palencia, M. (2018). Functional transformation of Fourier-transform mid-infrared spectrum for improving spectral specificity by a simple algorithm based on wavelet-like functions. *Journal of Advanced Research*, *14*, 53–62. https://doi.org/https://doi.org/10.1016/j.jare.2018.05.009

Queiroz, M. F., Melo, K. R. T., Sabry, D. A., Sassaki, G. L., & Rocha, H. A. O. (2015). Does the use of chitosan contribute to oxalate kidney stone formation? *Marine Drugs*, *13*(1), 141–158. https://doi.org/10.3390/md13010141

Rai, A. K., Singh, R., Singh, K. N., & Singh, V. B. (2006). FTIR, Raman spectra and ab initio calculations of 2-mercaptobenzothiazole. *Spectrochimica Acta - Part A: Molecular and Biomolecular Spectroscopy*, *63*(2), 483–490. https://doi.org/10.1016/j.saa.2005.05.034

Rashid, M., Sabir, S., Rahim, A. A., & Waware, U. (2014). Polyaniline/Palm Oil Blend for Anticorrosion of Mild Steel in Saline Environment. *Journal of Applied Chemistry*, *2014*, 973653. https://doi.org/10.1155/2014/973653

Rezaierod, A. R., Rahimi, A. R., & Chaghazardi, M. (2014). Corrosion inhibition and adsorption behavior of 1-(1-naphthalenylmethyl)quinolinium chloride on mild steel in hydrochloric acid medium. *Analytical and Bioanalytical Electrochemistry*, *6*(6), 657–665. file:///C:/Users/DEMIAN/Desktop/my wife project 2022/Corrosion_Inhibition_Adsorption_Behavior_and_Therm.pdf

Roy, P., Karfa, P., Adhikari, U., & Sukul, D. (2014). *Corrosion inhibition of mild steel in acidic medium by polyacrylamide grafted Guar gum with various grafting percentage : Effect of intramolecular synergism*.

Saha, S. K., Dutta, A., Ghosh, P., Sukul, D., & Banerjee, P. (2016). Novel Schiff-base molecules as efficient corrosion inhibitors for mild steel surface in 1 M

HCl medium: Experimental and theoretical approach. *Physical Chemistry Chemical Physics*, *18*(27), 17898–17911. https://doi.org/10.1039/c6cp01993e

Saini, A. K., Carlin, C. M., & Patterson, H. H. (1993). Confirmation of the presence of imine bonds in thermally cured polyimides. *Journal of Polymer Science Part A: Polymer Chemistry*, *31*(11), 2751–2758. https://doi.org/10.1002/pola.1993.080311111

Sangeetha, Y., Meenakshi, S., & Sairamsundaram, C. (2015). *International Journal of Biological Macromolecules Corrosion mitigation of N - (2-hydroxy-3-trimethyl ammonium) propyl chitosan chloride as an inhibitor on mild steel*. *72*, 1244–1249. https://doi.org/10.1016/j.ijbiomac

Shanmugapriya, R., Ravi, M., Ravi, S., Ramasamy, M., Maruthapillai, A., & J, A. S. (2023). Electrochemical and Morphological investigations of Elettaria cardamomum pod extract as a green corrosion inhibitor for Mild steel corrosion in 1 N HCl. *Inorganic Chemistry Communications*, *154*, 110958. https://doi.org/https://doi.org/10.1016/j.inoche.2023.110958

Sharma, H. B., Panigrahi, S., Sarmah, A. K., & Dubey, B. K. (2019). Bio-active corrosion inhibitor based on 8-hydroxyquinolinegrafted-Alginate: Experimental and computational approaches. Jo ur na l P re of. *Science of the Total Environment*, 135907. https://doi.org/10.1016/j.aca.2021.338884

Shokry, H. (2014). Molecular dynamics simulation and quantum chemical calculations for the adsorption of some Azo-azomethine derivatives on mild steel. *Journal of Molecular Structure*, *1060*, 80–87. https://doi.org/https://doi.org/10.1016/j.molstruc.2013.12.030

Shukla, S., & Quraishi, M. (2011). Effect of some substituted anilines-formaldehyde polymers on mild steel corrosion in hydrochloric acid medium. *Journal of Applied Polymer Science*, *124*. https://doi.org/10.1002/app.35668

Silva, F. R. F., Dore, C. M. P. G., Marques, C. T., Nascimento, M. S., Benevides, N. M. B., Rocha, H. A. O., Chavante, S. F., & Leite, E. L. (2010). Anticoagulant activity, paw edema and pleurisy induced carrageenan: Action of major types of commercial carrageenans. *Carbohydrate Polymers*, *79*(1), 26–33. https://doi.org/https://doi.org/10.1016/j.carbpol.2009.07.010

Singh, R. N., Kumar, A., Tiwari, R. K., & Rawat, P. (2013). A combined experimental and theoretical (DFT and AIM) studies on synthesis, molecular structure, spectroscopic properties, and multiple interactions analysis in a novel Ethyl-4-[2-(thiocarbamoyl)hydrazinylidene]-3,5-dimethyl-1H-pyrrole-2-carboxylate and it. *Spectrochimica Acta Part A: Molecular and Biomolecular Spectroscopy*, *112*, 182–190. https://doi.org/https://doi.org/10.1016/j.saa.2013.04.002

Solomon, M M, Umoren, S. A., Udosoro, I. I., & Udoh, A. P. (2010). *Inhibitive and adsorption behavior of carboxymethyl cellulose on mild steel corrosion in sulphuric acid solution*. *52*, 1317–1325. https://doi.org/10.1016/j.corsci.2009.11.041

Solomon, Moses M, Gerengi, H., Kaya, T., & Umoren, S. A. (2017). Performance Evaluation of a Chitosan/Silver Nanoparticles Composite on St37 Steel Corrosion in a 15% HCl Solution. *ACS Sustainable Chemistry & Engineering*, *5*(1), 809–820. https://doi.org/10.1021/acssuschemeng.6b02141

Song, C., Yu, H., Zhang, M., Yang, Y., & Zhang, G. (2013). Physicochemical properties and antioxidant activity of chitosan from the blowfly Chrysomya megacephala larvae. *International Journal of Biological Macromolecules*, *60*, 347–354. https://doi.org/10.1016/j.ijbiomac.2013.05.039

Srivastava, V., Chauhan, D. S., & Joshi, P. G. (2018). *PEG-Functionalized Chitosan : A Biological Macromolecule as a Novel Corrosion Inhibitor*. 1990–1998. https://doi.org/10.1002/slct.201701949

Tiu, B. D. B., & Advincula, R. C. (2015). Polymeric corrosion inhibitors for the oil and gas industry: Design principles and mechanism. *Reactive and Functional Polymers*, *95*, 25–45. https://doi.org/https://doi.org/10.1016/j.reactfunctpolym.2015.08.006

Tong, A., Tang, X., Zhang, F., & Wang, B. (2020). Study on the shift of ultraviolet spectra in aqueous solution with variations of the solution concentration. *Spectrochimica Acta Part A: Molecular and Biomolecular Spectroscopy*, *234*, 118259. https://doi.org/https://doi.org/10.1016/j.saa.2020.118259

Umoren, S. A., & Ebenso, E. E. (2008). Blends of polyvinyl pyrrolidone and polyacrylamide as corrosion inhibitors for aluminium in acidic medium. *Indian Journal of Chemical Technology*, *15*(4), 355–363.

Umoren, S A, Eduok, U. M., & Solomon, M. M. (2014). Effect of polyvinylpyrrolidone – polyethylene glycol blends on the corrosion inhibition of aluminium in HCl solution. *Pigment & Resin Technology*, *43*(5), 299–313. https://doi.org/10.1108/PRT-09-2013-0079

Umoren, Saviour A. (2011). Synergistic inhibition effect of polyethylene glycol–polyvinyl pyrrolidone blends for mild steel corrosion in sulphuric acid medium. *Journal of Applied Polymer Science*, *119*(4), 2072–2084. https://doi.org/https://doi.org/10.1002/app.32922

Umoren, Saviour A., & Solomon, M. M. (2020). *Polymeric Corrosion Inhibitors for the Oil and Gas Industry*. 303–320.

Umoren, Saviour A, Solomon, M. M., Madhankumar, A., & Ime, B. (2019). *ur*, *na l P of*.

Umoren, Saviour A, Solomon, M. M., Madhankumar, A., & Obot, I. B. (2020). Exploration of natural polymers for use as green corrosion inhibitors for AZ31 magnesium alloy in saline environment. *Carbohydrate Polymers*, *230*, 115466. https://doi.org/https://doi.org/10.1016/j.carbpol.2019.115466

Varma, R., & Vasudevan, S. (2020). Extraction, Characterization, and Antimicrobial Activity of Chitosan from Horse Mussel Modiolus modiolus. *ACS Omega*, *5*(32), 20224–20230. https://doi.org/10.1021/acsomega.0c01903

Vino, A. B., Ramasamy, P., Shanmugam, V., & Shanmugam, A. (2012). Extraction, characterization and in vitro antioxidative potential of chitosan and sulfated chitosan from Cuttlebone of Sepia aculeata Orbigny, 1848. *Asian Pacific Journal of Tropical Biomedicine*, *2*(1, Supplement), S334–S341. https://doi.org/https://doi.org/10.1016/S2221-1691(12)60184-1

Wang, Y., Wang, J., Yuan, Z., Han, H., Li, T., Li, L., & Guo, X. (2017). Chitosan cross-linked poly(acrylic acid) hydrogels: Drug release control and mechanism. *Colloids and Surfaces. B, Biointerfaces*, *152*, 252–259. https://doi.org/10.1016/j.colsurfb.2017.01.008

Wolkers, W. F., Oliver, A. E., Tablin, F., & Crowe, J. H. (2004). A Fourier-transform infrared spectroscopy study of sugar glasses. *Carbohydrate Research*, *339*(6), 1077–1085. https://doi.org/https://doi.org/10.1016/j.carres.2004.01.016

Xing, X., Wang, J., & Hu, W. (2017). *Piercing and solidification*. *126*(April), 322–330.

Yaagoob, I. Y., Goni, L. K. M. O., Mazumder, M. A. J., Ali, S. A., Alfantazi, A., & Verma, C. (2023). Surface and interfacial properties of poly(methyldiallylammonium chloride): Effect of hydrophobic pendant and synergism (KI) on corrosion of C1018CS in 15% HCl. *Journal of the Taiwan Institute of Chemical Engineers*, *149*, 105000. https://doi.org/https://doi.org/10.1016/j.jtice.2023.105000

Zeng, W., Chen, G., Zhang, Y., Wu, K., & Liang, Z. (2012). Studies on the UV spectrum of poly(γ-glutamic acid) based on the development of a simple quantitative method. *International Journal of Biological Macromolecules*,

51(1–2), 83–90. https://doi.org/10.1016/j.ijbiomac.2012.04.005

Zhang, B., Li, J., Lv, X., Cui, Y., & Xu, Y. (2015). Synthesis of polyaspartic acid/2-amino-2-methyl-1,3-propanediol graft copolymer and evaluation of its scale inhibition and corrosion inhibition performance. *Desalination and Water Treatment*, *54*(7), 1998–2004. https://doi.org/10.1080/19443994.2014.895779

Zhang, Z., Tian, N. C., Huang, X. D., Shang, W., & Wu, L. (2016). Synergistic inhibition of carbon steel corrosion in 0.5 M HCl solution by indigo carmine and some cationic organic compounds: experimental and theoretical studies. *RSC Adv.*, *6*(27), 22250–22268. https://doi.org/10.1039/C5RA25359